DSMC Simulations of Rarefied Granular Gases : Hydrodynamics, Rheology and Segregation

A Thesis
Submitted for the Degree of
Master of Science (Engineering)

by

Ronak Gupta

Engineering Mechanics Unit
Jawaharlal Nehru Centre for Advanced Scientific Research
(A Deemed University)
Bangalore – 560 064

APRIL 2017

My family and friends

CALVIN: If people sat outside and looked at the stars each night, I'll bet they'd live a lot differently.

HOBBES: How so?

CALVIN: Well, when you look into infinity, you realize that there are more important things than what people do all day.

HOBBES: We spent our day looking under rocks in the creek.

CALVIN: I mean other people.

Bill Watterson, Calvin and Hobbes

DECLARATION

I hereby declare that the matter embodied in the thesis entitled "**DSMC Simulations of Rarefied Granular Gases : Hydrodynamics, Rheology and Segregation**" is the result of investigations carried out by me at the Engineering Mechanics Unit, Jawaharlal Nehru Centre for Advanced Scientific Research, Bangalore, India under the supervision of **Prof. Meheboob Alam** and that it has not been submitted elsewhere for the award of any degree or diploma.

In keeping with the general practice in reporting scientific observations, due acknowledgment has been made whenever the work described is based on the findings of other investigators.

Ronak Gupta

CERTIFICATE

I hereby certify that the matter embodied in this thesis entitled "**DSMC Simulations of Rarefied Granular Gases : Hydrodynamics, Rheology and Segregation**" has been carried out by **Mr. Ronak Gupta** at the Engineering Mechanics Unit, Jawaharlal Nehru Centre for Advanced Scientific Research, Bangalore, India under my supervision and that it has not been submitted elsewhere for the award of any degree or diploma.

Prof. Meheboob Alam
(Research Supervisor)

Acknowledgements

I joined JNCASR, a bumbling, young student, unsure of my capabilities and yet eager to learn. Now, as I am nearing the end of my thesis, I am still bumbling, a little more sure of my abilities and a lot more eager to learn. For this and my research I have plenty of people to thank.

First and foremost, I'd like to thank my advisor Prof. Meheboob Alam, for giving me the opportunity to pursue my undergraduate thesis here at JNCASR, and then welcoming me in his group for carrying out my Masters thesis. From him, I have learnt to do science the right way, with a mix of passion, dedication and discipline. Every discussion with him is like a mini lesson. Under his tutelage, not only have I gained an invaluable research experience, but also learnt the nitty gritties that accompany it. Sir has always pushed me to do my best, for which I will always be grateful. I would also like to thank Prof K.R Sreenivas for his support and Prof Ganesh Subramanian for his brilliant course in fluid mechanics. Dr Rajaram Lakkaraju, who is now at IIT Kharagpur, introduced me to fluid mechanics research and has been supportive of my work ever since he guided me on an undergraduate project. I would like to thank him and Dr. Shibu Clement at BITS Goa for their constant encouragement. Dr. Nair, Mamta maam and Prabhu Sir made sure that their teaching went beyond textbooks and classrooms. Thank you!

Life at JNCASR has largely been a fun ride for which I have many people to thank for. I am part of a lab that is made of a diverse set of people, all of whom have helped me in so many ways. Thank you to Achal, Sunil, Nandu, Saikat, Ramki, Reddy, Pratik for being awesome labmates and facilitating my research. Thanks to them, I am now not only a more able researcher but a more politically and socially aware citizen of this country. Outside my lab, I'd like to thank Paaji, Rafi, Nakul, Praveen, Topi, Samarth, Sankalp, Meha, Priyanka, Shashank and Seeves for all their help and support (coz' when you dont know what to thank for, 'help' and 'support' always works). A special shoutout to my friends from BITS Goa, Ankita, Akshay, Aditi, Vinay, Nikhilesh, Anish, Francis and Avinash for not slapping their dollar laden wealth at my face and keeping from constantly reminding me of my relative poverty and near empty bank balance. A giant thank you to everyone who plays football, here at JNCASR. Thanks to them I am now half a dozen kilo's lighter. An even bigger thank you to the JNCASR Basketball Club. Thanks to them, I am alive and shooting splash bucket jump shots. Playing is such an underrated pleasure and on days when I was down and out, basketball rescued me.

My research work would be markedly more difficult to execute without the support staff of JNCASR. Thank you to everyone in the academic, adminsitrative, library, technical and auxillary staff for making my work life so much easier. I would remiss not to thank the Department of

Science and Technology for giving me a Graduate Scholarship that among other things, allowed me to soak in the wonderful city that is Bengaluru. Money doesn't buy you happiness but it does get you beer, food and an Uber.

Last but certainly not the least I want to thank my family. My parents always back me, on my best and worst days. My brother does the same, after making fun of me. Thanks Mama, Papa and Rishi!

Abstract

Rarefied gas dynamics show marked deviations from Navier-Stokes dynamics, which make them interesting to study. This thesis on rarefied 'granular' gas dynamics, aims to study a prototypical flow setup of smooth inelastic hard spheres flowing down a channel, dubbed granular Poiseuille flow (GPF). Using Direct Simulations Monte Carlo simulations, we have studied the effects of dissipation and rarefaction on the general hydrodynamics and rheology, and have elucidated the crucial role of boundaries in determining the occurrence of a Knudsen minima in a granular gas. The role of mass bidispersity on a dilute granular binary mixture is highlighted by adapting the 3D DSMC code developed, for simulating the Poiseuille flow of a dilute bidisperse granular mixture.

For a dilute GPF, rarefaction plays an important role in suppressing the effects of dissipation which are found to be dominant in the low Kn regime. This is highlighted by calculating hydrodynamic profiles and it is observed that the behavior of velocity is dependent on density, with inelastcity enhanced clustering playing a major role in enhancing slip and centerline velocities. Dissipation combined with rarefaction plays a non trivial role in the genesis of temperature bimodality, with each effect dominant within a certain regime. While, for a molecular gas, a heat flux results in the transverse direction (q_x), owing to the anisotropy of the thermal conductivity tensor, for a granular gas this heat flux becomes bimodal. The bimodality in q_x is tied to inelasticity as dissipation induced clustering causes density inhomogeneity. The heat flux perpendicular to the wall (q_y) is amplified, owing to the increase in temperature gradients caused by collisional cooling in a granular gas. Both, the bimodality in q_x and amplification of q_y are suppressed by rarefaction. Normal Stress differences are found to vary considerably across the channel with the centerline value of first normal stress difference increasing with increasing Kn, and taking a negative value in the limit of low e_n and low Kn. The effect of non-dimensional acceleration on some of these profiles is looked into.

Our simulations suggest the presence of a Knudsen minima, even for a granular gas, driven by thermal walls, a finding at odds with previous work. The conundrum is resolved by distinguishing between athermal and thermal boundary conditions. It is found that the nature of boundaries, essentially the difference in macroscopic boundary conditions between a molecular and granular gas play a crucial role in the occurrence of a Knudsen minima. Bulk dissipation in the later plays a largely subdominant role. A related issue of anomalous slip is analyzed.

Steady State profiles of hydrodynamic fields have been computed for the case of the Poiseuille flow of a dilute bi-disperse granular gas mixture with mass bidispersity. Nonequipartition of

granular temperature is enhanced with increasing mass ratio and inelasticity but is additionally a strong function of Knudsen number. Species velocities and mixture velocity begin to differ from each other as rarefaction kicks in. The total mixture number density becomes more uniform with increasing mass ratio, while species segregation follows a non monotonic trend with increasing mass ratio if the particles are not nearly elastic. Mixture velocity shows a similar trend.

Nomenclature

Roman Letters

x	:	position vector
t	:	Time
n	:	Particle number density
m	:	Mass of a particle
d	:	Diameter of a particle
R	:	Radius of particle
v	:	Velocity vector
u	:	Coarse grained average velocity vector
p_{ij}, P_{ij}	:	Pressure tensor
$\mathcal{N}_1$	:	First Normal Stress Difference
$\mathcal{N}_2$	:	Second Normal Stress Difference
q	:	Heat flux vector
T	:	Temperature
N	:	Number of Particles
V	:	Volume
f	:	Probability distribution function
Q	:	Mass Flowrate
k_B	:	Boltzmann Constant
Kn	:	Knudsen Number
a	:	Driving 'force' (shear rate, acceleration)
e_n	:	Normal coefficient of restitution
β	:	Wall roughness parameter
I	:	Segregation quantifying parameter
E	:	Collisional Energy Loss
w	:	Diameter ratio for binary system

Abbreviations

DSMC	:	Direct Simulation Monte Carlo
GPF	:	Granular Poiseuille Flow
MD	:	Molecular Dynamics
EDMD	:	Event Driven Molecular Dynamics
HCS	:	Homogenous Cooling State

Greek Letters

α	:	Coefficient of restitution
ρ	:	Mass density
θ_x	:	First Normal Stress Difference
θ_y	:	Second Normal Stress Difference
λ	:	Mean Free Path
η	:	Shear viscosity
$\boldsymbol{\kappa}$	:	Thermal conductivity tensor
σ_{ij}	:	Two particle Diameter used for binary systems
$\lambda_{q_{x,y}}$	:	Length defining distance of peaks (q_y) and troughs (q_x) from the wall
τ	:	Relaxation time in regularization
μ	:	Mass ratio for binary system
δ	:	Concentration ratio for binary system
ν	:	Collision Frequency
γ	:	Temperature ratio for binary system
Θ	:	Heaveside Function

Subscripts

$1, 2$	:	Particle number
α, β	:	Component of Tensor or Vector, α, β taken from set x,y,z
max	:	Maximum value of a quantity of a quantity
inc	:	Increment in a quantity
pre	:	Value before an event
$post$	:	Value after an event
avg	:	Average value of a quantity
o	:	Centerline value of a quantity
s	:	Slip value of a quantity
fw	:	Value of a quantity in the bin closest to wall

List of Figures

Contents

Chapter 1

Introduction

Who could ever calculate the path of a molecule? How do we know that the creations of worlds are not determined by falling grains of sand? (Victor Hugo, Les Miserables)

Granular matter, a collection of macroscopic grains is ubiquitous in nature. Snow avalanches, sand dunes, landslides are some examples of granular flows occurring in nature. While, commonplace in nature, granular materials are also critical in a wide variety of industrial processes (Rao & Nott 2008; Forterre & Pouliquen 2008; Jaeger & Nagel 1992). Large scale food and pharmaceutical industries depend on efficient storage and transport of granular materials and estimates suggest that there is $\sim 60\%$ wastage of power associated with problems regarding bulk transport of granular materials (Duran 2012). Gaining a better understanding of granular materials thus is extremely important from a practical standpoint.

((a)) Gravel ((b)) Food grains ((c)) Pills

Figure 1.1: Few examples of granular matter in our daily life.

In addition to the commercial and environmental importance of studying granular flows, such flows are intriguing from a physicists point of view. Granular materials show some unique features and have thus attracted the attention of scientists from different disciplines for a very long time. Dating back to the seminal work by Bagnold (Bagnold 1954) there have been numerous studies on granular flows to understand the myriad of interesting phenomena displayed by them. Examples of complex features exhibited by granular flows include, but are not limited to, jamming (Majmudar *et al.* 2007), clustering (Goldhirsch & Zanetti 1993), segregation (Ottino & Khakhar 2000), and Brazil Nut effect (Shinbrot & Muzzio 1998). Pattern formation and instabilities in other classical systems have granular counterparts. For example granular systems have been shown to exhibit a granular Leidenfrost effect (Eshuis *et al.* 2005), granular Rayleigh Bernard convection (Eshuis *et al.* 2010) and Faraday crispation patters (Faraday 1831).

Granular flows also often display a nontrivial and rich rheology with finite normal stress differences (Alam & Luding 2003*a*) and non trivial microstructural properties (Alam & Luding 2005).

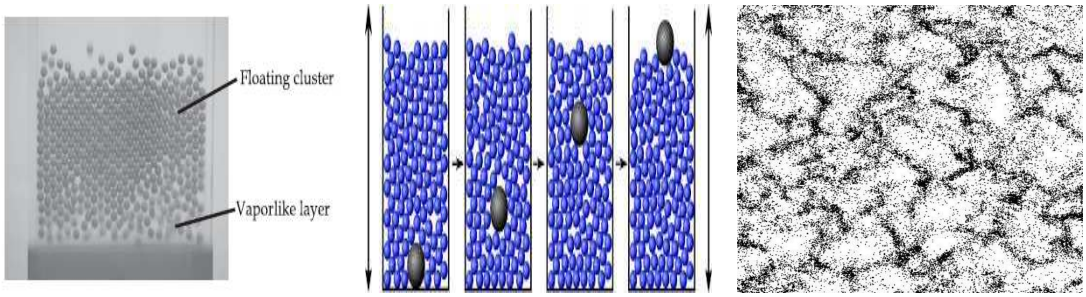

Figure 1.2: Left : granular Leidenfrost effect (Eshuis *et al.* 2005), Middle : Brazil Nut effect, right : Clustering in granular gases

The wealth of physics displayed by granular media can partly be accorded to the fact that granular matter can exist in all three states of matter, solid, liquid and gases (Jaeger *et al.* 1996). Granular matter can also coexist in two or more states and display phase transitions (Aranson & Tsimring 2006). While, granular media in each state of matter presents its own set of challenges and exhibits a wide range of specific features, the focus of this thesis is a granular gas (Umbanhowar 2003).

Figure 1.3: Granular states of matter - Left : sandpile (solid), Middle : Sand in hourglass (liquid), Right : sandstorm (gas)

Anyone observing typical granular media like a collection of sand particles knows that granular media has the capability of '*flowing*'. As far back as 55 B.C, Lucretius made one of the earliest recorded reference to the flow of granular materials and is quoted *"One can scoop up poppy seeds with a ladle as easily as if they were water and, when dipping the ladle the seeds flow in a continuous stream"* (Duran 2012). The flow of granular media has received considerable attention from the scientific community, owing to the different flow regimes that granular flows exhibit. While in the dense regime the flow is extremely slow and characterized by enduring force chains, at lower densities the flow is said to be in the kinetic regime where instantaneous

binary collisions dominate the transport. The ability of a set of hydrodynamic equations, much like the Navier Stokes equations, to capture the flow of granular materials is not wholly clear (Kadanoff 1999). The difficulty in forming traditional hydrodynamic continuum models for granular flow are compounded by the fact that except for a few exceptional cases, granular flows show no separation of length scales (Goldhirsch 1999). Also, the inter-particle collisions in the flow are inelastic and do not conserve energy, forcing the system out of equilibrium. Scientists have however achieved moderate success in capturing the hydrodynamics of granular flow, in particular the the flow of granular gases.

The fluid that we study in this thesis is a **granular gas** - an agitated and driven state of granular media. Owing to energy loss via collisions a collection of grains collapses to rest unless 'fluidized' by an input of energy via gravity, shear or shaking. This energetic state of then consists of particles that interact majorly via instantaneous binary collisions. Taking inspiration from traditional kinetic theory developed to study molecular gases (Chapman & Cowling 1970), hydrodynamic models to capture the dynamics of granular gases have been developed (Savage & Jeffrey 1981; Jenkins & Savage 1983; Haff 1983; Jenkins & Richman 1985; Campbell 1990)

Real granular flows in nature are complicated and suffer a large number of forces that present a challenge to model accurately. Many a times earth bound granular materials are suspended in an interstitial fluid, calling for a description that includes stressed due to the fluid. If the Bagnold number is high enough, these suspension based effects can be ignored. Besides the above complicating factors most granular materials found in nature have a non spherical shape and are characterized by a degree of polydispersity in shape, size and even inelasticity. For a theoretician or even a computational scientist modeling 'real' granular media poses a serious challenge and we usually resort to a simple paradigm to describe the behavior of a granular gas - a collection of smooth, inelastic, hard spheres having a fixed value of coefficient of restitution. Even this simple model has been found to capture a variety of rich dynamics exhibited by a granular gas.

1.1 Chapter organization

In the present study we consider flow of dry granular matter in an excited state as a granular gas. We study the flow of a granular gas in a simple geometry - a rectangular channel bounded by walls, and driven by a uniform acceleration. This flow is called a Poiseuille flow. It can be helpful to imagine a flow of gas in a pipe and replace the gas molecules by macroscopic granular particles to obtain a physical picture of a granular Poiseuille flow. As is seen in this study, the physics of GPF however differ considerably from that of a molecular gas flow, owing in part to the dissipative nature of collisions and the difference in boundary conditions.

Chapter 2
In this chapter we describe the Direct Simulation Monte Carlo algorithm in detail by listing kinetic theory calculations to arrive at the physical principles at the heart of the method. We present some test cases to bench mark the problem.

Chapter 3

This chapter describes an effort to study the general hydrodynamics and rheology of a dilute GPF driven by thermal walls. In particular the aim is to isolate the effects of dissipation and rarefaction on some quantities of interest and briefly examine the effect of change in acceleration on some of these quantities.

Chapter 4

Here we discuss the problem of Knudsen minima in a granular gas and explain the conundrum of why a minima is shown to be absent in previous simulations (Alam *et al.* 2015) but appears in the recent simulations. We carry out simulations for different wall boundary conditions.

Chapter 5

In this chapter we add a degree of complexity to the system by introducing mass bidispersity. We outline how the present DSMC code is adopted for simulating binary mixtures and look at typical features of granular mixtures like energy non equipartition and segregation. Effect of rarefaction and mass ratio on equipartition, flow rate and velocities is discussed.

Chapter 2

Direct Simulation Monte Carlo (DSMC) Method

2.1 Introduction

With the advent of computing technology the field of computational fluid dynamics has seen a parallel rise. Today, while there exist a number of sophisticated techniques to simulate continuum equations, a number of algorithms have sprung up to simulate particle systems as well. Chief among them is Molecular Dynamics (MD) (Alder & Wainwright 1959), which exactly simulates the behavior of a system by computing individual particle trajectories. Given the force and/or torque acting on the system the position and velocity of each particle is determined which makes it an expensive method, limiting its usage to small systems. Efficient modifications of traditional MD like Event Driven Molecular Dynamics (Rapaport 1980) have vastly improved the efficiency of the algorithm, allowing the simulation of systems contains millions of particles. Yet, there exist limitations of MD which have been well documented elsewhere. For instance, the computation of collision partners in a rarefied gas becomes impractical for an event driven simulation method.

In the 1960's G.A Bird introduced a stochastic method for simulating particle dynamics called Direct Simulation Monte Carlo (DSMC) method (Bird 1963, 1994). Originally introduced as a method to simulate near continuum, transition and free molecular regimes of a dilute gas flow, the method has since then grown to be the preferred technique for simulating various physical phenomena in rarefied gas dynamics, and has demonstrated the ability to faithfully reproduce characteristic physics of a host of equilibrium and non equilibrium processes. Going beyond its application in dilute molecular gas flows, variants of DSMC have been used for modeling dense gases (Montanero & Santos 1997), binary mixtures and granular gases. DSMC owes its remarkable efficiency indirectly to the non deterministic nature of the algorithm where it differs from MD. MD, essentially integrates Newton's equations of motion, which are universal and deterministic. DSMC, on the other hand doesn't compute particle trajectories and instead maps a system containing real particles onto a set of 'quasi' particles that act as agents to integrate the Boltzmann equation. While this statistical approach is a deviation from other particle schemes, it allows DSMC to be efficient, especially in computing rarefied gas flows. We will discuss the concept of 'quasi' particles later in the chapter. It will be instructive to revisit the Boltzmann physics in order to understand the core physics behind the working of DSMC.

2.2 Boltzmann Equation

The Boltzmann equation is the appropriate equation for investigating the non equilibrium dynamics of the flow of gases. While the Navier-Stokes equations give a continuum description of fluid behavior, the equations are only valid for systems characterized by a small Kn. The Boltzmann equation on the other hand can capture relevant physics in regimes where hydrodynamic gradients occur at length scales of the order or even smaller than the mean free path, λ. Because the Boltzmann equation is an Integro-differential equation, its mathematical complexity limits analytical solutions. Physicists often rely on limiting solutions or numerical techniques like DSMC to obtain predictions from the Boltzmann equation. Unlike continuum physics which regards matter as a continuum and formulates balance equations for its macroscopic quantities, Kinetic theory describes the dynamics of gases at a molecular level in terms of changes in probabilities. The quantity of prime importance in Kinetic theory is the single particle distribution function $f(\vec{r}, \vec{v}, t)$. This function is basically a probability distribution that when integrated over suitable limits $d\vec{r}$ and $d\vec{v}$, gives us the number of particles with position coordinates and velocity within the bounds of $d\vec{r}$ and $d\vec{v}$ respectively. If we can track the evolution of the distribution function in time and space, it allows us to obtain the complete description of the system. By taking moments of the function we can obtain macroscopic number density ($n(\vec{r}, t)$), velocity ($\vec{u}(\vec{r}, t)$), and Temperature ($T(\vec{r}, t)$).

$$n(\vec{r}, t) = \int f(\vec{r}, \vec{v}, t) d\vec{v} \tag{2.1}$$

$$n(\vec{r}, t)\vec{u}(\vec{r}, t) = \int \vec{v} f(\vec{r}, \vec{v}, t) d\vec{v} \tag{2.2}$$

$$\frac{3}{2} n(\vec{r}, t) k_B T(\vec{r}, t) = \frac{m}{2} \int (\vec{v} - \vec{u}(\vec{r}, t))^2 f(\vec{r}, \vec{v}, t) d\vec{v} \tag{2.3}$$

The single particle distribution function changes due to three processes : particle motion (streaming), external forcing, and intermolecular binary collisions. The Boltzmann equation is given by

$$\frac{\partial f(\vec{r}, \vec{v}, t)}{\partial t} + \nabla_r f(\vec{r}, \vec{v}, t) \cdot \vec{v} + \nabla_v f(\vec{r}, \vec{v}, t) \cdot \frac{\vec{F}}{m} = \left. \frac{\partial f(\vec{r}, \vec{v}, t)}{\partial t} \right|_{coll} \tag{2.4}$$

The left hand side of the equation represents the change in f, due to particle motion (second term) and external force (third term). The right hand side of the equation is the time varying change in f due to binary collisions which is calculated using a collision operator. As is obvious by the above formulation, unlike a collection of Newton's equations, the Boltzmann Equation doesn't discuss the motion of particles. Rather it measures how the probabilities (dictated by the distribution function) change with time. Using information provided by real particles motion and velocities we can construct the distribution function and then by coarse graining calculate hydrodynamic fields. This is the crux of almost any particle algorithm. While MD does this by simulating a set of real particles that are directly representative of the physical

system being simulated, DSMC uses another approach. For solving the Boltzmann equation, DSMC integrates the equation using 'quasi' particles. These 'quasi' particles can be imagined as sub-units or agents of probability increment, $\delta f(\vec{r}, t)$. Using a collection of these quasi particles, increments in the velocity distribution function are calculated due to collisions, streaming and external force.

2.3 DSMC : Physics*

2.3.1 Collision Frequency in a Homogeneous Hard Sphere Gas

As discussed in the above section, the distribution function experiences a change if the number of particles in a certain phase space $f(\vec{r}, \vec{v}, t)d\vec{r}d\vec{v}$ changes. The change in the distribution function due to streaming is reflected in the convective type $\nabla_r f(\vec{r}, \vec{v}, t)\cdot\vec{v}$ term in the Boltzmann equation. Further, we proceed to calculate the total number of collisions, N_c that occur in a time interval dt and volume element V. This term will allow us to calculate the change in the distribution function due to intermolecular collisions and thus intregrate the Boltzmann equation. It will become clear later in the chapter how this calculation is incorporated into the DSMC algorithm. Let's define a quantity ν for the above mentioned task. $\nu(\vec{v}_1, \vec{v}_2, \vec{e})$ is the number of collisions per unit time that occur between particles having relative velocity $\vec{v}_1 - \vec{v}_2$ and relative orientation $\vec{e}$. This term, the collision frequency will lead to the number N_c, central to DSMC's working. For deriving ν we will resort to geometry. Consider two particles, both having radius R, velocities $\vec{v}_1$ and $\vec{v}_2$, and positions $\vec{r}_1$ and $\vec{r}_2$ respectively. If particle 2 is put to rest, particle 1 will collide with 2 at an orientation $\vec{e}$ with relative velocity $\vec{v}_{12}$ tracing a generalized collision cylinder in time Δt having length $\vec{v}_{12}\Delta t$ and cross section $(2R)^2 d\vec{e}$. The scenario is graphically shown in the schematic 2.1.

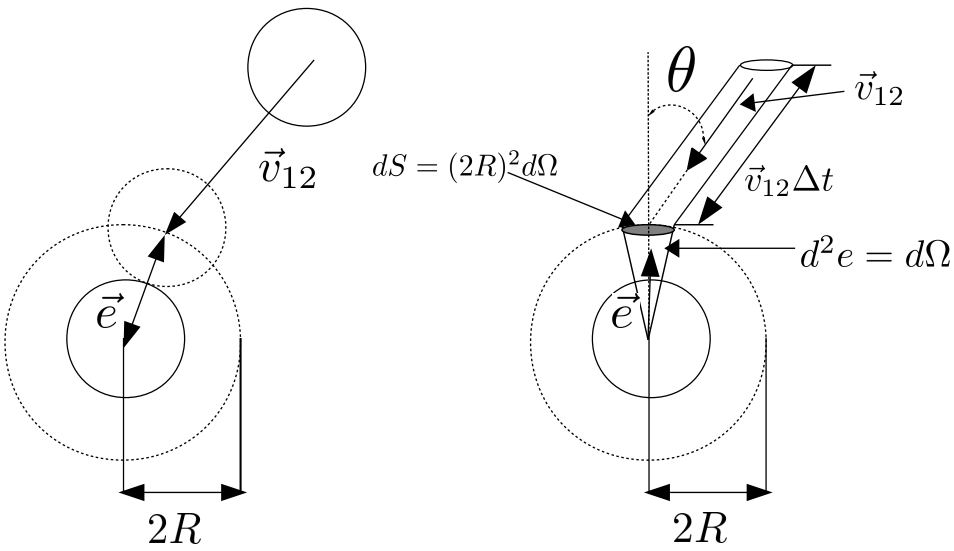

Figure 2.1: Schematic showing the collision of two particles. Parameters used to calculate collision frequency also shown

*This section is an expanded version of the derivation found in (Pöschel & Schwager 2005; Brilliantov & Pöschel 2004)

Each particle 2 will have a corresponding collision cylinder and there will be N_2 such particles in a volume $d\vec{e}$.

$$N_2 = f(\vec{v}_2, t)d\vec{v}_2 d\vec{e} \tag{2.5}$$

The number of particles of type 1 contained in the volume of the cylinder (dV) is N_1.

$$N_1 = f(\vec{v}_1, t)d\vec{v}_1 \frac{dV}{dt} \tag{2.6}$$

The distribution functions are independent of position because the derivation is made for a uniform hard sphere gas. The extension for non uniform gases can be taken care of within the framework itself and will be discussed in a later section. Hence each particle of type 2, having its own cylinder, will have suffer a direct collision with N_1 particles per unit time. We are finally in a position to calculate the collision frequency as the product of N_1 and N_2. By visual inspection

$$dV = (2R)^2 d\vec{e}|\vec{v}_{12} \cdot \vec{e}|\Delta t \tag{2.7}$$

Using the formulas for N_1, N_2 and dV we obtain

$$\nu(\vec{v}_1, \vec{v}_2, \vec{e}) = f(\vec{v}_1, t)f(\vec{v}_2, t)(2R)^2|\vec{v}_{12} \cdot \vec{e}|d\vec{v}_1 d\vec{v}_2 \vec{e} \tag{2.8}$$

We make use of the Heaviside function (Θ) to discriminate between particles that are approaching towards and away from each other and finally

$$\nu(\vec{v}_1, \vec{v}_2, \vec{e}) = \Theta[\vec{v}_{12} \cdot \vec{e}]f(\vec{v}_1, t)f(\vec{v}_2, t)(2R)^2|\vec{v}_{12} \cdot \vec{e}|d\vec{v}_1 d\vec{v}_2 \vec{e} \tag{2.9}$$

We now need to integrate the obtained collision frequency all orientations, velocities and volume of the system to come up with the number of particle collisions in time Δt and volume V

$$\frac{dN_c}{dt} = \int \nu(\vec{v}_1, \vec{v}_2, \vec{e})d\vec{v}_1 d\vec{v}_2 d\vec{e} dr \tag{2.10}$$

Since ν is independent of position the volume integral is trivial and a division by a factor of half is needed to avoid double counting. On plugging the derived formula for $\nu(\vec{v}_1, \vec{v}_2, \vec{e})$

$$\frac{dN_c}{dt} = \frac{V}{2} \int \Theta[-\vec{v}_{12}.\vec{e}]f(\vec{v}_1, t)f(\vec{v}_2, t)(2R^2)|\vec{v}_{12}.\vec{e}|d\vec{v}_1 d\vec{v}_2 d\vec{e} \tag{2.11}$$

For an arbitrary vector $\vec{a}$ the following identity helps us simplify the above expression and obtain (2.13)

$$\int \Theta(-\vec{a}.\vec{e})|\vec{a}.\vec{e}|d\vec{e} = \pi|\vec{a}| \tag{2.12}$$

$$\frac{dN_c}{dt} = \frac{V}{2}\pi(2R^2) \int f(\vec{v}_1, t)f(\vec{v}_2, t)|v\vec{_{12}}|d\vec{v}_1 d\vec{v}_2 \tag{2.13}$$

The definition of the systems number density n and average relative velocity, $\langle|\vec{v}_{12}|\rangle$ follow and are used to obtain the final expression for $\frac{dN_c}{dt}$ which after multiplying by the time interval of

interest Δt gives us a number for N_c (2.16)

$$n = \int f(\vec{v}, t) d\vec{v} = \frac{N}{V} \tag{2.14}$$

$$\langle |\vec{v}_{12}| \rangle = \frac{\int f(\vec{v}_1, t) f(\vec{v}_2, t) |\vec{v_{12}}| d\vec{v}_1 d\vec{v}_2}{\int f(\vec{v}_1, t) f(\vec{v}_2, t) d\vec{v}_1 d\vec{v}_2} \tag{2.15}$$

$$N_c = \frac{2\pi R^2 N^2 \langle |\vec{v}_{12}| \rangle \Delta t}{V} \tag{2.16}$$

(2.16) gives us an expression for the total number of collisions that occur in a time interval Δt and volume V, given that the number of particles in the volume is N. It is seen that besides a constant pre-factor, N_c is dependent on the term $\langle |\vec{v}_{12}| \rangle$ which requires knowledge of the distribution function *apriori* as seen in (2.15). The brilliance of DSMC is that it allows us to subvert this limitation and in the next section we will see how the method succeeds in doing that.

2.3.2 Algorithm Details

As mentioned previously, DSMC basically aims to integrate the Boltzmann equation and process a number of collisions as given by the collision frequency obtained by kinetic theory calculations. As such the 'particles' in DSMC serve the purpose of satisfying this aim and should not be regarded as *real* particles. Thus even though DSMC resembles a particle method it is beneficial to imagine the 'simulated particles' as agents to integrate the Boltzmann equation. We can define a quantity N_e that denotes the number of physical or real particles each simulated particle represents.

$$N_e = \frac{\bar{n}}{N/V} \tag{2.17}$$

In (2.17) $\bar{n}$ is the physical systems number density. The particle number density ($\frac{N}{V}$) in the simulation has no physical meaning and just holds statistical significance. As such it can be arbitrarily increased without changing the value of $\bar{n}$ and not breaching the low density limitation of DSMC. If N_e is not equal to 1 the factor is simply multiplied to increase or decrease the collision frequency. Including this parameter the formula for N_c becomes

$$N_c = \frac{2\pi R^2 N^2 N_e \langle |\vec{v}_{12}| \rangle \Delta t}{V} \tag{2.18}$$

From now on this factor will only be included in the final formulas and omitted in intermediate steps of the derivation. Although all the results derived till now and further have assumed homogeneity they are equally applicable for non uniform systems. For such systems we divide the domain into regions where local equilibrium and homogeneity is assumed. We claimed that the DSMC method is designed to avoid this inconvenience of calculating $\langle |\vec{v}_{12}| \rangle$. An appropriate acceptance rejection procedure is designed so that while we randomly select a certain N_p number of pairs of particles only those satisfying the acceptance rejection criteria actually collide. As a result of this scheme we process number of collisions in a time Δt as required by collision

frequency in (2.16). The acceptance criteria for collisions is

$$P_{12} = \frac{\Theta(\vec{v}_{12}.\vec{e})|\vec{v}_{12}.\vec{e}|}{v_{12}^{max}} > \text{rand}[0,1) \tag{2.19}$$

P_{12}, the probability of collision between two particles, can also be written as the ratio of actual colliding pairs (N_c) and selected pairs for collision (N_p).

$$P_{12} = \frac{N_c^{\Delta t}}{N_p^{\Delta t}} = \frac{\langle\Theta(\vec{v}_{12}.\vec{e})|\vec{v}_{12}.\vec{e}|\rangle}{v_{12}^{max}} = \frac{1}{v_{12}^{max}}\frac{1}{4\pi n^2}\int d\vec{e}d\vec{v}_1 d\vec{v}_2 f(\vec{v}_1)f(\vec{v}_2)\Theta(\vec{v}_{12}.\vec{e})|\vec{v}_{12}.\vec{e}| \tag{2.20}$$

For simplifying (2.20) we use the following identities

$$\langle\Theta(\vec{v}_{12}.\vec{e})|\vec{v}_{12}.\vec{e}|\rangle = \frac{\int d\vec{e}d\vec{v}_1 d\vec{v}_2 f(\vec{v}_1)f(\vec{v}_2)\Theta(\vec{v}_{12}.\vec{e})|\vec{v}_{12}.\vec{e}|}{\int f(\vec{v}_1,t)f(\vec{v}_2,t)d\vec{v}_1 d\vec{v}_2 d\vec{e}} \tag{2.21}$$

$$\int f(\vec{v}_1,t)f(\vec{v}_2,t)d\vec{v}_1 d\vec{v}_2 d\vec{e} = \int d\vec{e}\int f(\vec{v}_1,t)f(\vec{v}_2,t)d\vec{v}_1 d\vec{v}_2 = 4\pi n^2 \tag{2.22}$$

We use the vector identity below to simplify (2.20) and further use the definition of $\langle|v_{12}|\rangle$ to obtain (2.25) :

$$\int \Theta(\vec{v}_{12}.\vec{e})|\vec{v}_{12}.\vec{e}|d\vec{e} = \pi|v_{12}| \tag{2.23}$$

$$\frac{N_c^{\Delta t}}{N_p^{\Delta t}} = \frac{1}{v_{12}^{max}}\frac{1}{4n^2}\int d\vec{v}_1 d\vec{v}_2 f(\vec{v}_1)f(\vec{v}_2)|v_{12}| = \frac{1}{4v_{12}^{max}}\langle|v_{12}|\rangle \tag{2.24}$$

Finally we obtain the result for N_p and multiply it with a factor of N_e :

$$N_p^{\Delta t} = \Delta t\frac{dN_c}{dt}\frac{4v_{12}^{max}}{\langle|v_{12}|\rangle} = \frac{8\pi R^2 N^2 v_{12}^{max}\Delta t N_e}{V} \tag{2.25}$$

The result (2.25) importantly does not contain the troublesome term $\langle|v_{12}|\rangle$ and instead contains the term v_{12}^{max} which is a user defined bound on the maximum value that $\vec{v}_{12}.\vec{e}$ and hence $|\vec{v}_{12}|$ can take during the simulation. Using the above described physical principles the DSMC algorithm is as follows.

- Initialize the particle positions and velocities and set an initial bound on v_{12}^{max}
- Propagate each particle as the assumed force dictates and process boundary conditions
- If the simulation is for the case of a non Homogenous gas sort the particles in cells according to positions.The cells must typically be a fraction of the mean free path.
- In each cell select $N_p = \frac{1}{2}N_{cell}\omega_{max}$, where $\omega_{max} = 4\pi\sigma^2 n_{cell}|\vec{e}.\vec{v}_{ij}|_{max}\Delta t$, pairs of particles randomly.
- For each pair select a random vector in 3D which is the pre-collision contact vector $\vec{e}$. If the collision is accepted according to the rule given in (2.19) change the velocities of particles i,j to $\vec{v}_i'$ and $\vec{v}_j'$ respectively as given by the collision rule below. Else move to the

next pair of selected particles. The normal coefficient of restitution is given by e_n.

$$\vec{v_i'} = \vec{v_i} - \frac{m_j}{m_i + m_j}(1 + e_n)(\vec{e}.\vec{v}_{ij})\vec{e} \tag{2.26}$$

$$\vec{v_j'} = \vec{v_j} + \frac{m_i}{m_i + m_j}(1 + e_n)(\vec{e}.\vec{v}_{ij})\vec{e} \tag{2.27}$$

- Calculate averages of required hydrodynamic quantities and keep repeating steps from 3-5 till number of time-steps specified are completed

As seen in the above mentioned algorithm DSMC in unique in the sense that the collision stage is decoupled from the particle movement stage. This also allows DSMC to have a much less stringent restriction on time-step Δt than traditional event driven Molecular dynamics (EDMD). In DSMC, Δt is usually set to a fraction of the effective mean time between collisions. In contrast EDMD sets the time-step to the time between two successive collisions. To summarize this section, we have outlined in some details the physics behind the working of DSMC. By resorting to Kinetic theory concepts, DSMC uses a 'parliament' of simulated particles to represent a physical system. Randomness lies at the heart of this algorithm as particles collide, regardless of position, with the contact vector before collision selected randomly. The streaming stage and boundary conditions implementation is akin to a traditional particle method and similar coarse graining is done to obtain averaged quantities. Because the method is designed to solve the Boltzmann equation, the algorithm described is limited in its working to dilute systems where the assumption of molecular chaos can be invoked. While variants of the method have been introduced to solve the Enskog equation, a good approximation to model dense gases, throughout this thesis we will restrict our study to dilute gases and hence use DSMC in its classical form.

2.4 Test Cases

In this section we present results of test cases that validate the developed code and demonstrate its capability to simulate a host of prototypical granular gas systems. The test cases also confirm that the various steps in the DSMC algorithm like averaging, boundary condition implementation and collision routines are correctly implemented in the code.

2.4.1 Freely Cooling Granular Gas

A freely cooling granular gas is one of the simplest kind of granular system. The system is not acted upon by any force and because of the continual inelastic collisions it loses all energy and ultimately comes to a state of complete collapse. The decrease in granular temperature follows a cooling law first derived by Haff (Haff 1983) and is thus called the Haff's law.

$$\frac{dT}{dt} \propto -\bar{n}(2R)^2(1 - {e_n}^2)T^{\frac{3}{2}} \tag{2.28}$$

(2.28) is a simple initial value ODE and can be integrated to obtain the final form of Haff's law

$$T(t) = \frac{T(0)}{(1+\frac{t}{\tau})^2} \tag{2.29}$$

The relaxation time τ for a three dimensional case is given by ((Brilliantov & Pöschel 2004))

$$\tau^{-1} = \frac{8}{3}(1-{e_n}^2)R^2\bar{n}\sqrt{\pi T(0)} \tag{2.30}$$

(2.28) along with (2.30) can be rigorously derived from kinetic theory but for sake of brevity we will omit the derivation. Interested readers are directed to (Puglisi 2001). Fig 2.2(a) shows decaying granular temperature (T) versus time (t) as predicted by Haff's Law and present code. The parameters in the simulation were set to ($e_n = 0.8$, $R = 1$, $\bar{n} = 0.01$) for which (2.30) predicts a $\tau = 58.805$. As seen from the figure the agreement between theory and simulation is excellent. Fig 2.2(b) shows the normalized probability distribution for v_x plotted over a Maxwellian distribution. The overlap confirms the existence of a homogenous cooling state (HCS).

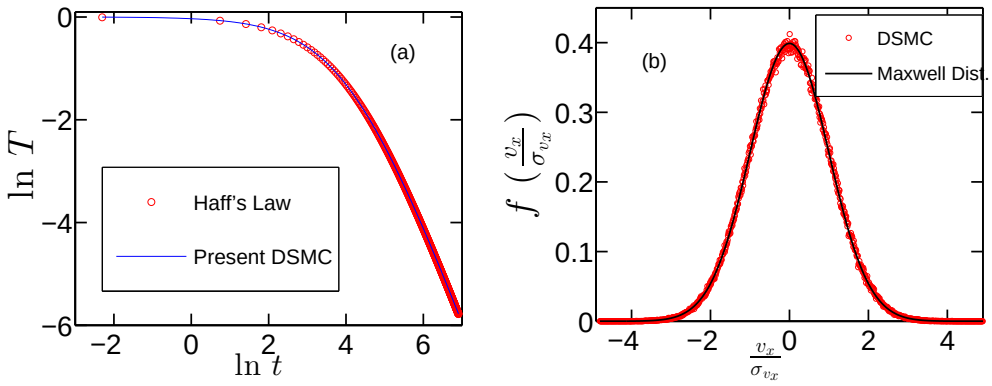

Figure 2.2: (a): ln T vs ln t for a system of 10^5 particles compared with Haff's law prediction, (b) Distribution function for v_x for a system of 10^6 particles and $e_n = 0.8$

A molecular gas with $e_n = 1$ under no forcing and periodic boundaries will remain homogeneous and uniform. A granular gas however loses this property due to the appearance of clustering in the system. The resulting transient state is called as an Inhomogeneous Cooling System (ICS). An HCS for a granular gas however is still a system of interest and DSMC allows us to maintain a granular gas in an HCS. If the simulation box is not split into cells, the system is artificially maintained in an HCS which allows us to measure properties of interest. Dividing the domain into cells leads to an non uniform granular gas and the system begins to show clustering, enhanced by larger degree of inelasticity in the system as seen in Fig 2.3. The present DSMC code is able to simulate and reproduce the essential features of an HCS, namely the temperature decay in accordance with Haff's law and a Maxwellian distribution for its velocity components. Fig 2.3 presents no quantitative check but demonstrates the ability of the code to capture phenomena occurring in non-uniform systems.

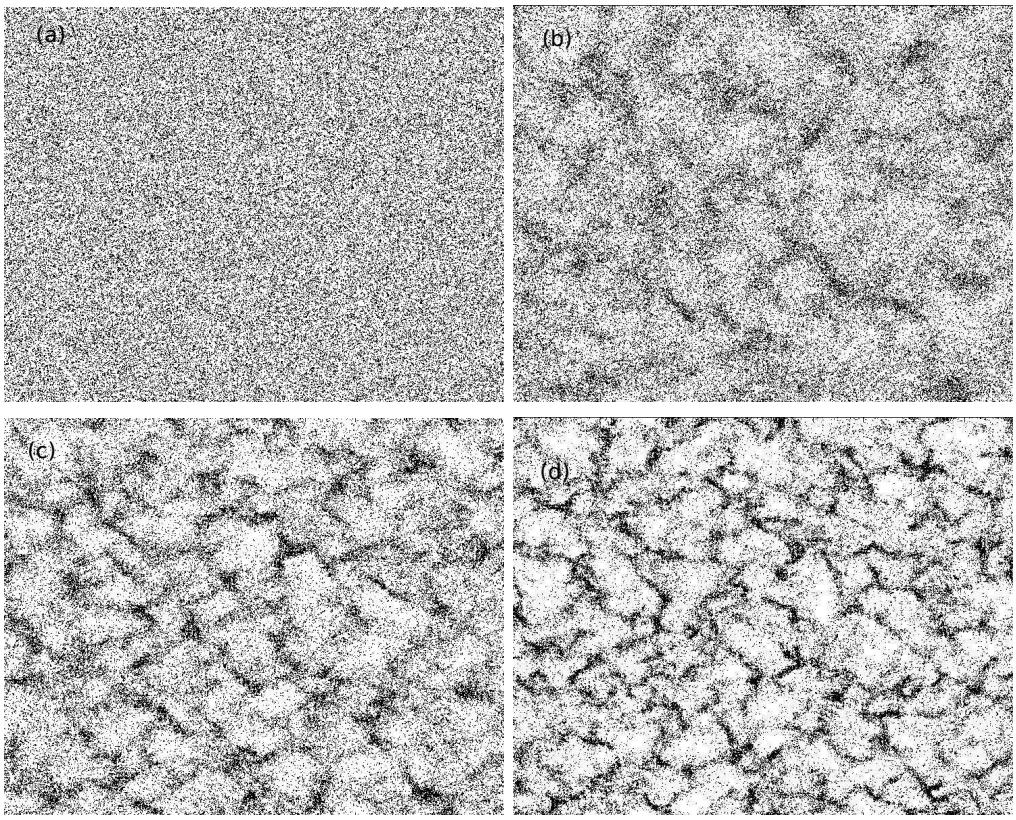

Figure 2.3: System snapshots for the cooling state of a gas of different e_n's at $t = 1000$ for N = 10^5. (a): $e_n = 1$, (b): $e_n = 0.9$, (c): $e_n = 0.8$, (d): $e_n = 0.6$

2.4.2 Uniform Shear Flow of Dissipative Gases

In this section we simulate the uniform shear flow of a granular gas as done in (Astillero & Santos 2005). If we transfer the problem to the local Larangian frame of reference, it can be shown that the solution to the Boltzmann equation for the case of a uniform shear flow is homogeneous with uniform density and temperature. The boundaries for the simulation setup are not real boundaries but rather virtual ones where we apply the Lee-Edwards boundary condition (Lees & Edwards 1972). A schematic of the problem is shown in Fig 2.4.

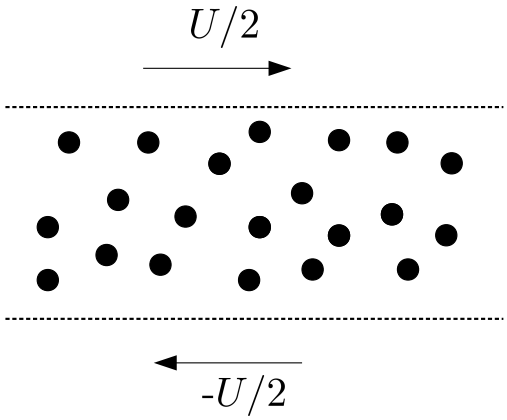

Figure 2.4: A simple schematic showing the setup for a uniform shear flow of a gas enclosed by two boundaries traveling with equal speed in opposite directions

The imposed shear rate injects energy into the system which is balanced by the collisional energy loss due to inelasticity. Initially the system will be in a transient state and gradually evolve to a steady state with a characteristic pressure and temperature. In Fig 2.5 we plot the evolution of granular temperature and normalized shear component pressure with the number of collisions per particle (s). It is observed that the agreement with DSMC simulations of (Astillero & Santos 2005) is reasonable. The slight mismatch in the temperature profile could be due to error in extraction of data from a log-log plot or slight mismatches in the imposed shear rate ($a\tau^0$). A detailed analysis of the system revealed a difficulty in achieving a steady state for the lower value of shear rate. While the match till the plotted value of s is good, due to unavailability of data beyond $s = 40$ we cannot make a quantitative comparison to comment further. This section, however demonstrates the ability of the code to handle transient processes.

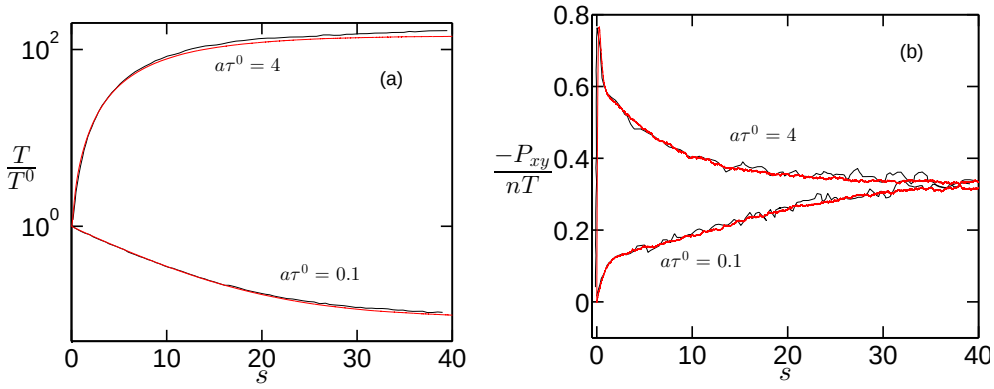

Figure 2.5: (a): $\frac{T}{T^0}$ vs s, (b): $\frac{-P_{xy}}{nT}$ vs s for a system with ($N = 10000$, $a\tau^0 = (4, 0.1)$, $e_n = 0.9$). Red lines : Present DSMC, Black Lines : DSMC results from (Astillero & Santos 2005)

2.4.3 Couette-Fourier Flow of a Granular Gas

In (Reyes Vega Francisco & Vincente 2013) the authors studied the presence of several base states in a granular gas subject to shear (a) and a temperature difference ($\Delta T = T_+ - T_-$). A schematic of the system is shown in Fig 2.6.

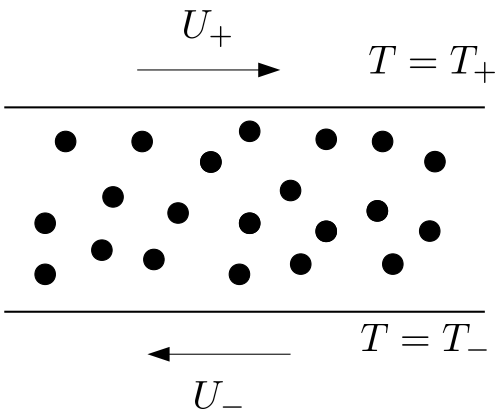

Figure 2.6: A simple schematic showing the setup for a Couette-Fourier flow of a gas enclosed by two boundaries traveling with equal speed in opposite directions and kept at different temperatures

Grad's method was supplemented by DSMC solutions that revealed five types of Couette-Fourier steady states with uniform shear flow existing as a special case as a line in the $\Delta T = 0$ plane. The simulations were run for a bounded system with boundaries behaving as standard thermal walls whose implementation will be discussed in a later chapter. In Fig 2.7 we plot a reduced shear viscosity coefficient (η^*) and normal stress difference components (θ_x, θ_y) w.r.t to the square of a reduced shear rate (a). For the results presented, simulations were run with a value of $\frac{T_+}{T_-} = 10$ and the shear rate was modified by varying U. As seen in Fig 2.7 the agreement between the present DSMC and simulations from (Reyes Vega Francisco & Vincente 2013) is good, especially considering that we have reported data on transport coefficients which have to be bulk averaged throughout the domain. The reason for deviation of DSMC data from Grad's results at lower shear rates is unclear at the moment. While, this mismatch has been tied to the curvature of temperature profiles by Reyes Vega Francisco & Vincente (2013), a thorough study investigating the above problem may give better answers. This Fourier-Couette system presents a good test case, as the system settles in inhomogeneous steady state with hydrodynamic variables namely density, velocity and temperature showing dependence on the wall normal direction. It is evident that our code is able to handle such inhomogeneous systems and this paves the way forward to study the dynamics of a similar non-uniform steady state - Granular Poiseuille Flow, using the current DSMC code.

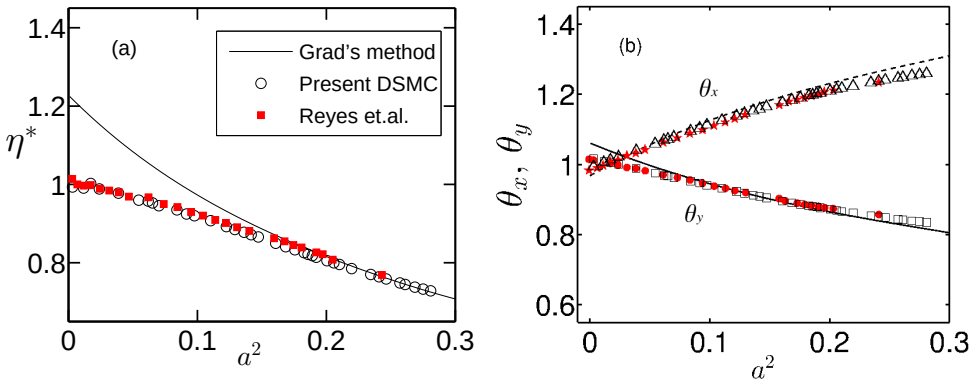

Figure 2.7: (a): η vs a^2, (b): θ_x, θ_y vs a^2. In (b) Solid lines : Grad's solution from (Reyes Vega Francisco & Vincente 2013), Filled Symbols : DSMC results from (Reyes Vega Francisco & Vincente 2013), Open Symbols : Present DSMC. Simulations are run for N = 30000, n = 0.0021, $Kn = 0.0667$

Chapter 3

Hydrodynamics and Rheology of Dilute Granular Poiseuille Flow

3.1 Introduction

Poiseuille flow (Poiseuille 1847; Hagan 1839), namely the flow of a fluid confined between bounding walls and driven by a force or pressure difference is a prototypical fluid flow that has received considerable attention over the years. Owing to its simple configuration, it is one of the few cases which admits an analytical solution to the Navier-Stokes equations, at least on satisfying a few physical assumptions. In its simplest form, Poiseuille flow has been studied for a little less than two decades with earlier instances of derivations of Poiseuille law made by eminent scientists of the time (Mathieu 1863; Stokes 1845). The Poiseuille flow of a molecular gas has also been extensively studied using an array of numerical, theoretical and experimental techniques (Ohwada *et al.* 1989; Cercignani & Daneri 1963; Graur *et al.* 2009; Wang & Li 2004). Clubbed along with Fourier Law the combined Navier-Stokes-Fourier equations have proven to be unable to predict a host of features unique to a rarefied molecular gas flow (Cercignani 2000*a*; Karniadakis & Beşkök 2001; Kogan 1969). The unique features like the presence of normal stress differences, transverse heat flux and temeprature bimodality are typically signatures of rarefaction (Uribe & Garcia 1999). A natural extension of this line of research is the study of rarefied granular gas flows in a channel configuration. Previous work on granular Poiseuille flow has focused on the role of wall roughness, slip velocity and rheology in a moderately dense flow (Chikkadi & Alam 2007, 2009; Alam & Chikkadi 2010). Most granular flows of interest, however could be in the rarefied regime (Goldhirsch 2003) and thus a study of a dilute granular gas flow could be of practical relevance. Alam *et al.* (2015) studied two rarefaction signatures, Knudsen minimum and temperature bimodality in a dilute granular gas. The objective of the present study is to study the role of dissipation and rarefaction on the hydrodynamics and rheology of a dilute granular Poiseuille flow. By systematically studying the effects in tandem we can ascertain if the well known rarefaction effects in molecular gases have counterparts in granular gases and isolate the role played by dissipation in those phenomena. Such a study is likely to be useful in the formulation of theories for granular flow and can also act as a check for existing hydrodynamic models. In this study we numerically solve the inelastic Boltzmann equation using the well known DSMC algorithm (Bird 1994) to study the Poiseuille flow of a dilute granular gas, that has been approximated by a system of smooth hard spheres of diameter d and mass m. The grains flow between two parallel walls that are kept at a pre-described temperature and as such can be imagined as *thermal* walls (Tehver *et al.* 1998) that allow us to study the bulk dynamics of the system. The cooling due to inelastic collisions is eventually balanced by the shear energy due to a constant body force, forcing the system into a steady state that is analyzed

for calculating hydrodynamic and rheological quantities. Several interesting features regarding heat flux and normal stress differences have been uncovered and the role of body force on the bulk dynamics is briefly investigated.

3.2 Simulation Details

In order to simulate a body force driven Poiseuille flow we apply a constant acceleration on every constituent particle. The acceleration acts as a driving force that adds energy into the system. For the case of a molecular gas a steady state is facilitated by use of the *thermal* wall boundary conditions which allows us to run DSMC simulations without using a thermostat. Generally, particle simulations for driven gases employ schemes for keeping the total energy of the system from blowing up (Hünenberger 2005). For studying steady state properties of granular gases in absence of boundary forcing, stochastic or Gaussian thermostats are routinely used to prevent eventual rest state and balance the inelastic cooling (Garzó 2004). Our curent system however includes a driving acceleration which is energy providing, forcing a nonequilibrium steady state with energy balance. For all simulations we distribute hard spheres of specified diameter and mass, initialized with some random thermal velocity. Our simulation domain is a cuboid as shown in Fig 3.1 The domain is divided into *layers* with divisions only in the direction perpendicular to the horizontal walls (y direction). Layer splitting instead of dividing domain into cubic boxes is done because it is known to us *a priori* that the flow has gradients only in the y direction. For all simulations we fix the particle mass (m), diameter (d), Boltzmann constant (k_B), wall temperature (T_w) and non dimensional acceleration ($\hat{a}$) as :

$$m = 1 \tag{3.1}$$

$$d = 1 \tag{3.2}$$

$$k_B = 1 \tag{3.3}$$

$$\hat{a} = \frac{aW}{\frac{2k_B T_w}{m}} \tag{3.4}$$

3.2.1 Boundary Conditions

Boundary conditions implementation in DSMC is similar to MD as we treat the simulation particles as physical particles for application of any boundary condition. Since the averaging cells are basically layers with non unit dimension only in the direction perpendicular to the wall, the only relevant coordinate of the particle required for sorting is the y coordinate (See schematic shown in Fig 3.1 for coordinate system choice). Thus the x and z coordinates of the particles are not updated or stored. However, we could assume that our domain is periodic in both those directions and update x and z in the following way :

$$x^{t+\Delta t} = fmod(x^t + x_{inc} + L_x, L_x) \tag{3.5}$$

$$z^{t+\Delta t} = fmod(z^t + z_{inc} + L_z, L_z) \tag{3.6}$$

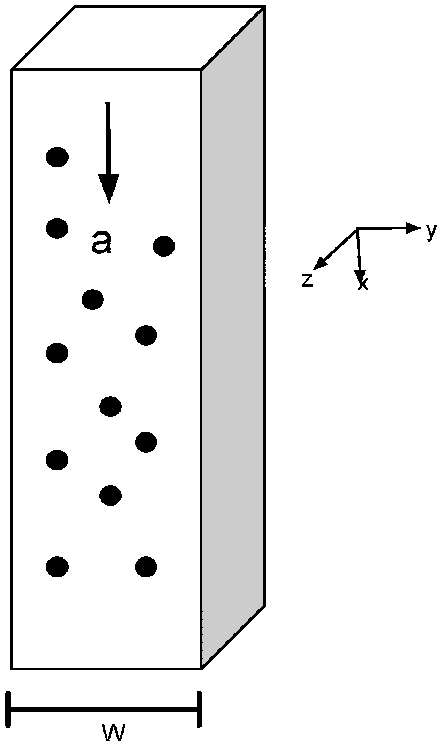

Figure 3.1: Simple schematic showing the Poiseuille flow of hard spheres in a cubic box domain. **a** represents the acceleration. Coordinate system used is shown on the side

x_{inc} and y_{inc} are the increment in the respective coordinates due to free streaming in case of y and ballistic motion for x. In absence of collision with the wall the above are defined as :

$$x_{inc} = v_x^t \Delta t + \frac{1}{2} a \Delta t^2 \tag{3.7}$$

$$y_{inc} = v_y^t \Delta t \tag{3.8}$$

If the particle collides with the wall that is normal to the y direction these expressions change as the particles acquires a velocity different from what it had before collision with the wall. These post collision velocities are assigned in accordance with the type of boundary present at the wall physically. In these simulations we model the boundaries as thermal walls (Cercignani 2000*a*). Thermal wall boundary conditions have been employed for various computational studies for rarefied molecular and granular gases (Tehver *et al.* 1998; Hrenya *et al.* 2008; Mansour *et al.* 1997). In this scheme x and z components of velocity forget their initial velocity and gain a velocity taken from a Gaussian distribution with variance corresponding to the temperature of the wall (T_w) and mean corresponding to the wall velocity which in this case is 0 (v_G is velocity sampled from a Gaussian distribution with zero mean and unit variance). The x component of the velocity gets accelerated for the time it spends between the end of the time step and collision with the wall(t_{post}). The y component of the velocity is sampled from a biased Gaussian distribution (v_{BG}), also called a Rayleigh distribution (Pöschel & Schwager 2005) and reflected. The values of x_{inc} and y_{inc} for a particle collision are then defined as in (3.12) and (3.13) with

t_{pre} and t_{post} defining time pre and post collision respectively:

$$v_x^{t+\Delta t} = \sqrt{\frac{k_B T_w}{m}} v_G + a t_{post} \tag{3.9}$$

$$v_y^{t+\Delta t} = \sqrt{\frac{2k_B T_w}{m}} v_{BG} \tag{3.10}$$

$$v_z^{t+\Delta t} = \sqrt{\frac{k_B T_w}{m}} v_G \tag{3.11}$$

$$x_{inc} = v_x^t(t_{pre}) + \frac{1}{2}a(t_{pre})^2 + \sqrt{\frac{k_B T_w}{m}} v_G t_{post} + \frac{1}{2}a {t_{post}}^2 \tag{3.12}$$

$$y_{inc} = v_y^t(t_{pre}) + v_y^{t+\Delta t} t_{post} \tag{3.13}$$

3.2.2 Averaging Procedure

After a certain time into the simulations when a steady state has been reached we begin spatial averaging of hydrodynamic quantities which are sampled after certain time steps and then time averaged as well. The entire domain is split into cells as shown in Fig 3.2. All the particles in a particular bin are used for spatial averaging. These cells, also referred to as sampling cells may or may not coincide with the cells used for computing collisions. In this chapter however the sampling and collision cells coincide for almost all cases. For calculation of heat flux, temperature and pressure field the peculiar velocity is required which in turn requires a bin-wise average of velocity. We calculate the average velocity in each bin for a certain number of time steps post steady state and use that average in the averaging for the other fields. Post the attainment of steady state snapshots are used as samples for obtaining averaged quantities. For high values of Kn ($Kn \geq 1$) particles undergo very few collisions per time-step. Most molecules travel from wall to wall without suffering a collision with another particle. This is why snapshot samples must be taken after a number of time-steps over which sufficient number of collisions have occurred. The average density of a quantity $\psi(\mathbf{v})$ is :

$$\langle \psi(\mathbf{v}) \rangle_y = \frac{1}{N_t} \sum_t^{N_t} \frac{1}{V_c} \sum_{i \in c} \psi(\mathbf{v}_i(t)) \tag{3.14}$$

Here $\mathbf{v}_i$ is velocity of particle i and N_t is the number of time steps over which the quantity is sampled. The inner sum is over all particles in cell (layer) c which is centered at position y. The other variables are:

$$\rho(y) = N_e \langle m \rangle_y \tag{3.15}$$

$$\vec{u}(y) = \langle m\vec{v} \rangle_y / \rho \tag{3.16}$$

$$T(y) = \frac{m}{3k_b \rho(y)} \langle (v_x - {u_x}^2) + (v_y - {u_y}^2) + (v_z - {u_z}^2) \rangle \tag{3.17}$$

$$P_{\alpha\beta}(y) = N_e \langle m(v_\alpha - u_\alpha)(v_\beta - u_\beta) \rangle_y \tag{3.18}$$

$$q_\alpha(y) = \frac{1}{2} N_e \langle m(v_\alpha - u_\alpha)|v - u|^2 \rangle_y \tag{3.19}$$

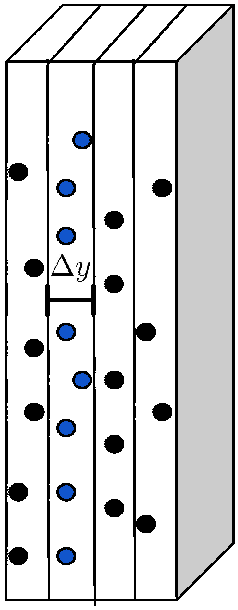

Figure 3.2: Simple schematic showing cells used to calculate average quantities. The spheres in blue denote particles which will be considered for averaging in the particular bin shown with width Δy

For DSMC simulations we need to set a bound on the parameter v_{12}^{max} for finding out the number of collision pairs to be chosen in a time-step per cell. We set this parameter initially to 3 times the most probable velocity and then dynamically update it. The cell width is set to be about one third of the initial equilibrium mean free path or less. The effect of bin size has an effect on the boundary value of fields since a lesser bin width effectively measures a point closer to the wall than a bin with larger width. In the bulk however there isn't much deviation.

3.2.3 Control parameters

Forcing parameter : $\hat{a}$

We present simulations for two values of $\hat{a}$, 0.5 and 10 where W is the width of the system. The parameter $\hat{a}$ measures the strength of the body force acting on a particle traveling a length L that is to say that for O(1) Kn, when $L \sim \lambda$, it measures the strength of the body force term in between two successive collisions. As such $\hat{a}$ can be thought of as a forcing parameter that is responsible for driving an initially homogeneous system at equilibrium, out of equilibrium. A constant $\hat{a}$ ensures that the system is subject to the same shear and allows us to make a proper dynamical comparison. This can be seen in the shear stress profiles presented in Fig **??**(c), where after scaling the profiles collapse. The velocity profiles are normalized by a characteristic velocity u_c and the density profiles are normalized by the average number density in the channel ρ_{avg}. Pressure tensor components are normalized by P_c and heat flux profiles are normalized by

q_c. The normalization factors for velocity, density, pressure and heat flux are given by

$$\begin{aligned} T_c &= T(0) \\ u_c &= \sqrt{2k_B T_w/m} \\ \rho_c &= \rho_{avg} \\ P_c &= \frac{1}{2}\rho_{avg} {u_c}^2 \\ q_c &= \frac{1}{2}\rho_{avg} {u_c}^3 \end{aligned}$$

Knudsen number

The Knudsen number (Kn) measures the degree of rarefaction in the system and is the ratio of the mean free path and a characteristic length scale. In the simulations in this chapter we define a sort of *global* Knudsen number as used in (Hrenya *et al.* 2008). Instead of measuring Kn as a result of simulations as done in recent simulations (Alam *et al.* 2015) we set Kn as an input parameter for the simulation and define it apriori as :

$$Kn = \frac{\lambda}{W} \tag{3.20}$$

$$\lambda = (\sqrt{2}\pi n d^2)^{-1} \tag{3.21}$$

It is important to note that defining Kn as a global parameter used as an input for the simulation prevents it from including non-equilibrium effects like clustering. Effectively, such a definition allows to set, *apriori* a Kn for different $\hat{a}$ and e_n. For changing the Kn two routes can be taken, (i) We can vary the channel width keeping the number density and hence λ constant. We will however have to adjust the value of a in each simulation to keep the parameter $\hat{a}$ constant, (ii) We can change the number density keeping the channel width constant. This is convenient as a single value of a will ensure $\hat{a}$ is constant across all Kn. We have used the second method for varying Kn in our simulations. We did however run a test case using the first method as well and results obtained are identical for a single value of $\hat{a}$.

3.2.4 Code Validation

We have tested the code by comparing our results for a molecular gas (Mansour *et al.* 1997). For the case of $\hat{a} = 0.3$ and $Kn = 0.1$ with number density $n = 0.00121$ the temperature and velocity profiles are shown in Fig 3.3(a) and Fig 3.3(b) respectively. There is good quantitative match for both fields, the slight mismatch however can be accorded to the difference in number of sampling cells or collision cells, time step set for the simulation or number of snapshots used to obtain time averaged quantities. In Fig 3.4 we compare the flowrate results of our DSMC code with those taken from (Hadjiconstantinou 2003).The non dimensional flowrate for this particular validation is calculated as :

$$Q = \frac{\int_{-L_y/2}^{+L_y/2} \rho(y) u_y(y) dy}{\rho_{avg}\sqrt{\frac{2k_B T_w}{m}}\hat{a}L_y} \tag{3.22}$$

The quantitative agreement is good and a flow rate minimum for the case of a molecular gas is found at $Kn \sim 1$.

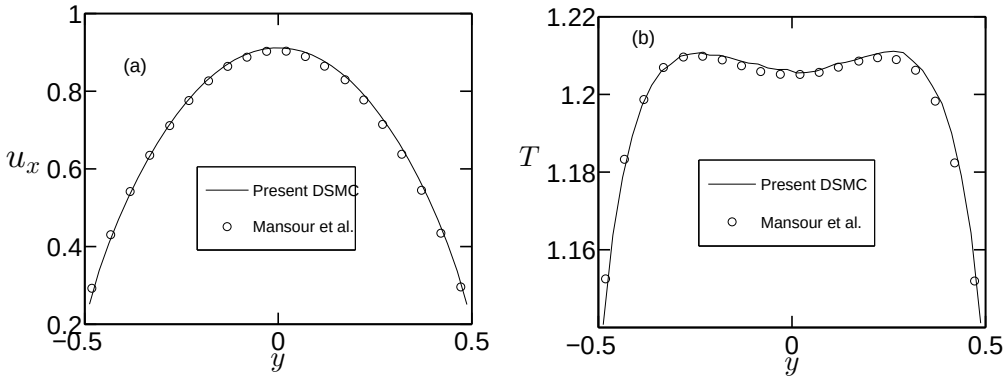

Figure 3.3: (a): Streamwise velocity and (b): Temperature plots showing quantitative agreement with (Mansour *et al.* 1997)

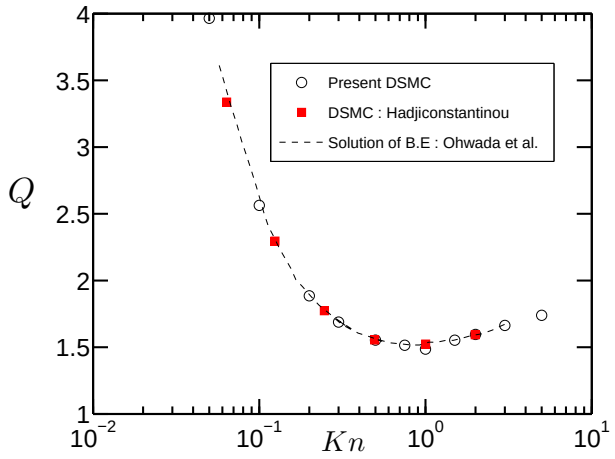

Figure 3.4: Non dimensional flowrate vs Knudsen number: results from present DSMC code ($\hat{a}$=0.05) and (Hadjiconstantinou 2003)

3.3 Molecular Gas : elastic hard spheres

We first show the results for the flow of elastic hard spheres for a fixed value of $\hat{a}$ for different Kn. This also acts like another check for the code and set parameters as the qualitative and quantitative results are mostly known for the flow of elastic hard spheres. These simulations are run for $\hat{a} = 0.5$.On observing the velocity profiles (u_x) in Fig 3.5(a) we see that the slip velocity increases with increasing Kn which is expected as deviations from the no slip boundary condition, that is an appearance of a wall slip is a O(Kn) effect. Bulk velocity decreases with increasing Kn and profiles become flatter,but somewhere around $Kn \sim 1$ the bulk velocity starts to increase again. This effect influences the temperature (T) profiles as well and one can observe the increase in bulk temperature after $Kn \sim 1$. The temperature profiles presented in Fig 3.5(b) exhibit bimodality and there is a temperature 'slip' at the walls. Density (ρ) profiles

in Fig 3.5(c) show near uniform density in the bulk of the channel with peaks at the walls corresponding to particles gathering near a low temperature region. The direction of the flux, q_x is parallel to the flow near the walls and opposite to the flow in the bulk but the profiles makes a transition at an arbitrary Kn post which the entire flux is unidirectional and parallel to the flow. The profiles for P_{xy} show that the shear stress (p_{xy}) is nearly independent of Kn as seen in Fig3.7(b). These results will be invoked later in the chapter and discussed in detail to compare with similar profiles for granular Poiseuille flow.

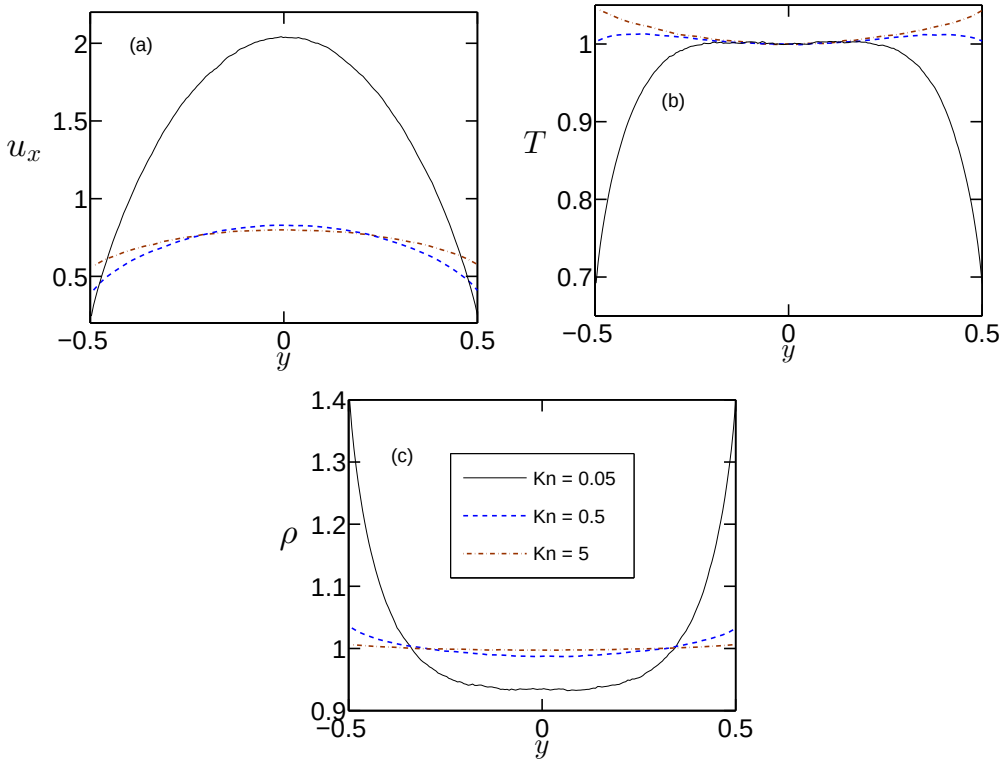

Figure 3.5: (a): u_x vs y, (b): T vs y and (c): ρ vs y plots for the Poiseuille flow of a molecular gas at $\hat{a} = 0.5$

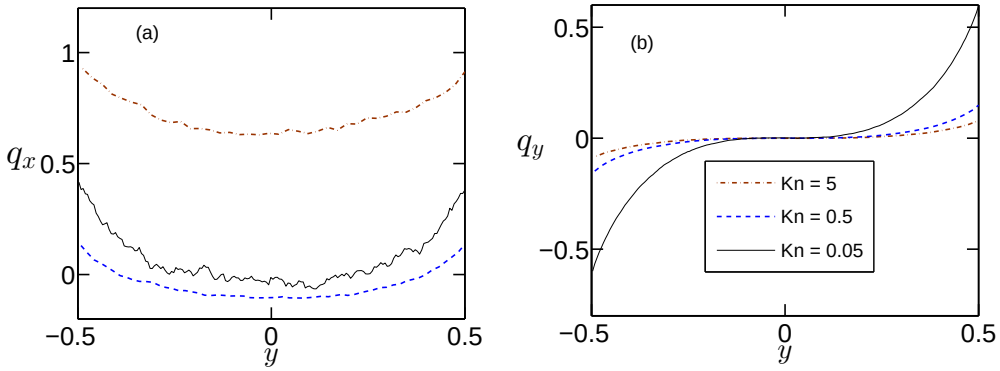

Figure 3.6: (a): q_x vs y, (b): q_y vs y for a molecular gas at $\hat{a} = 0.5$

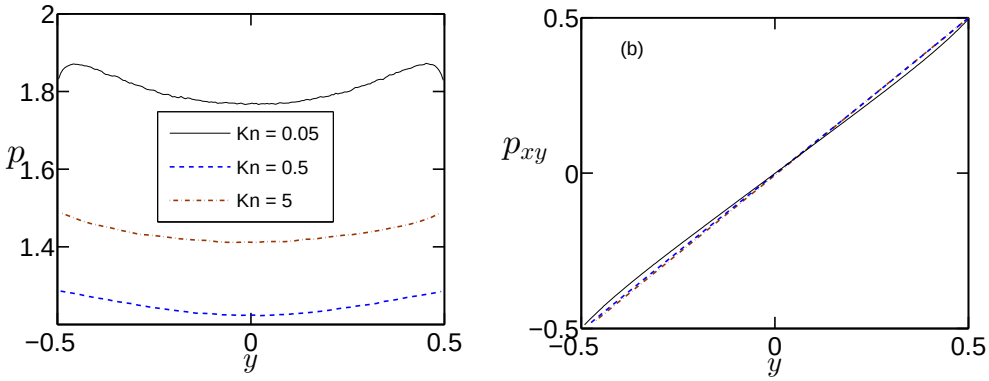

Figure 3.7: (a): p vs y, (b): pxy vs y for a molecular gas at $\hat{a} = 0.5$

3.4 Hydrodynamics of GPF

3.4.1 Density Profiles

In this section we present results for $Kn = 0.05$,1 and $e_n = 0.7$,0.9,0.99,1. The simulations for these sets are run for a value of $\hat{a} = 0.5$. Density profiles for a granular gas and molecular gas (See Fig 3.5(c)) are markedly different, owing to energy loss, E due to inelastic collisions($E \propto (1 - e_n^2)$). A granular gas exhibits a density inhomogeneity that is characterized by a density peak in the center of the channel, in stark contrast to elastic and nearly elastic particles for which density profiles are nearly homogeneous, except at the walls. Collisional cooling leads to the formation of a low shear rate zone near the channel center where particles tend to gather. For higher values of Kn, owing to rarefaction induced de-clustering, the density becomes uniform across the channel, even for a granular gas which shows only a slight variation in density across the width, as seen in Fig 3.8(b). This is indicative of the fact that the effects of inelasticity are suppressed in the rarefied regime where wall-particle collisions are dominant in number. We define two quantities:

$$\rho_o = \rho(0) \tag{3.23}$$

$$\rho_{fw} = \frac{1}{2}(\rho(-0.5) + \rho(0.5)) \tag{3.24}$$

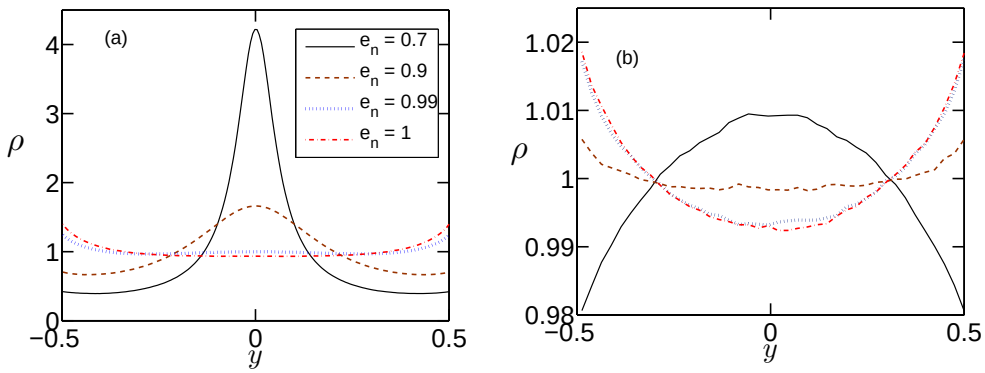

Figure 3.8: ρ vs y at $\hat{a} = 0.5$, (a): $Kn = 0.05$, (b): $Kn = 1$

With increase in Kn, due to decrease in inter-particle collisions, ρ_o decreases for a granular gas. This decrease is accompanied by a corresponding increase in ρ_{fw}, both of which tend to a value of one, indicating the onset of a rarefied regime with uniform fields. On the other hand elastic and nearly elastic particles show an opposite trend with $\rho(\rho_{fw})$ increasing(decreasing) to a value of one (Fig 3.9(c,d)). The evolution of density field for a molecular gas with increasing Kn is also clearly seen in Fig 3.5(c). Fig 3.9(a) reveals that the value of the density peak at the center line strongly increases with increasing dissipation and correspondingly the value of ρ_{fw} decreases as the value of e_n reduces (Fig 3.9(b)). This phenomena can be used to explain why the value of velocity slip increases with increasing dissipation.

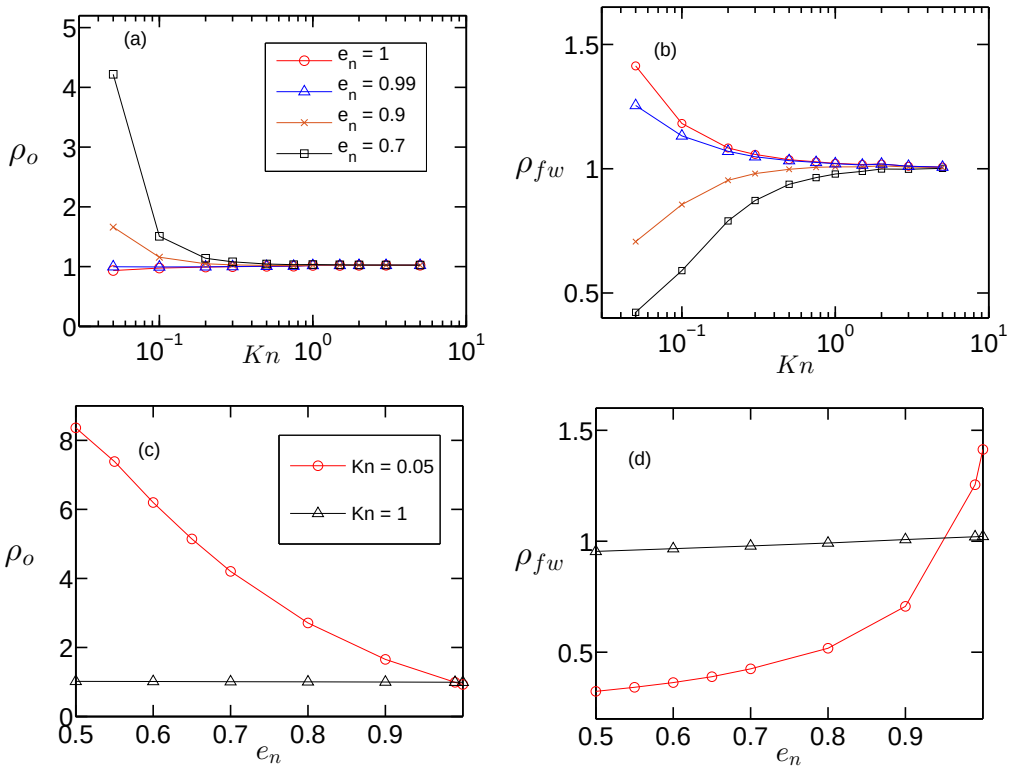

Figure 3.9: (a): ρ_o vs Kn, (b): ρ_{fw} vs Kn, (c): ρ_o vs e_n, (d): $\rho_f w$ vs e_n

The variation of density in the wall normal direction also directly affects the Kn field in the channel, with local value of Kn showing a variation in y and the amount of deviation from its equilibrium preset value depending on the inhomogeneity in the density field. As expected for Kn=1, the local Kn variation is very small for both elastic and granular particles as seen in Fig 3.10(b). The local Kn referred to as Kn_y is calculated as :

$$Kn_y = \frac{(\sqrt{2}\pi n(y) d^2)^{-1}}{W} \tag{3.25}$$

In the above equation $n(y)$ is the local binwise number density corresponding to the number of *real* particles in a bin.

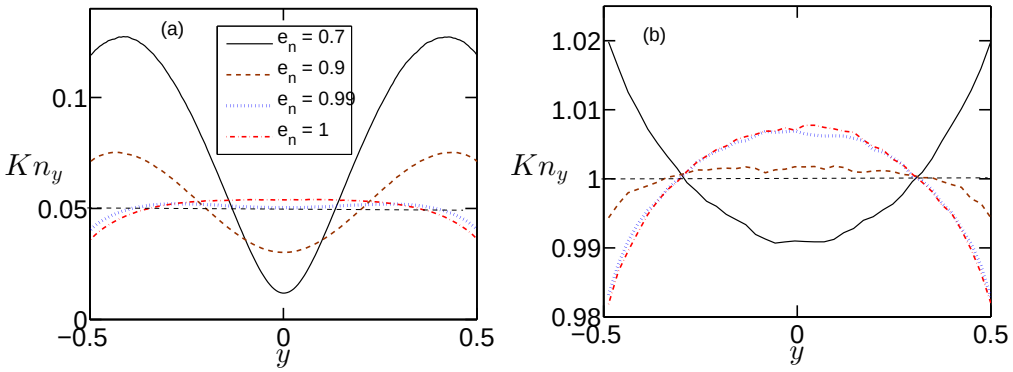

Figure 3.10: Kn_y profiles for different Kn, e_n and $\hat{a} = 0.5$, (a): $Kn = 0.05$, (b): $Kn = 1$. Dashed lines indicate the pre set value of global Kn

3.4.2 Velocity field

We observe that the streamwise velocity shown in Fig 3.11 retains the typical parabolic profile for weak inelasticity and higher Kn. For $Kn = 0.05$ and $e_n = 0.7$ the profile is no more parabolic. The centerline velocity (u_o) also is a function of both Kn and e_n as seen in Fig 3.11(c,d). The initial decrease of u_o with increasing Kn (Fig 3.11(c)) can be tied to the decrease in drift velocity due to lesser number of inter-particle collisions. This decrease is characteristic of elastic as well as inelastic particles, with inelastic particles maintaining a higher value of centerline velocity (Fig 3.11(d)) due to enhanced bulk velocities aided by a clustering effect.

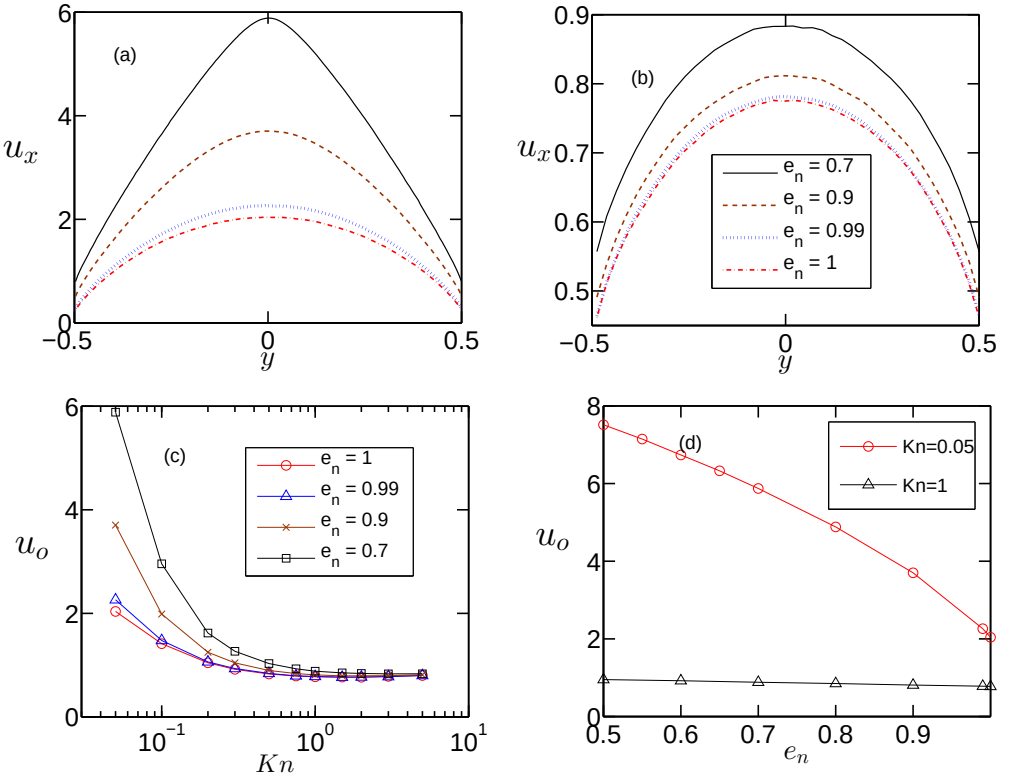

Figure 3.11: (a): u_x vs y at $Kn = 0.05$, (b): u_x vs y at $Kn = 1$, (c): u_o vs Kn, (d): u_o vs e_n

Slip Velocity

Slip velocity is also an interesting feature and is calculated as:

$$u_s = \frac{1}{2}(U(-0.5) + U(0.5)) \tag{3.26}$$

For the case of particles with $e_n = 1$, i.e a molecular gas driven by thermal walls, the slip velocity is an order Kn effect. In the limit of $Kn \to 0$ slip disappears and a finite slip occurs only at finite values of Kn and can thus be categorized as a rarefaction effect. This can be seen in Fig 3.11, where the line corresponding to e_n=1, shows a linear increase (on the log scale) with Kn and a zero extrapolated slip value at $Kn = 0$. For inelastic particles ($e_n < 0.99$) slip velocity shows a non monotonic trend with Kn, accompanied by an initial decrease and followed by an eventual increase with Kn. The slight drop in u_s for $e_n = 0.7$ for very low Kn could be a result of the velocity profile showing large deviation from a Gaussian or an imperfect fit. The initial decrease can be explained by looking at the density profiles in Fig 3.9(b). Due to clustering induced by dissipative collisions of particles, there is a relative decrease in density near the wall leading to a formation of a rarefied layer. With an increase in Kn, the central density peak decreases, leading to an increase in density near the wall and leading to a decline in slip velocity. Dissipation induced clustering is also responsible for the slip velocity increasing with decreasing e_n, in the low Kn limit, as seen in Fig 3.12(b). The slip variation in Fig 3.12(a) is similar to what is reported in the least dense case in (Wu *et al.* 2016), where the authors compare the slip variation to the anomalous slip variation reported in (Alam *et al.* 2015). It is critical to note that the boundary conditions used in (Alam *et al.* 2015) were *athermal* and 'anomalous' nature of velocity slip was accorded to its continual decrease even beyond an $O(1)$ Kn. A detailed analysis on the effect of boundaries on slip characteristics will be taken up as future work.

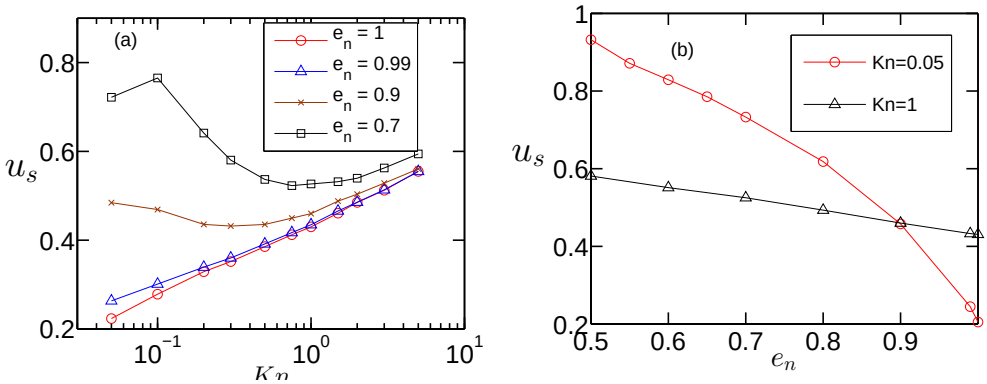

Figure 3.12: Variation of slip velocity with Kn, e_n for $\hat{a} = 0.5$. (a): u_s vs Kn, (b): u_s vs e_n

3.4.3 Granular Temperature

According to Campbell in (Campbell 1990), "This concept of a granular temperature is perhaps the single most important key to understanding the behavior of rapid granular flows..." A system with a driving force leads to particles having kinetic energy due to which shear work is generated. In the presence of inelastic collisions the balance between shear work and inelastic dissipation

results in a granular temperature. Invoking an equation of state in the low Kn we can infer that regions of high density will usually be accompanied by a region of low temperature, with particles less energetic and mobile. Regions of low density allow regions of high temperature and highly mobile and energetic particles. The clustering of granular particles near the channel center hence leads to the formation of a low temperature region in the center as is clearly observed in Fig 3.13(a).

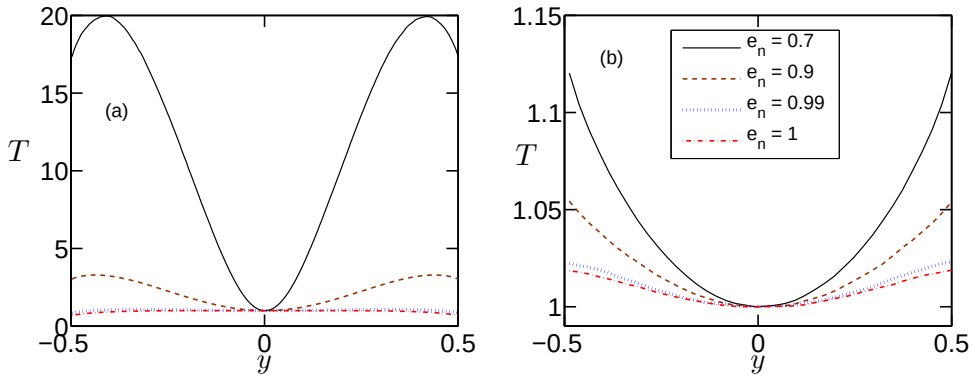

Figure 3.13: Temperature profiles for $\hat{a}$=0.5, (a): T vs y at $Kn = 0.05$, (b): T vs y at $Kn = 1$

Temperature bimodality

Using DSMC simulations, it was reported in (Mansour *et al.* 1997) that molecular gas dynamics can show considerable deviation from the dynamics predicted by the Navier-Stokes equation. One of the consequences of this deviation was a bimodality in temperature that occurs as rarefaction effect and was later shown to be a $O(Kn^2)$ effect. The phenomenon for temperature bimodality for a granular gas was investigated in detail in (Alam *et al.* 2015), where the authors concluded that there exist two regimes of bimodality in a granular gas - dissipation induced and rarefaction induced. Another important finding from the study was that inelasticity, below a certain e_n ensures that the temperature profiles always remains bimodal. Inelasticity increases the bimodality as is seen in Fig 3.14(b). To quantify bimodality we define an 'excess temperature', ΔT

$$\Delta T = \frac{T_{max} - T(0)}{T(0)} \tag{3.27}$$

ΔT measures the degree of temperature bimodality and a higher value of ΔT indicates a greater amount of bimodality in the temperature profile. From Fig 3.14(a) it is clear that a molecular gas owes its origin for temperature bimodality to rarefaction. We see that on decreasing Kn the value of ΔT reduces and the bimodality would disappear in the limit of $Kn \to 0$. Adding even a small amount of inelasticity however changes the situation and inelasticity amplifies the bimodality in temperature at low Kn. ΔT for e_n=0.99 is an order of magnitude higher than that of a molecular gas at Kn=0.05. Moreover ΔT initially decreases and then begins to increase with Kn. This non monotonicity indicates the presence of two dominant regimes in causing a bimodality in temperature profile. Dissipation is active at lower Kn and rarefaction kicks in as we gradually move to higher values of Kn. It isn't clear why this non monotonic behavior is not seen for the curves representing e_n=0.7,0.9. The plot for e_n=0.99 however motivates a a phase plot in the $Kn - e_n$ space that shows regions in which dissipation and rarefaction are

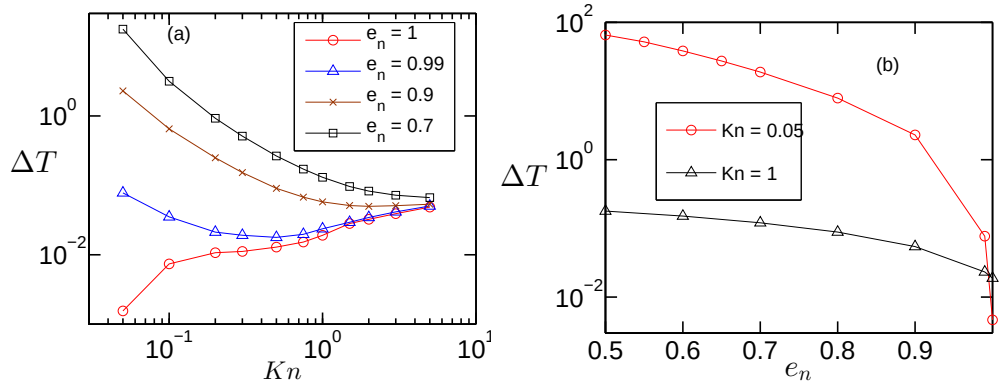

Figure 3.14: (a): ΔT vs Kn, (b): ΔT vs e_n

independently dominant in causing temperature bimodality.

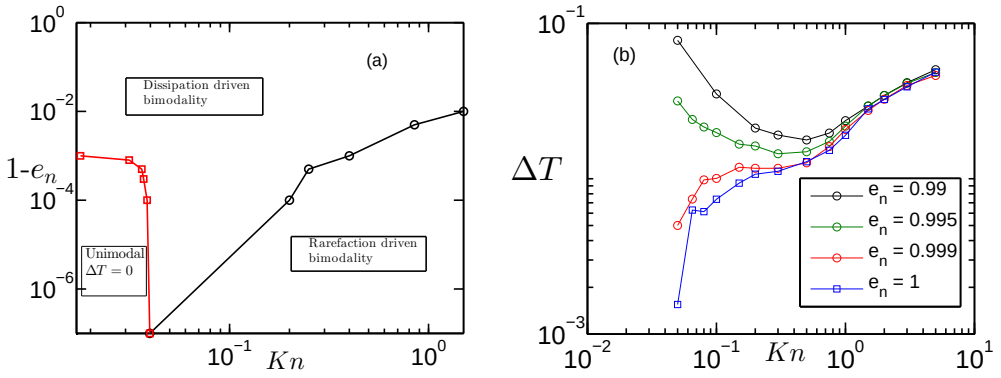

Figure 3.15: (a): Temperature bimodality phase diagram in the $(Kn, 1-e_n)$ plane for $\hat{a} = 0.5$, (b): ΔT vs Kn for different values of e_n used to calculate phase boundaries

The points for the unimodal region boundary were obtained by quadratically fitting 3-4 points for $0.05 < Kn < 0.2$ for $e_n \geq 0.999$ and extrapolate to obtain the value of Kn at which $\Delta T = 0$. It is observed that ΔT begins to increase with decreasing Kn beyond $Kn = 0.05$ for $e_n < 0.999$. This means that temperature profiles will be always be bimodal for $e_n < 0.999$. The points for the phase boundary separating the dissipation and rarefaction dominated regions are obtained by plotting ΔT *vs* Kn and seeing around what Kn the line corresponding to $e_n \neq 1$ begin to follow the line for $e_n = 1$. The value for e_n are chosen keeping in mind that a unique value for Kn is obtained as it is seen that the simulation accuracy does not allow for suitable differentiation for values of e_n very close together, at least for this region of the phase boundary.

Temperature Slip

Similar to velocity slip temperature profiles also exhibit a slip which means that the fluid temperature at the wall is different from the set temperature T_w. The temperature slip, T_{fw} is defined as :

$$T_{fw} = \frac{1}{2}(T(-0.5) + T(0.5)) - T_w \tag{3.28}$$

T_{fw} first decreases and then increases for $e_n = 0.7$,0.9 and at $Kn \sim 0.2$ there is a transition for a granular gas as beyond this Kn, T_{fw} for a granular gas is less than that for a molecular

gas. This could be because of the increase in ρ_{fw} with Kn for a granular gas, which leads to an enhanced collision frequency in the bin near the wall and hence a greater loss due to collisional cooling, leading to values of T_{fw} less than that of a molecular gas. For $Kn = 0.05$, T_{fw} increases with decreasing e_n, but interestingly follows the opposite trend at $Kn = 1$.

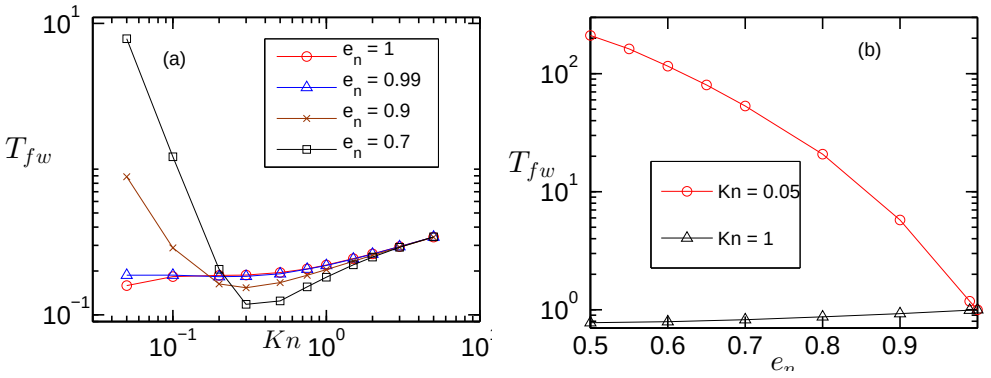

Figure 3.16: (a): T_{fw} vs Kn, (b): T_{fw} vs e_n. Profiles in (b) have been scaled by their respective values of $T_{fw}(e_n = 1)$

3.5 Rheology of GPF

While Navier-Stokes equations predict non varying pressure across a channel, DSMC results show a clear deviation from that prediction. The pressure exhibits a parabolic variation across the channel with the minimum pressure at the center. The effect of inelasticity is prominent on the pressure seen in Fig 3.17, there is departure from the near parabolic pressure profile for e_n = 0.7 which results from the corresponding density inhomogeneity for the case. Note that for $Kn = 1$ the curves are qualitatively the same and inelasticity simply displaces the curves. The shear stress profiles shown in Fig 3.17(c,d) are linear for all Kn and small degree of inelastcity. Because for a set of Kn the value of $\hat{a}$ is kept constant the shear stress profiles collapse for $e_n \sim 1$. For $Kn = 1$ all shear stress profiles collapse to a near linear profile confirming that inelasticity loses dominance for higher Kn. The deviation from linearity in the shear stress at $Kn = 0.05$ is the reason why corresponding velocity profiles show a deviation from the classical parabolic profile that is predicted by the Navier-Stokes equations.

3.5.1 Pressure, Shear Stress and Normal Stress Differences

The first normal stress difference coefficient ($\mathcal{N}_1$) and second normal stress difference ($\mathcal{N}_2$) are defined in the following way :

$$\mathcal{N}_1 = \frac{p_{xx} - p_{yy}}{p} \tag{3.29}$$

$$\mathcal{N}_2 = \frac{p_{yy} - p_{zz}}{p} \tag{3.30}$$

Normal Stress differences are indicators of a fluids' Non-Newtonian behavior as for a Newtonian fluid both $\mathcal{N}_1$, and $\mathcal{N}_2$ are zero. Unlike for a prototypical uniform shear flow, for the case of a dilute granular Poiseuille flow there is a variation in the normal stress differences across the

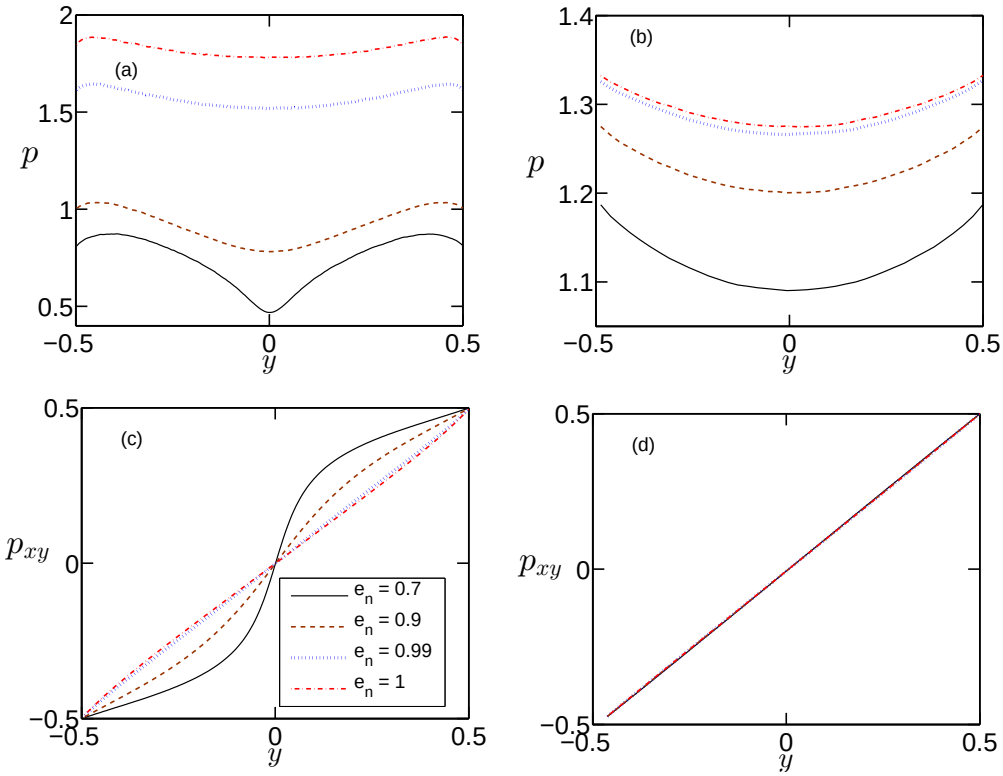

Figure 3.17: (a): p vs y at Kn=0.05, (b): p vs y at Kn=1, (c): p_{xy} vs y at Kn=0.05, (d): p_{xy} vs y at Kn=1

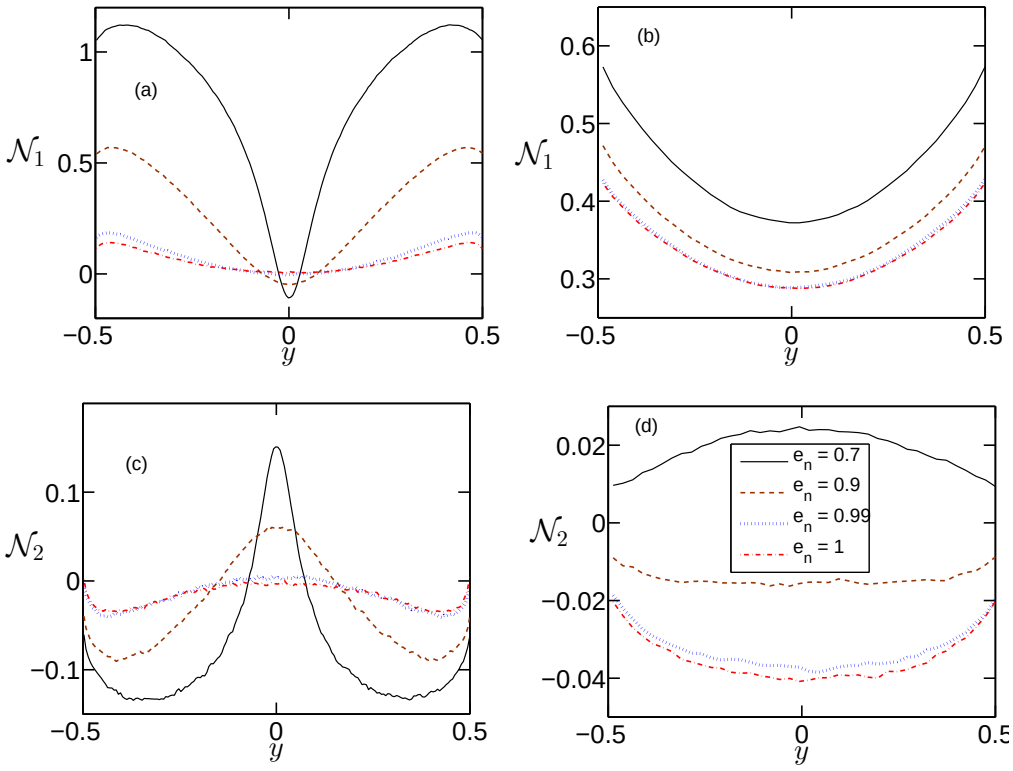

Figure 3.18: (a): $\mathcal{N}_1$ vs y at Kn=0.05, (b): $\mathcal{N}_1$ vs y at Kn=1, (c): $\mathcal{N}_2$ vs y at Kn=0.05, (d): $\mathcal{N}_2$ vs y at Kn=1

channel. It is seen in Fig 3.18 the variation in the normal stress differences across a channel are enhanced at low Kn and for higher dissipation. The variation of centerline normal stress differences ($\mathcal{N}_1(0)$,$\mathcal{N}_2(0)$) is plotted in Fig 3.19. It is observed that while $\mathcal{N}_1(0)$ increases with Kn, the behavior of $\mathcal{N}_2(0)$ is not as straightforward. For elastic and nearly elastic particles $\mathcal{N}_2(0)$ initially decreases and then increases. This behavior is shown by the curve for $e_n = 0.9$ as well. The value of Kn at which $\mathcal{N}_2(0)$ begins to increases shifts to larger values of Kn as dissipation increases. The curve for $e_n = 0.7$ may show a transition at a higher Kn than simulated currently.

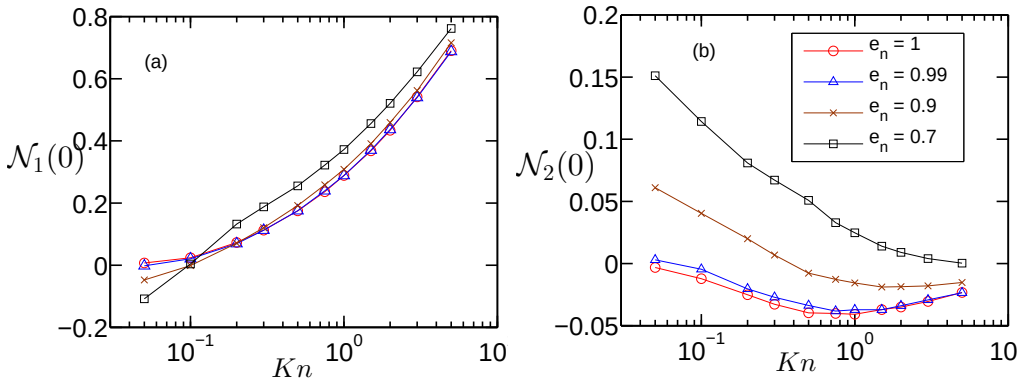

Figure 3.19: (a): $\mathcal{N}_1(0)$ vs Kn, (b): $\mathcal{N}_2(0)$ vs Kn

3.5.2 Heat flux

A heat flux normal to the wall, q_y, is seen owing to temperature gradient in the wall normal direction. q_y profiles for a granular gas (Fig 3.20) differ significantly from that of a molecular gas. While the normal heat flux for a molecular gas is tangential to the zero line close to the bulk, q_y for a granular gas is amplified and cuts the zero line at the center. This difference is likely due to the amplification of temperature gradients due to inelasticity, which causes a corresponding increase in heat flux. The qualitative difference between profiles for different e_n seems to be suppressed at high Kn. To quantify the deviation in q_y profiles we specify two

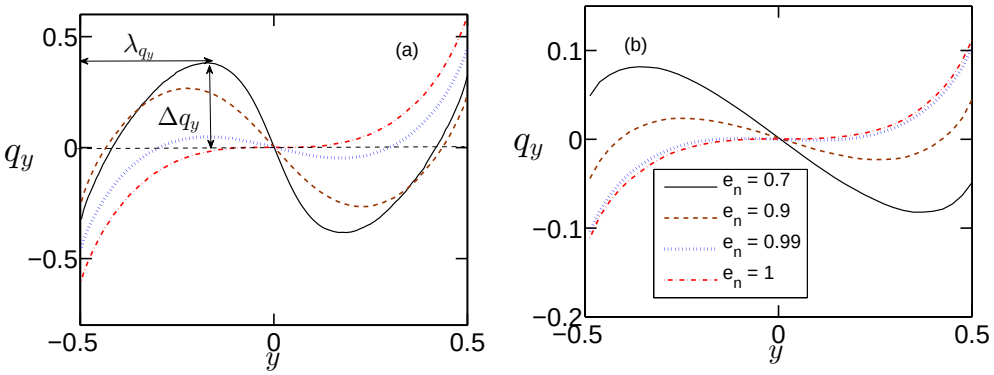

Figure 3.20: (a): q_y vs y at Kn=0.05, (b): q_y vs y at Kn=1

quantities, Δq_y and λ_{q_y}, which are marked in Fig 3.20(a). It must be noted that both the

quantities defined will take a zero value for e_n=1 at all Kn. Δq_y decreases with increasing Kn and e_n, indicating that while the appearance of a nonzero Δq_y is purely due to inelasticity, rarefaction suppresses it. The quantity, λ_{q_y} shows a nonmonotonic behavior with both Kn and e_n.

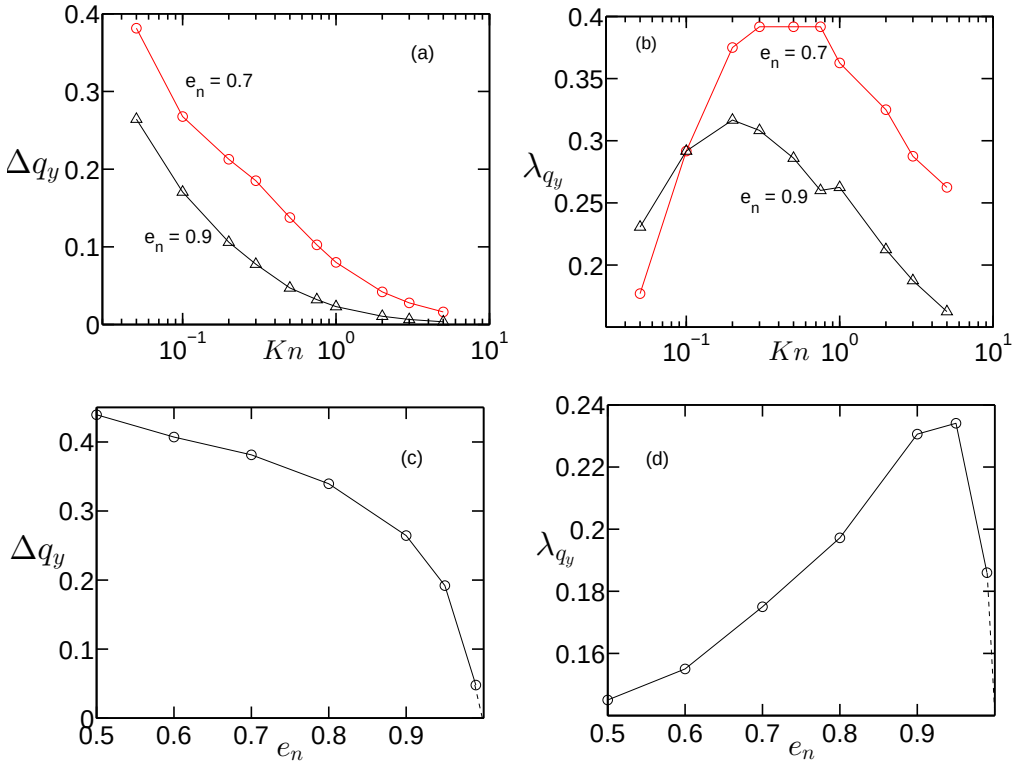

Figure 3.21: (a): Δq_y vs Kn, (b): λ_{q_y} vs Kn, (c): Δq_y vs e_n at $Kn = 0.05$, (d): λ_{q_y} vs e_n at $Kn = 0.05$

Another rich feature of the Poiseuille flow of a gas is the appearance of a heat flux parallel to the wall (q_x), in the direction of the flow. This heat flux is not driven by the x component of ∇T since that value is zero and all gradients have components only in the y direction perpendicular to the walls. The flux appears due to an anisotropy in the thermal conductivity tensor $\boldsymbol{\kappa}$. Essentially, shear provided by a constant acceleration is responsible for non zero off-diagonal elements and unequal diagonal elements in $\boldsymbol{\kappa}$ (Saha & Alam 2014). This shear induced anisotropy manifests as a non-zero parallel heat flux in the absence of a temperature gradient - a rarefaction effect in molecular gases that is a marked departure from Navier-Stokes dynamics and is predicted by Burnett (Uribe & Garcia 1999), BGK (Tij & Santos 1994) and Grad Expansion theories (Risso & Cordero 1998). Readers are referred (Saha & Alam 2014; Kogan 1969; Grad 1949) for detailed discussion on the origin of this heat flux. While for $e_n = 1$ the profiles for q_x are unimodal (Fig 3.22(a)), inelasticity causes bimodality in the parallel heat flux profiles as seen in Fig 3.22(a).

This phenomena has not been reported before and it will be interesting to look at it from a more quantitative standpoint for which we define the quantities Δq_x and λ_{q_x} in Fig3.22(a). The bimodality in parallel heat flux seems to be tied to the non homogeneity in density across the

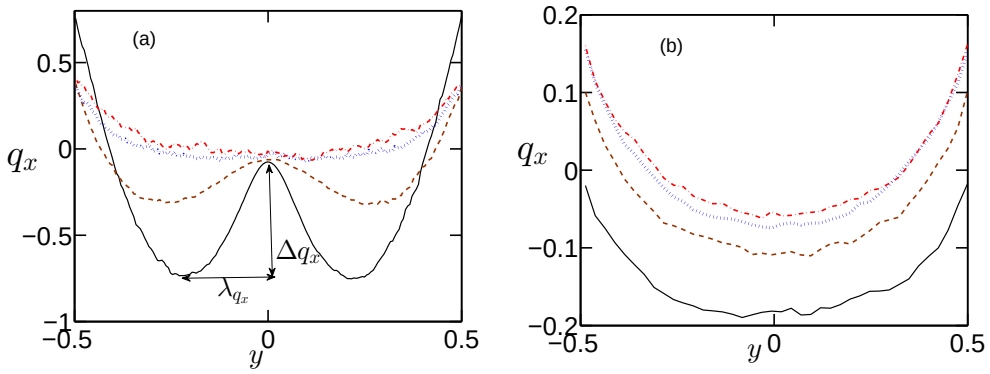

Figure 3.22: q_x profiles for different Kn, e_n and $\hat{a}$=0.5, (a): $Kn = 0.05$, (b): $Kn = 1$

channel with the occurrence of density peaks near the channel center marking a clear deviation from the case of molecular gas. Δq_x decreases with increasing Kn and increases when the inelasticity in the system increases as seen in Fig 3.23, a behavior mirrored by the behavior of ρ_o, the centerline density. The bimodality in heat flux disappears beyond a certain Kn, indicating the crucial and possibly singular role played by dissipation in its genesis. Like λ_{q_y} the behavior of λ_{q_x} is also non-monotonic with both Kn and e_n. While the reason for this non-monotonicity is unclear at this point, λ_{q_x} tending to a zero value for either e_n or Kn going to zero should be expected since q_x profiles are unimodal for elastic particles and the appearance of a parallel heat flux is a consequence of finite Kn (Kogan 1969).

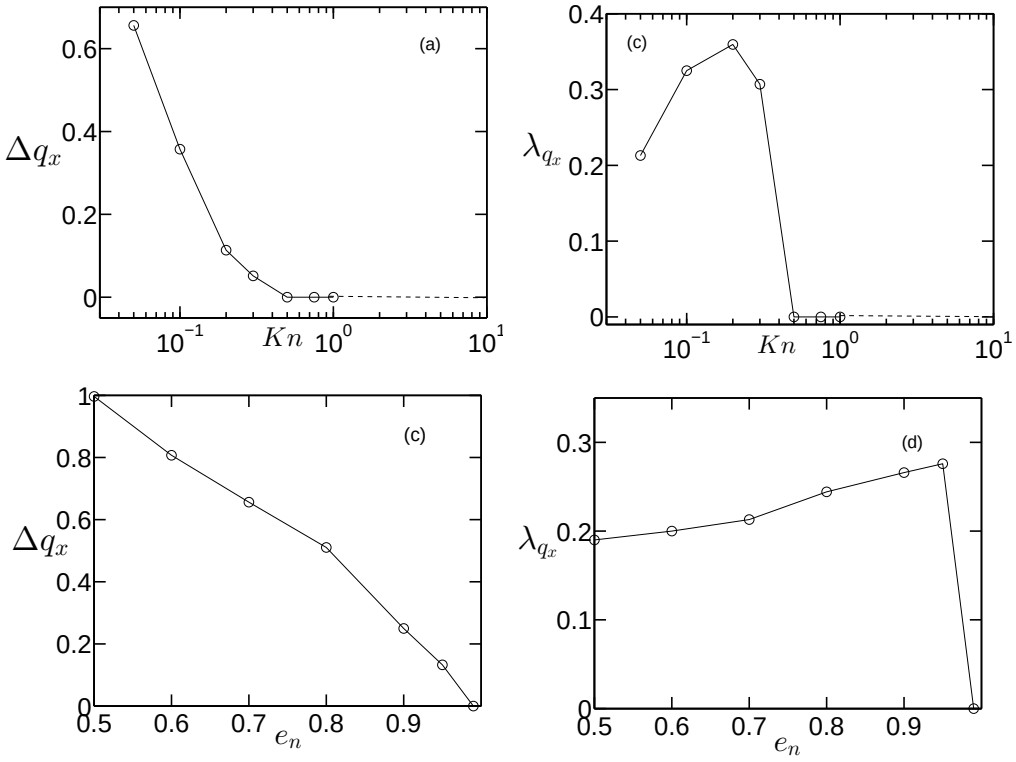

Figure 3.23: (a): Δq_x vs Kn for $e_n = 0.7$, (b): λ_{q_x} vs Kn for $e_n = 0.7$, (c): Δq_x vs e_n at $Kn = 0.05$, (d): λ_{q_x} vs e_n at $Kn = 0.05$

3.6 Flowrate and Knudsen Minimum

Flowrate across a channel defined in (3.22) has received considerable attention owing to a phenomena dubbed as a *Knudsen Minimum* effect or *Knudsen Paradox* (Knudsen 1909). The flowrate shows a non-monotonic variation with Kn, initially decreasing with Kn and then increasing relatively slowly post a minima that usually exists at $Kn \sim O(1)$ for a molecular gas. Here we find that the Poiseuille flow of a granular gas also shows the phenomena of a Knudsen minimum. As seen in Fig 3.24(a) the flowrate for all the e_n curves plotted typically decreases steeply with Kn and exhibits a minima close to Kn=1, after which there is a slow increase with Kn. The presence of a clear Knudsen minimum for a granular gas seems to be at odds with the results presented in (Alam *et al.* 2015), where the authors finding indicates an absence of a Knudsen minimum for a granular gas, except for very smooth walls and nearly inelastic particles. However, another recent work, (Wu *et al.* 2016) reported the presence of a Knudsen minimum for a granular gas driven by thermal walls, as used in the current simulations. Another interesting feature uncovered in our current study is the delay of a minima for a granular gas as observed in Fig 3.24(b). It is seen that as inelasticity increases the Kn number at which a minima occurs is pushed towards the right on the Kn line. The flowrate at lower Kn increases with decreasing e_n due to enhanced bulk velocities aided by density clustering in the channel center.

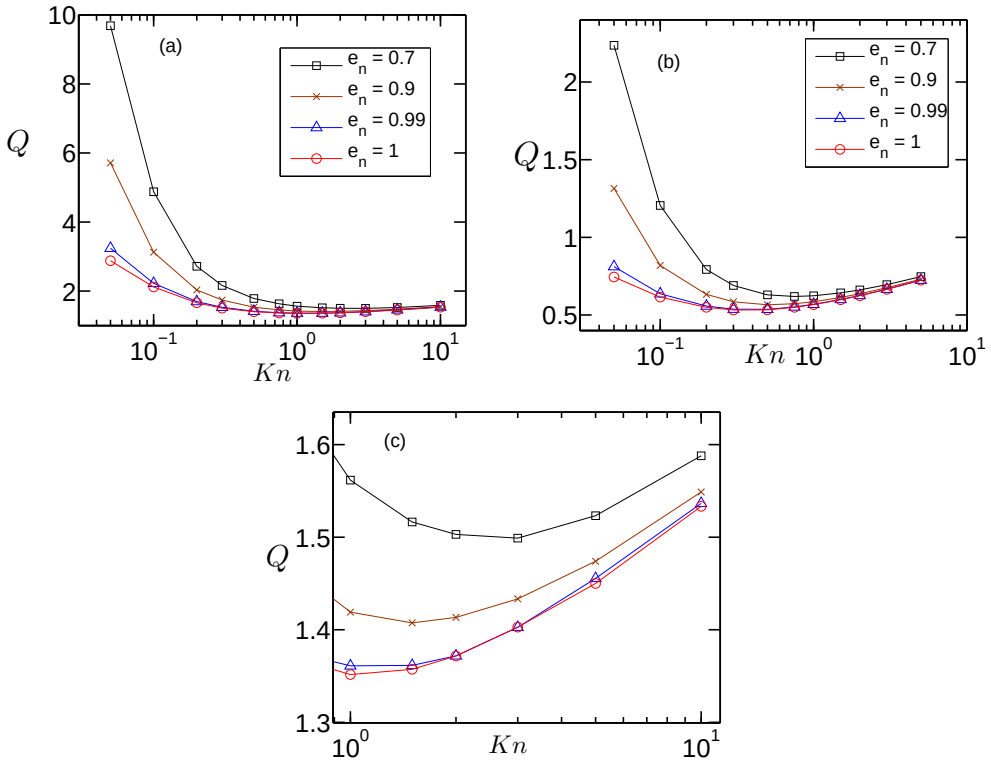

Figure 3.24: (a): Q vs Kn for different e_n for $\hat{a} = 0.5$, (b): Q vs Kn for different e_n for $\hat{a} = 10$, (c): zoomed portion of (a) to highlight the delaying of minimum with decreasing e_n

3.7 Effect of $\hat{a}$

While the value of $\hat{a}$ for a molecular gas driven by gravity is small, it can assume a large value for a granular gas owing to particles relatively larger mass and diameter and smaller thermal velocity when compared to a molecular gas. We briefly discuss the effect of varying (increasing) $\hat{a}$ on the behavior of the system under analysis and first direct attention towards mass flowrate. As seen in Fig 3.24(b) the qualitative characteristics of the behavior of Q w.r.t to e_n and Kn doesn't change on changing $\hat{a}$. There is a clear presence of a Knudsen Minima and it is observed that the point of minima occurs at a lower value of Kn ($Kn \sim 0.5$ for $e_n = 1$) than what is observed for the case of $\hat{a} = 0.5$. Fig 3.25 shows that the non-dimensional mass flowrate decreases with increasing value of $\hat{a}$.

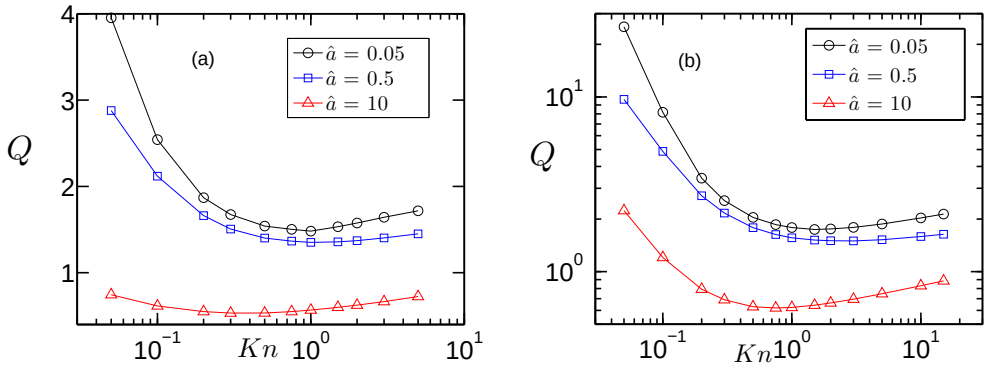

Figure 3.25: (a): Q vs Kn for $e_n = 1$ and different $\hat{a}$, (b): a): Q vs Kn for $e_n = 0.7$ and different $\hat{a}$

The qualitative nature of profiles for $\Delta q_{x,y}$ and $\lambda_{q_{x,y}}$ (not shown) remain the same for $\hat{a} = 10$ with the point of nonmontonic transition for $\lambda_{q_{x,y}}$ shifting to a lower value of Kn. $\hat{a}$ has a significant impact on the normal stress differences of the flow as s demonstrated in Fig 3.26. The magnitude and rate of increase of $\mathcal{N}_1(0)$ is larger for a larger value of $\hat{a}$. The effect of $\hat{a}$ on $\mathcal{N}_2(0)$ is not as trivial and we notice that both for elastic and inelastic particles $\mathcal{N}_2(0)$ varies non monotonically with Kn for $\hat{a} = 10$, even becoming negative for a range of Kn. The effect of $\hat{a}$

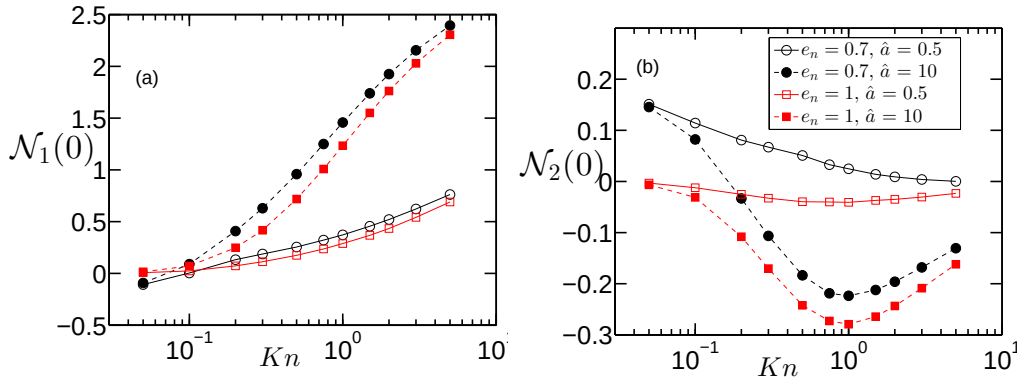

Figure 3.26: (a):$\mathcal{N}_1(0)$ vs Kn, (b): $\mathcal{N}_2(0)$ vs Kn

on temperature bimodality is shown in Fig 3.27(a). For a value of $\hat{a} = 10$, ΔT is non monotonic for $e_n = 0.7$ and $e_n = 1$ in contrast with what is observed for $\hat{a} = 0.5$. In Fig 3.28 we plot

three points on the bimodality phase plot (Fig 3.15) which have been simulated for $\hat{a} = 5$. It is observed that the transition from dissipation to rarefaction dominated bimodality occurs at a lower Kn for a higher value of $\hat{a}$.

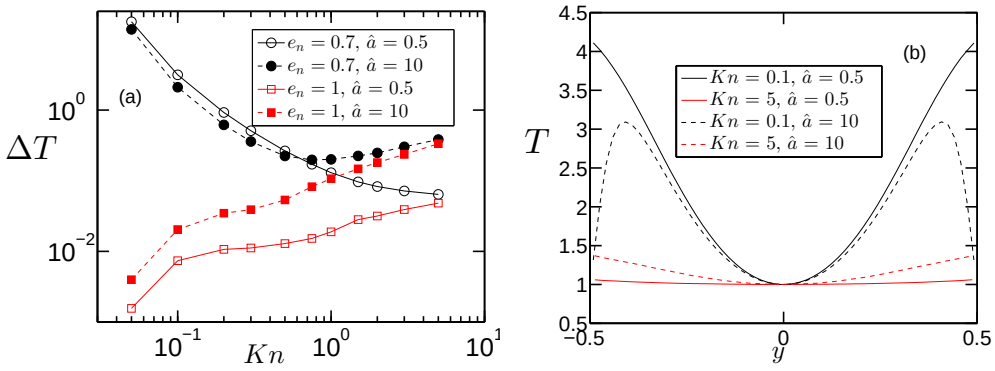

Figure 3.27: (a):ΔT vs Kn, (b): T vs y for $e_n = 0.7$ at $Kn = 0.1{,}5$ and $\hat{a} = 0.5{,}10$

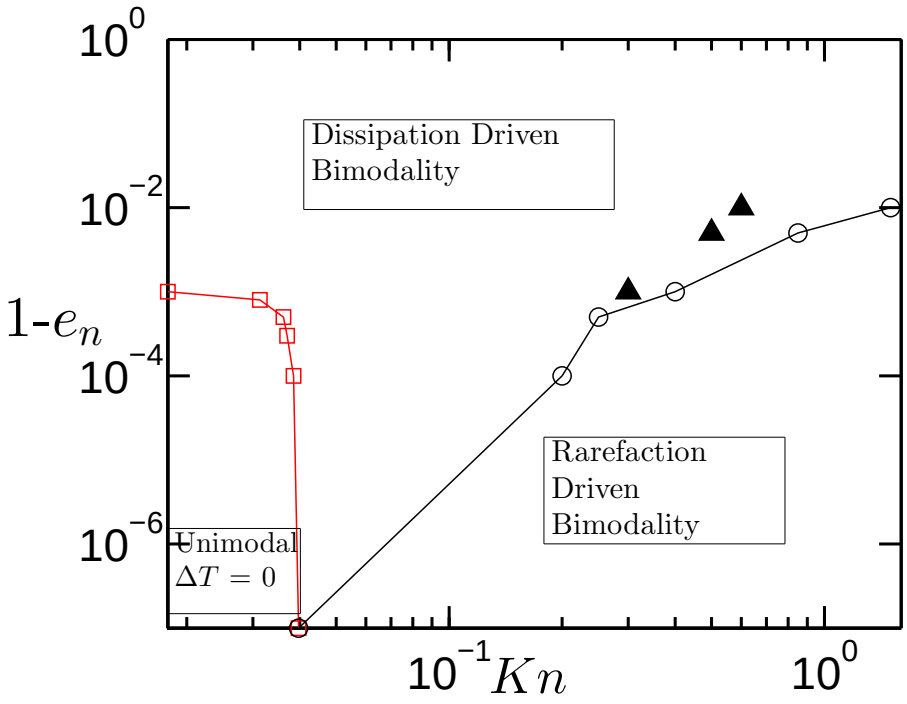

Figure 3.28: Same plot as Fig 3.15 with black triangles indicating corresponding points for e_n = 0.99,0.995,0.999 for $\hat{a} = 5$

Generally, the higher the value of $\hat{a}$, the more the viscous heating, leading to higher value of temperature and a higher effective Kn, than the pre-set average global Kn ((Wu *et al.* 2016)). This might explain some of the differences due to a higher $\hat{a}$ that occur in the quantities discussed above. For the same value of global Kn, the simulation for a higher value of $\hat{a}$ may represent a higher value of effective Kn. The non monotonicity in ΔT and $\mathcal{N}_2(0)$ for $\hat{a} = 10$ might be due to a higher range of Kn accessed for those cases. The early transition from dissipation to rarefaction dominated bimodality could also owe its origin to the same phenomena. It

must, however, be pointed out that there doesn't exist a simple linear relationship that ties the hydrodynamics of the flow across a range of $\hat{a}$ and for higher values of $\hat{a}$, the dynamics might be governed by nonlinear effects as well.

3.8 Conclusion

Using DSMC simulations we have studied the role of dissipation and rarefaction on the hydrodynamics and rheology of a dilute Poiseuille flow. Density inhomogeneity and clustering induced by dissipation plays a major role in influencing velocity profiles as well as temperature across the channel. The density inhomogeneity is also responsible for inducing bimodality in the transverse heat flux. Inelasticity amplifies the perpendicular heat flux in the bulk. Profiles of pressure and normal stress differences have been computed and some comment is made on the variation of centerline values of normal stress difference with Knudsen number. Role of acceleration is discussed in brief. While, we have uncovered some interesting results regarding the rheology of a dilute GPF, constructing a theoretical framework that can predict such novel features should be the next step. An explanation for negative centerline value of first normal stress difference for low e_n and Kn, and non monotonic variation of centerline value of second normal stress difference with Kn must be found along with a more complete description of the effects of increasing non dimensional acceleration.

Chapter 4

Role of Boundaries on Knudsen Minima Phenomenon

4.1 Introduction

The mass flow rate of a rarefied gas in a channel has received considerable attention due its interesting nonmonotonic behavior with Kn. This behavior, dubbed the Knudsen paradox was first proposed by Knudsen (Knudsen 1909) when he studied the effect of varying pressure heads on the flowrate of rarefied gases in a capillary tube. Flowrate was first found to decrease with increasing Kn after which it attained a minima and then displayed an increase, in contrast with the behavior predicted by the Navier Stokes equation. By taking the kinetic theory route this paradox was explained much later than Knudsen's original experiments (Cercignani & Daneri 1963). The issue of a Knudsen minima in a dilute granular gas was investigated in Alam *et al.* (2015) where the authors found that except for nearly smooth walls and nearly inelastic particles, Knudsen minima is absent. The results concerning the occurrence of Knudsen minimum in the previous chapter seem to be at odd with those in (Alam *et al.* 2015). In the following discussion we will show that energy transfer at the boundaries are critical in affecting the granular temperature near the wall (T_w), which is correlated to the density near the wall and hence directly affects the local Kn and slip velocity characteristics. By carrying out simulations for an athermal wall characterized by a bulk roughness parameter and a more general class of athermal walls we aim to highlight the crucial role played by boundaries in the occurrence of a Knudsen minima, hence attempting to solve the conundrum posed in (Alam *et al.* 2015), while at the same time making an attempt to discuss some anomalies associated with slip velocity.

4.2 Smooth Walls

For a certain region in the β,e_n phase space (Fig 4.1(a)) it was shown in (Alam *et al.* 2015) that the flowrate shows a nonmonotonic variation with Kn, exhibiting a minimum and a maxima. β is seen as an average roughness parameter that is frequently used in studies to approximate a rough wall (Campbell 1990), with β = -1,1 acting as the perfectly rough and perfectly smooth limits. The wall collision scheme is implemented as follows:

$$v_x^{t+\Delta t} = -\beta v_x^t + a t_{post} \tag{4.1}$$

$$v_y^{t+\Delta t} = -v_y^t \tag{4.2}$$

$$v_z^{t+\Delta t} = -\beta v_z^t \tag{4.3}$$

As seen in Fig 4.1(b) the flowrate does indeed initially decrease to a local minima and then increase to a maxima, post which it starts to decrease again.The reason for this nonmonotonic variation in flowrate is not clear at the first look.

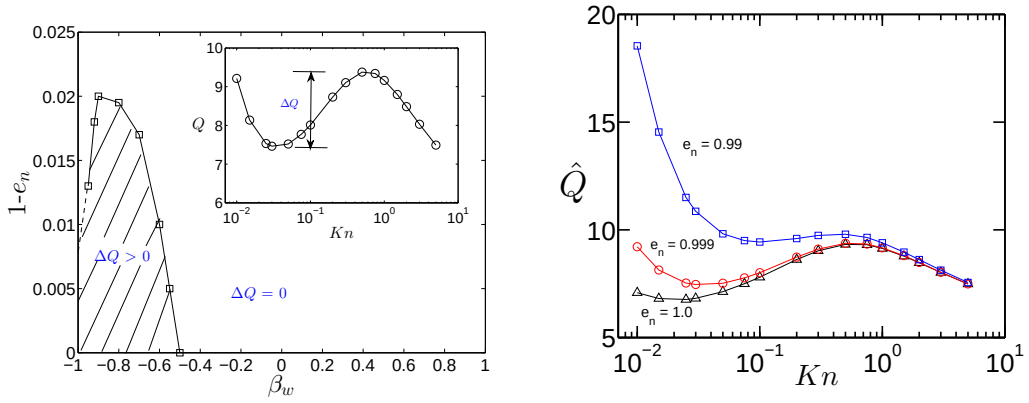

Figure 4.1: Left : Phase diagram in the (β_w, e_n) plane delineating regions of monotonic and nonmonotonic flowrates. Inset shows $\hat{Q}$ vs Kn for β_w, e_n = (-0.9, 0.9999). Right : $\hat{Q}$ vs Kn for three simulations having different e_n and β=-0.9

If we look at profiles for the case of $e_n = 0.9999, \beta = 0.9$ we notice that slip and centerline velocity both show anomalous variation with Kn. While it is expected that at values of e_n that are so close to 1 the density variation across the channel will be negligible, even the most subtle density variations and corresponding granular temperature variations can lead to the referred anomalous behavior. In Fig 4.2(a) we see how again density near the wall correlates with temperature near the wall with regions of decreasing granular wall temperature causing layers with higher density. The nonmonotonic variation of T_{fw} and the corresponding opposite trend shown by values of ρ_w lead to the anomalous variation in slip velocity as seen in Fig 4.2(b)

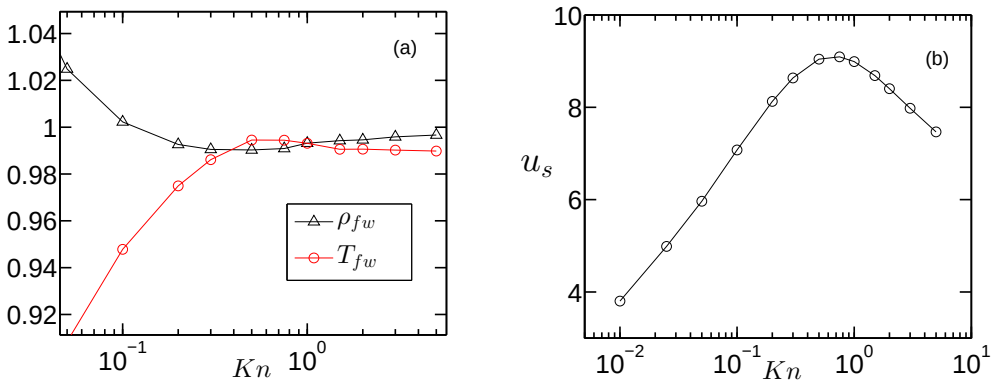

Figure 4.2: For smooth wall simulations - (a): T_{fw},ρ_{fw} vs Kn, (b):u_s vs Kn

4.3 Thermal Walls

A thermal 'heated' wall boundary condition is one that is frequently implemented for studying flows of a molecular gas (Cercignani 2000*a*; Kogan 1969; Karniadakis & Beşkök 2001). A thermal

wall can be imagined as a boundary connected to a heat reservoir at a certain temperature. The wall then is in thermal equilibrium with the reservoir. A gas molecule hitting the wall forgets its initial velocity characteristics and is re-emitted from the wall having adopted the wall temperature. While for the case of a molecular gas this boundary condition is a physically realizable one, for the case of a granular gas the concept of a heated thermal wall isn't as straightforward. This is because for granular gas the temperature is a quantity that is a byproduct of a flow and cannot be fixed or specified as an independent quantity. For the case of a vibrating wall with a certain high frequency the vibrating boundary can be approximated as a thermal boundary with a fixed temperature, but for stationary walls as in the case of a Poiseuille flow, the idealization of a thermal wall is not applicable. Thermal wall driven granular flows have however been the focus of several studies (Reyes Vega Francisco & Vincente 2013; Hrenya *et al.* 2008; Wu *et al.* 2016) and the present work can prove to be useful in uncovering features of another such prototypical flow. The following question can be posed - "*If we follow a protocol as has been done for molecular gas studies and study the Poiseuille flow of a granular gas driven by gravity and bounded by thermal walls does a Knudsen minima occur?*" For the purpose of the current discussion about the role of boundaries we show results for a value of $a = 0.01$. For all boundaries other than the thermal walls we cannot formulate a parameter like $\hat{a}$ as in the other wall boundaries we do not impose a wall temperature as we do in the case of thermal walls. For the following results we will nondimensionalize velocity with $\sqrt{aW}$, density with ρ_{avg} and temperature with its centerline value T_o. We recall the definition of nondimensional flowrate $\hat{Q}$

$$\hat{Q} = \frac{\int_{-L_y/2}^{+L_y/2} \rho(y) u_y(y) dy}{\rho_{avg} \sqrt{aW} L_y} \tag{4.4}$$

$\hat{Q}$ is plotted vs Kn for two e_n as well as for an elastic case and $\hat{a} \sim 10$ which corresponds to $a = 0.01$ and $T_w = 1$ and a clear minimum in flowrate is observed along with a log like increase post minimum Fig 4.3. The delay in the appearance for minimum with decreasing e_n can be accorded to the greater collisional contribution to drift velocity and hence with decreasing Kn there is an earlier transition from a ballistic to collisional regime.

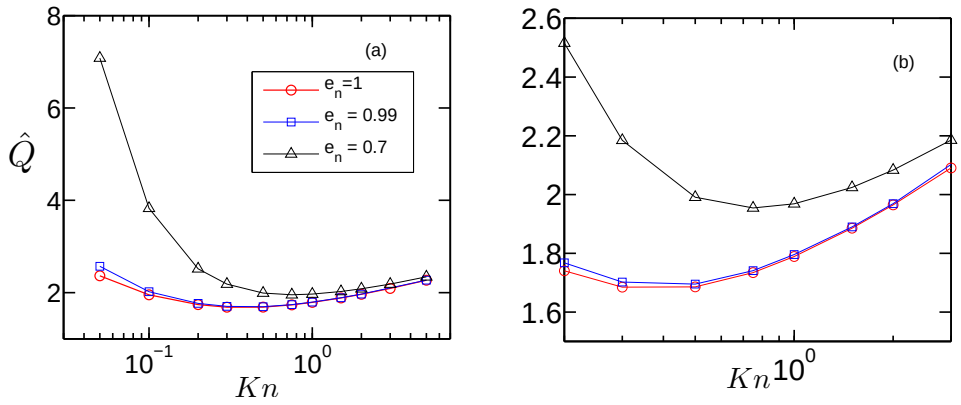

Figure 4.3: For thermal wall simulations - (a): $\hat{Q}$ vs Kn, (b):Magnified region showing occurrence of minima

It is instructive to observe the temperature and density near the walls on the same plot as in

Fig 4.4(a) . The plot is suggestive of the fact that the two quantities are correlated. Particles tend to gather near low temperature regions which are produced because the thermal walls act as a sink of energy. The height of the central density peak decreases with increasing Kn as particle particle collision lose dominance. This decrease in density peak is accompanied by an increase in ρ_{fw}. Gradually as rarefaction effects start kicking in both ρ_c and ρ_{fw} tend to 1, the latter *decreasing* to 1 and the former *increasing* to 1. Due to rarefaction, greater number of wall particle collisions lead to higher value of temperature slip, a trend which is accompanied by lower values of density near the wall. This decrease in ρ_{fw} leads to a layer near the wall that is rarefied and experiences greater slip. Essentially what is seen is that gradually increasing value of T_{slip} caused by the boundary interactions specific in the case of thermal walls, leads to an increasingly rarefied layer next to the wall where slip velocities are high and increase with increasing Kn as seen in Fig 4.4(b). This increase in slip velocity coupled with increase in centerline velocity (Fig 4.4(b)) (tied to increase in centerline density) ensures that flowrate increases after the initial decrease. Bulk dissipation doesn't prevent the occurrence of a Knudsen minimum at the current parameter values. We can refer to this surviving Knudsen minimum as $'artificial'$ due the artificial nature of thermal boundaries for a granular Poiseuille flow. However this exercise is helpful in indicating that the Knudsen paradox in a granular gas is crucially dependent on boundaries or rather how different the boundaries for a granular and molecular gases can behave. The Knudsen paradox in a granular gas crucially depends on the nature of the walls that bound the flow and if the walls are modeled as Thermal or Athermal.

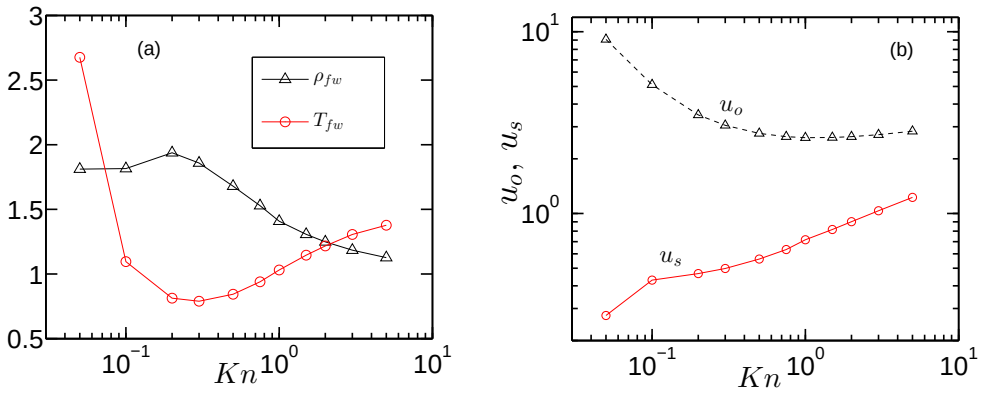

Figure 4.4: For thermal wall simulations at $e_n = 0.7$ - (a): T_{fw},ρ_{fw} vs Kn, (b):u_s,u_o vs Kn

4.4 Adiabatic Walls

In this section we present results from simulations that include boundaries imagined as idealistic walls that do not allow for any slip or energy transfer and are hence referred to athermal or no flux/no slip walls (Khain 2009). Since these walls don't allow energy exchange they cannot be used for a molecular gas simulation without an external thermostat. *For a thermal wall case the wall played a crucial role in bringing the system that gains energy due to shear provided by a body force, to a steady state. For an adiabatic wall, devoid of energy exchange mechanism, will we see any evidence of a Knudsen minimum in case of a granular gas flow?* Our results show that a Knudsen minimum is absent for such athermal walls as seen in Fig 4.5, again driving home the

point made in the previous section that the absence or presence of a flowrate minimum in the Poiseuille flow of a granular gas is primarily governed by the type of boundary interaction. The simulation results presented in this section are also for a = 0.01 and $e_n = 0.7$. We cannot define the parameter $\hat{a}$ for these simulations as we do not specify a temperature for the wall *apriori*. The reflection rule for the adiabatic boundary states that in the wall normal direction the particle simply reverses the direction of its incoming velocity. In the wall tangential direction the particle forgets it's incoming velocity and is reflected back with wall tangential velocity components v_x and v_z taken from a Gaussian distribution with zero mean and variance corresponding to the temperature of the bin adjacent to the wall ($T_{adjacent}$).

$$v_x^{t+\Delta t} = \sqrt{\frac{k_B T_{adjacent}}{m}} v_G + a t_{post} \tag{4.5}$$

$$v_y^{t+\Delta t} = -v_y^t \tag{4.6}$$

$$v_z^{t+\Delta t} = \sqrt{\frac{k_B T_{adjacent}}{m}} v_G \tag{4.7}$$

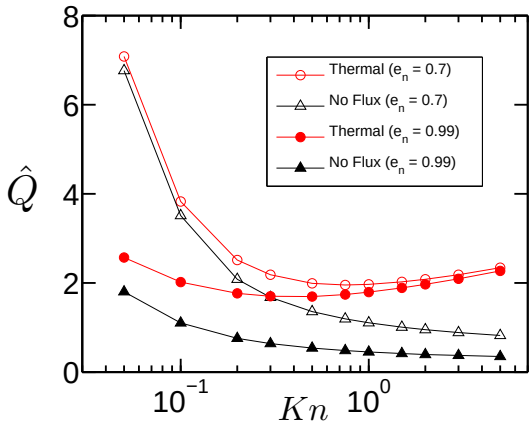

Figure 4.5: $\hat{Q}$ vs Kn for adiabatic boundaries

The absence of a minimum for the case of a wall with no energy flux can be explained by looking at the plot for slip velocity. The slip velocity keeps decreasing with Kn (Fig 4.6(b)) instead of the usual increase of slip velocity with increasing Kn. This anomalous behavior is tied to the density behavior near the walls.

Unlike the case of thermal walls where a temperature drop near the wall lead to increasing particle density, an adiabatic wall has no density peak near the wall, because of a lack of a temperature drop near the wall. The density at the centerline meanwhile keeps decreasing with increasing Kn leading to relative increase in density near the wall. Instead of a rarefied layer that enhances slip, these walls lead to denser layers that lead to decreasing slip velocities. Again, as in the discussion for thermal walls we see that the density near the wall is closely tied to the behavior of temperature slip. The temperature slip decreases with increasing Kn which leads

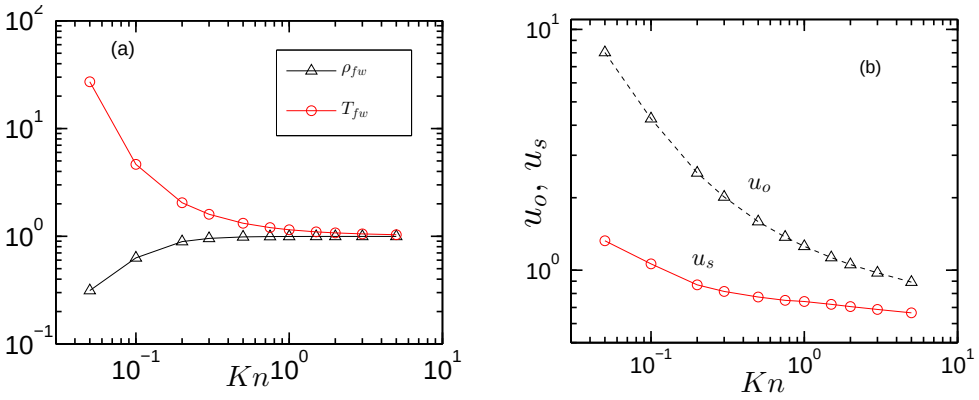

Figure 4.6: For no flux wall simulations at $e_n = 0.7$. (a): T_{fw}, ρ_{fw} vs Kn, (b):u_s, u_o vs Kn

to an increasing density near the wall as seen in Fig 4.6(a). The increasing density near the wall means that the centerline density decreases that leads to a decrease in centerline velocity which again is in contrast with the thermal wall case. Although the results have been shown for a gas well outside the elastic limit, simulations were run for $e_n = 0.99$ and no evidence for a minima was found.

4.5 Conclusion

The absence of a minima in flowrate for athermal walls reveals the importance of boundary interactions and energy gain/loss on influencing even averaged properties like flowrate. Since the wall boundaries used in simulations reported in Chapter 3 are the same as those used for molecular gas simulations (Cercignani 2000*b*), we can conclusively state that the absence of the Knudsen minimum seen in (Alam *et al.* 2015) can be accorded to the difference in *macroscopic* boundary conditions between a granular and molecular gas and bulk dissipation, an essential feature of a granular gas, plays a subdominant role. Our simulations indicate that inelastic dissipation does not prevent a minimum in flowrate, because if it did the Poiseuille flow of a granular gas with thermal walls, the subject of the study in Chapter 3, would fail to observe a minimum. The issue of boundary conditions for a granular fluids is not trivial and has received attention (Hui *et al.* 1984) in the last few years. The issue of Knudsen minima along with anomalous slip can maybe be better resolved if effort is made to map the athermal wall conditions to thermal wall conditions by either using a pre defined temperature or specifying an accommodation coefficient for momentum at the walls (Alam *et al.* 2015). Work in this direction is in progress. Future work is directed at finding out the mechanistic role played by different boundaries in the occurrence of a Knudsen minimum in a granular gas.

Chapter 5

Binary Granular Poiseuille flow : Role of Mass Bidispersity

5.1 Introduction

While granular flows are important in a plethora of industrial and natural flow processes, the majority of studies regarding granular flows have been restricted to monodisperse granular flows. Most of the naturally occurring and industrial flows however are characterized by a certain degree of polydispersity in size, shape or concentration, which makes it important to study polydisperse granular flows. Unfortunately these systems are significantly difficult to study when compared to a monodisperse system due to the large parameter phase. From a physics standpoint, granular mixtures are a hot bed of phenomena specific to them, most interesting of which is a tendency to segregate. Particles species in a granular mixture show often show segregation under external forcing (Ottino & Khakhar 2000) but also due to a difference in material properties like mass, size (Savage & Lun 1988) or even due to differences in degree of inelasticity (Serero *et al.* 2006). Another typical behavior exhibited by granular mixtures is that they don't share the same granular temperature, indicating a breakdown of equipartition of energy. The breakdown of equipartition for energy in granular systems has been observed in studies employing theory (Martin & Piasecki 1999; Barrat & Trizac 2002), simulations (Montanero & Garzó 2002; Alam *et al.* 2002; Alam & Luding 2003*b*; Galvin *et al.* 2005) and experiments (Wildman & Parkar 2002; Feitosa & Menon 2002). To reduce the complexity posed by a high degree of polydispersity, researchers work on binary mixtures consisting of two species of granular particles. Several theories have been proposed to model typical features observed in binary granular mixtures (Farrell *et al.* 1986; Jenkins & Mancini 1989; Willits & Arnarson 1999; Iddir & Arastoopour 2005; Serero *et al.* 2006). Some of these theories are based on certain assumptions like Maxwellian velocities, equipartition of energy and equal species velocity, and have still proven to be fairly successful in predicting certain properties of binary granular mixtures. Yet to investigate flows outside limits set by theory, like particles having high amount of inelasticity and specific wall boundaries, it often becomes imperative to resort to computer simulations. A large amount of granular mixture studies have focused on unbounded (Alam & Luding 2003*b*) or vibrated driven systems (Knight *et al.* 1993). The focus of the present study however is a binary granular Poiseuille flow, which includes both, a shear and wall boundary. Binary granular mixtures for a Couette (Liu *et al.* 2007) and channel flow (Liu *et al.* 2008) were studied via numerical modeling of equations derived from kinetic theory for moderately dense gases. We use DSMC simulations to study the effect of rarefaction and dissipation on some hydrodynamic properties, while also trying to ascertain if and what kind of segregation occurs for a dilute granular gas flow. The presence of walls along with a uniform acceleration leads to a non uniform steady state which

is analyzed for calculating velocity and temperature profiles of the mixture along with density and segregation across the channel width.

5.2 DSMC for binary mixtures

Binary mixtures refer to gases in which constituent particles are of two different types. They may differ in mass and/or diameter and number density. The system is also generally characterized by three coefficients of restitution, one each characterizing collisions between particle of the same type and another for collisions between particles of different types. This wide parameter space makes the system difficult to analyze theoretically but numerically solving the Boltzmann equation for a bidisperse system via DSMC is a viable solution. The extension of the traditional DSMC as described in the previous section to binary mixtures is not very complicated. At the onset it is fairly obvious that the system will now be charcaterised by three different collision frequencies, one each for 1-1, 2-2 and 1-2 type of collisions. This indicates that while previously a collision routine is run only once in a time-step, for a binary mixture it will have to be executed four times (1-1, 2-2, 1-2, 2-1). For each of these the N_p factor is modified to account for the differences in collision frequencies. Care must however be taken to specify cell size and time step to account for the different physical scales present in the problem due to the mixture's bidisperse nature. We define the following quantities that will be useful in setting up the simulation method.

$$\sigma_{ij} = \frac{1}{2}(\sigma_i + \sigma_j) \tag{5.1}$$

$$\mu_{ij} = \frac{m_j}{m_i + m_j} \tag{5.2}$$

In the above i = 1,2 and j = 1,2.Also, while the number of simulated particles in DSMC hold a strictly statistical significance the ratio of number of simulated particles of the two types should follow :

$$\frac{N_1}{N_2} = \frac{n_1}{n_2} \tag{5.3}$$

The algorithm for implementing DSMC for a binary mixture of gas is as follows :

- Initialise the positions and velocities for each particle. The usual practice is to assign positions by a random number chosen from a uniform distribution and the chose the velocities from an equilibrium Maxwell Boltzmann velocity distribution function for each specie corresponding to an initial temperature.
- Propogate each particle and process boundary conditions
- Sort particles in cells based on their positions. Each cell will now contain N_1^{cell} type 1 particles and N_2^{cell} type 2 particles.
- To simulate the collisions between particles of species i and j in a certain cell choose $N_p = \frac{1}{2} N_i^{cell} \omega_{max}^{ij}$ pairs of particles randomly. Here $\omega_{max}^{ij} = 4\pi\sigma_{ij}^2 n_j v_{12}^{max}$ and n_j refers to the local number density of species j in the cell for which collisions are being processed.

- For each pair of particles (k, l) choose a random vector equally distributed in 3D. The velocities of the accepted pairs of particles are changed according to the below collision rule.

$$\vec{v}_k' = \vec{v}_k - (\mu_{ji})(1 + \alpha_{ij})(\vec{e}.\vec{v}_{kl})\vec{e} \tag{5.4}$$

$$\vec{v}_l' = \vec{v}_l + (\mu_{ij})(1 + \alpha_{ij})(\vec{e}.\vec{v}_{kl})\vec{e} \tag{5.5}$$

  As metioned in the paragraph above, for each cell the collision routine will have to be run four times as $i = 1, 2$ and $j = 1, 2$. In addition k denotes a particle of species i and l denotes a particle of species j

- Calculate averages of required hydrodynamic quantities and repeat 2-5 till specified number of time-steps are completed.

5.3 Homogenous Cooling State for a Granular Mixture

In this section we present simulations done for a test case using the aforementioned DSMC code for binary mixtures. DSMC simulations performed for the homogeneous cooling state of a granular gas mixture (Montanero & Garzó 2002) are used as a test case for this section. As has been found for a variety of granular systems, there is an absence of equipartition of energy for the HCS. While each individual species shows a temperature decay their ratio ($\gamma = \frac{T_1}{T_2}$) saturates to a constant value after sometime which is reported. γ depends on different parameters, namely reduced density (n^*), mass ratio (μ), concentration ratio (δ), diameter ratio (w) and normal coefficient of restitution (e_n). The dependence of the relative temperature ratio on some of these parameters is plotted in Fig 5.1 and it is found that the quantitative agreement between the simulations reported in (Montanero & Garzó 2002) and the present DSMC code is excellent.

The successful match paves the way ahead for us to use the code developed for binary mixtures and study the Poiseuille flow of a dilute granular gas. Since the mass of the particle enters the boundary condition for thermal walls, and also the a governing parameter $\hat{a}$, it introduces a level of complexity to the system. Hence, all the simulations in this chapter have been carried out for athermal walls with a single value of roughness parameter (β_w = -0.9). For the case of athermal walls, the numeric value of acceleration, a, doesn't matter as it gets scaled out of the dynamics. The value of a is set to 0.01 for all simulations in this chapter. Because the parameter space for a binary granular gas is so large, in this chapter, we vary only on mass ratio and study some basic characteristics of this specific case of a binary granular Poiseuille flow with mass bidispersity.

5.4 Binary Granular Poiseuille Flow

This chapter is a result of preliminary analysis of simulations carried out for a dilute binary granular Poiseuille flow and quantities and features that have been looked at in detail for the monodisperse case will not be looked at. Rather, we will discuss some general features of the binary gas flow and report effects of rarefaction and dissipation, along with segregation.

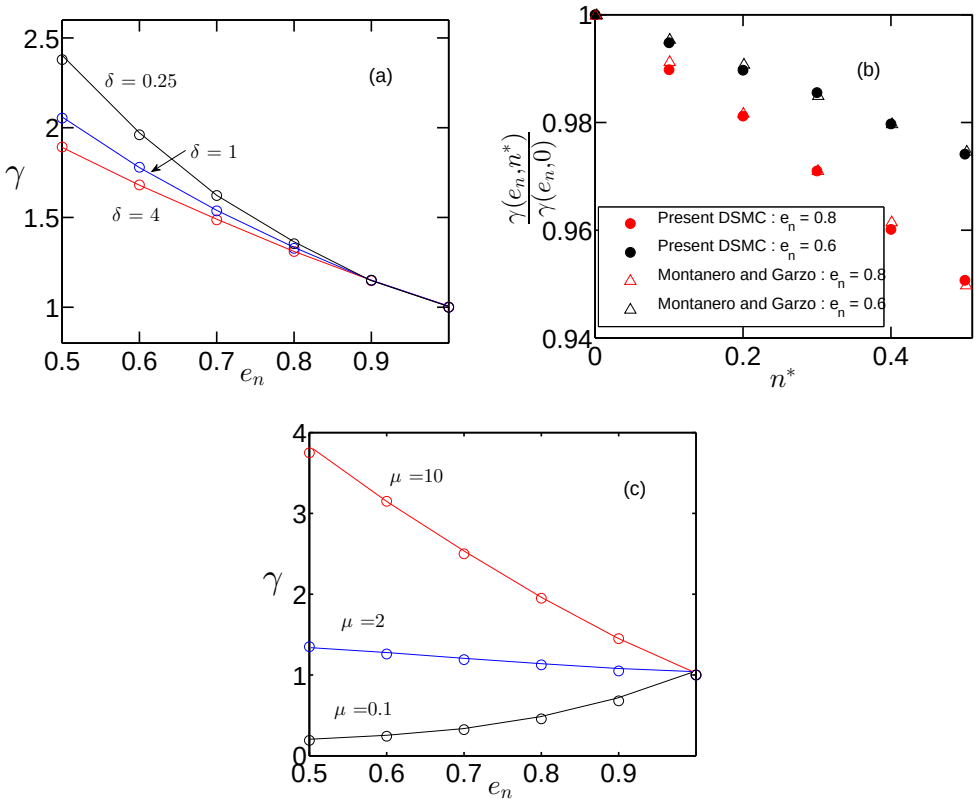

Figure 5.1: (a): γ vs e_n for different values of δ and $n^* \sim 0$, (b): γ vs n^* for (δ,w,μ) = 0.5,2,2, (c): γ vs e_n for $n^* \sim 0$, (w,μ) = 1,4. The solid lines in (a) and (c) are obtained by joining the respective symbols indicating DSMC results from (Montanero & Garzó 2002)

5.4.1 Velocity Field

The mean velocities of the individual species (u_1,u_2) are defined in the same way as was for the monodisperse case. The mean velocity for the mixture (v_m) is calculated as

$$\vec{u^m} = \frac{\rho^1 \vec{u}^1 + \rho^2 \vec{u}^2}{\rho^m} \tag{5.6}$$

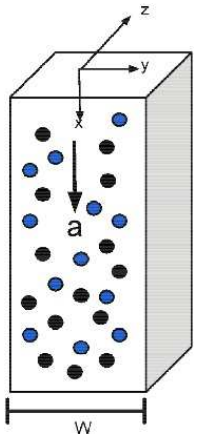

Figure 5.2: Schematic for binary GPF. Two colours represent particles of different masses.

$$\rho^m = m^1 n_{avg} + m^2 n_{avg} \tag{5.7}$$

Note, the superscripts (1,2) indicate the specific species value and the superscript, m, indicates the field for the mixture. Because the number density ratio for the mixture is 1, the initial average values of n for both species is the same (n_{avg}). The Kn reported is thus calculated using $n^m_{avg} = n^1_{avg} + n^2_{avg} = 2n_{avg}$. The mass ratio, ($m_r$) is defined as the ratio of the heavier particle (2) to the lighter particle (m). The velocity field for both species and mixture retains the typical parabolic velocity profile with deviation from the parabolic profile occuring for inelastic particles at lower value of Kn as seen in Fig 5.3(a). More interestingly, while there is no discernible difference between the species and mixture velocity for the low Kn case, for a higher value of Kn the species have different mean velocities (Fig 5.3(b)). This phenomena will be discussed a little later in the chapter.

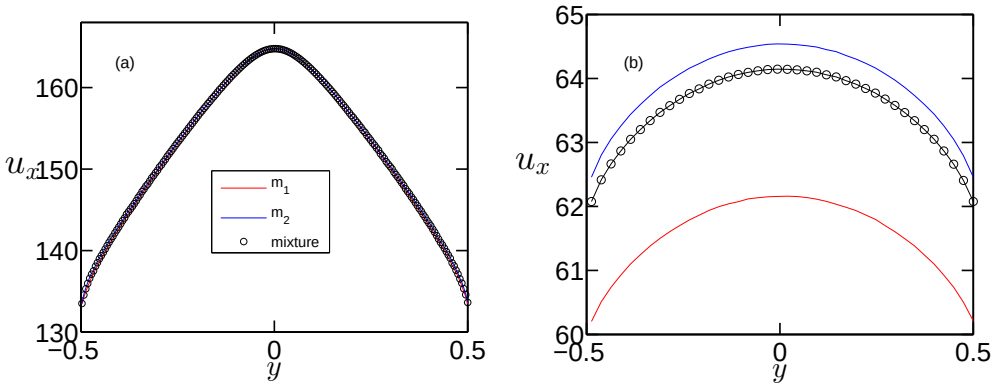

Figure 5.3: (a): u_x vs y for $Kn = 0.05$, $e_n = 0.7$ and $m_r = 5$, (b): u_x vs y for $Kn = 1$, $e_n = 0.7$ and $m_r = 5$,

In Fig 5.4 we see that the centerline velocity for the mixture follows a non monotonic trend for inelastic particles. For nearly elastic particles this trend is absent. The reason for the nonmonotonic variation for centerline velocity is not clear at this point. We return to the issue of different mean species velocities in Fig 5.5 and notice that for all m_r and e_n, and low to moderate values of Kn the difference in centerline species velocity ($\Delta u_o = u^2_o - u^1_o$) remains very small, but attains finite value with increasing Kn. The collapse of individual and mixture velocities at low Kn for our case agrees with the results reported for moderate density mixtures in a Couette and channel flow (Liu *et al.* 2007, 2008). Δu_o increases with increasing Kn. It has a similar dependence on m_r, but the dependence on m_r, seems to decrease with increasing mass ratio. As seen in Fig 5.5(a,b) the dependence of Δu_o on e_n doesn't show a characteristic trend but one can conclude that it is a relatively weak dependence. Our results highlight the importance of including a difference in mean velocities when developing kinetic theories for binary mixtures (Mei *et al.* 2015). It is important to point out at this point that because the initial average number density and diameter is the same for each particle species their individual Kn, if we can attach a quantity like that, is the same. Hence, simulated separately each species, even with different masses would have the same steady state mean velocity. A non zero value of Δu_o is a consequence of the bidispersity of the system and results from the interaction of these individual non-equal mass species.

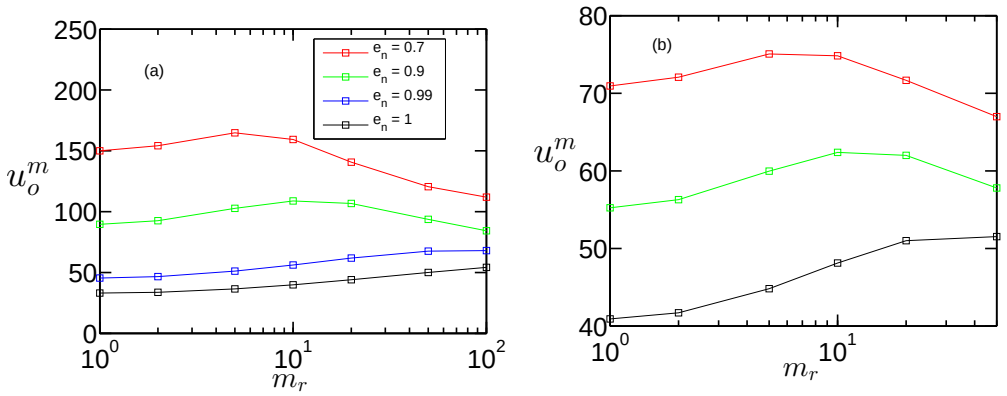

Figure 5.4: u_o^m vs m_r for different e_n, (a): $Kn = 0.05$, (b): $Kn = 0.5$

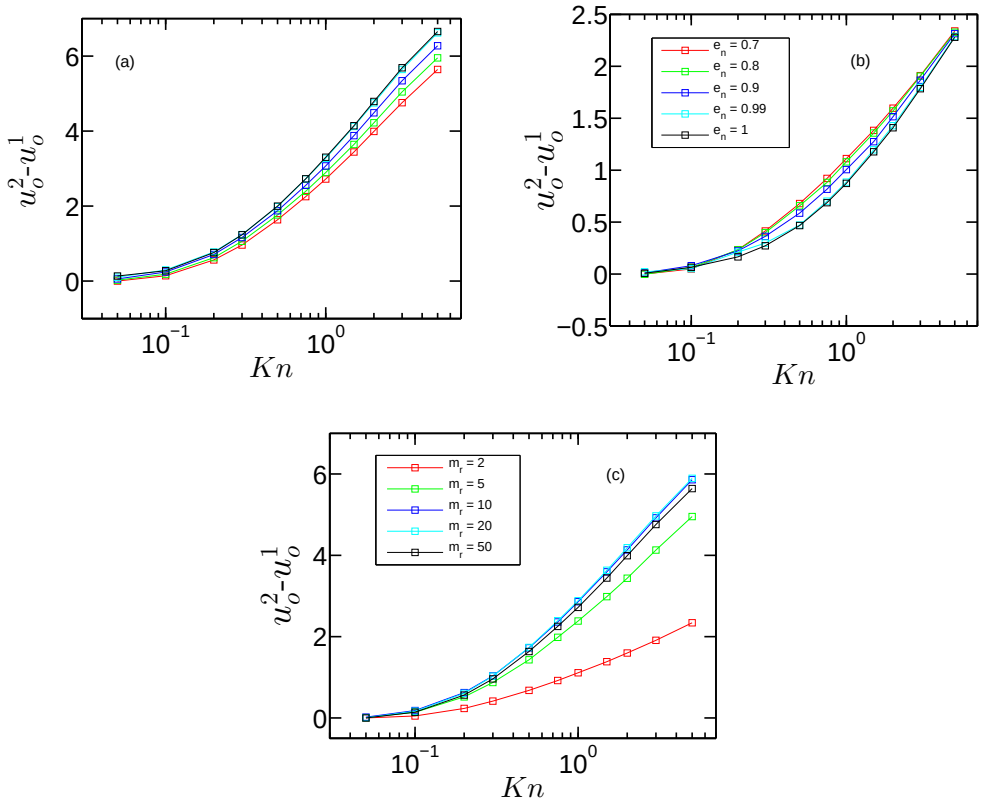

Figure 5.5: (a): Δu_o vs Kn for $m_r = 50$ (b): Δu_o vs Kn for $m_r = 2$, (c): Δu_o vs Kn for $e_n = 0.7$. Legend for (a) and (b) are same.

5.4.2 Flowrate

In this section we very briefly describe the characteristics of the mass flow rate exhibited by a binary granular gas poiseuille flow. Profiles of flowrate along with the related issue of Knudsen minima has been extensively discussed in the previous chapters and will not be revisted in this chapter. The flowrate for the mixture is defined by

$$\hat{Q}^m = \frac{\int_{-W/2}^{+W/2} \rho^m(y) u_x^m(y) dy}{\rho_{avg}^m \sqrt{aW} W} \tag{5.8}$$

For the value of β_w, a monodisperse flow shows a monotonically decreasing flowrate for all values of e_n >0.985 (Fig 4.1). The bidisperse flow rate for $e_n = 0.7$. shows a similar trend. In Fig 5.6(a) we observe that at $Kn = 0.05$, the value of flowrate is nonmonotonic with mass ratio. This follows from the nonmonotonic variation of centerline mixture velocity at the same value of Kn. It is also observed that at least for all values of $m_r \leq 20$, the flowrate becomes rather insensitive to variation in mass ratio, beyond the initial nonmonotonicty displayed at lower values of Kn. As seen in In Fig 5.6(b) the flowrate shows nonmonotonicty, albeit of a very small magnitude, for e_n=0.99 as this combination of (β_w, e_n) lies inside the $(\Delta Q > 0)$ region of the phase plot in Fig 4.1. For the largest value of m_r, however this nonmonotonicity seems to disappear, indicating that maybe for high values of m_r, Fig 4.1 might have to be modified. Similar nonmonotonicty and possible loss at higher m_r is expected for the case of $e_n = 1$, but low Kn runs are not done for that case and hence no conclusive comment can be made.

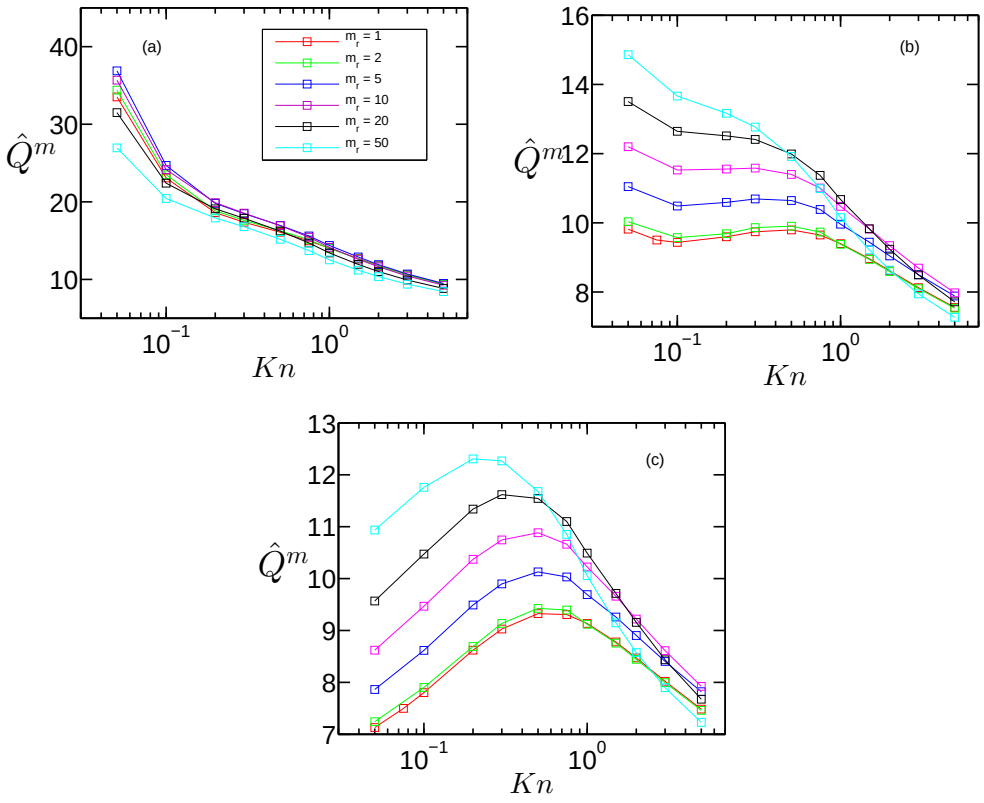

Figure 5.6: $\hat{Q}$ vs e_n for different values of m_r (a):$e_n = 0.7$ (b): $e_n = 0.99$, (c): $e_n = 1$

5.5 Granular Temperature

In this section we refrain from discussing temperature profiles features like slip and bimodality like we did for the monodisperse case and instead restrict our discussion to the case of non-equipartition of energy, which is a classical feature of binary granular mixtures. The granular temperature for a species and mixture is defined as follows

$$T^i = \frac{1}{3} m^i \langle C^{i2} \rangle \tag{5.9}$$

$$C^i = \vec{v} - \vec{u}^m \tag{5.10}$$

$$T^m = \frac{n^1 T^1 + n^2 T^2}{n^1 + n^2} \tag{5.11}$$

We see in Fig 5.7 that there is a significant difference in the temperature profiles for both species, signalling a breakdown of equipartition. Particles of species 2, the heavier species, have a greater granular temperature. From Fig 5.7(b) we notice that the degree of nonequipartition of energy between the two species, at least in the center, seems to have increased for the case of $Kn = 1$. To the best of our knowledge the effect of rarefaction on temperature nonequipartition has not been studied before and we only provide a brief insight. To quantify nonequipartition we define two parameters namely γ_o and γ_{avg}.

$$T^i_{avg} = \frac{\int_{-W/2}^{+W/2} T^i(y)dy}{W} \tag{5.12}$$

$$\gamma_{avg} = \frac{T^2_{avg}}{T^1_{avg}} \tag{5.13}$$

$$\gamma_o = \frac{T^2_o}{T^1_o} \tag{5.14}$$

As seen in Fig 5.8 and 5.9 both γ_o and γ_{avg} seem to be a strong function of Kn, with γ_{avg} showing a nonmonotonic behavior. The experiments reported in (Feitosa & Menon 2002) indicate that the breakdown of energy equipartition is predominantly a bulk effect. Our DSMC simulations for a dilute gas flow however show that rarefaction beyond a certain transitional Kn, amplifies the nonequipartition of energy. Fig 5.8 shows that nonequipartition is also amplified by an increasing m_r, a result which is not surprising and in agreement with the simulations for different prototype flows reported in (Alam & Luding 2002, 2003*b*; Liu *et al.* 2007, 2008). For a uniform shear flow, there is a single defining temperature for the system which is shown to exhibit as a nonmonotonic variation with m_r (Alam & Luding 2002, 2003*b*). For a inhomogeneous flow like Poiseuille flow however the temperature is a function of the coordinate normal to the wall. A preliminary check failed to observe a similar trend for the average mixture temperature in the channel, though a roughly similar trend was found for centerline temperature. Here we must

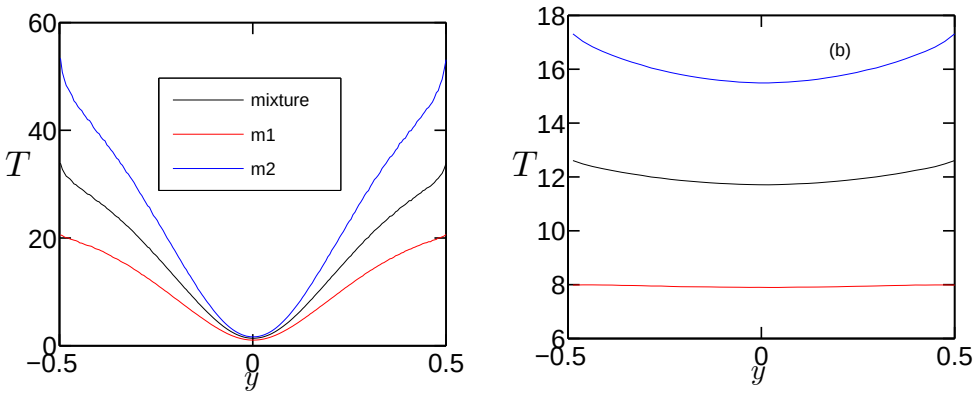

Figure 5.7: (a): T vs y for Kn, e_n, m_r = (0.05,0.7,5) (b): T vs y for Kn, e_n, m_r = (1,0.7,5)

note that the simulated mass ratio's are not entirely unrealistic as particles with hollow structures may have very low densities making it possible to achieve high mass ratios in experiments (Liu *et al.* 2008).

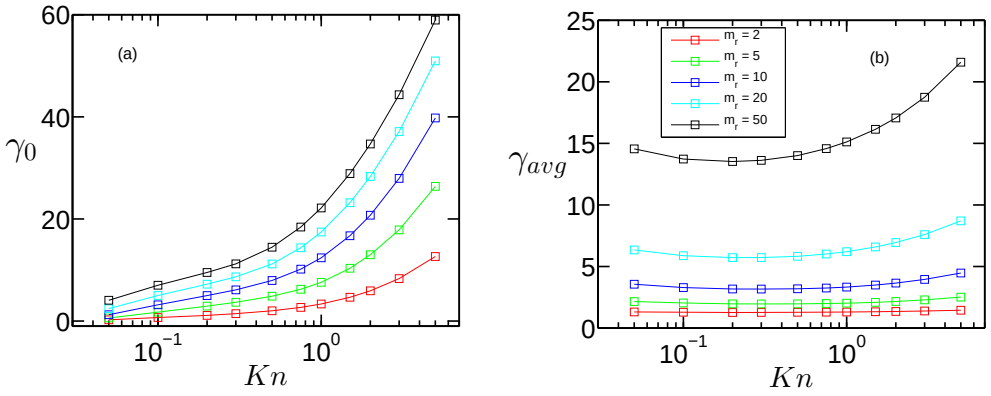

Figure 5.8: (a): γ_o vs Kn (b): γ_{avg} vs Kn, for different values of e_n and $m_r = 5$

Fig 5.9 shows that in the low Kn limit nonequipartition is a result of inelasticity (Alam & Luding 2003*b*), however elastic particles show a marked amount of nonequipartition at higher Kn. The genesis of this nonequipartition of energy however could be rarefaction, a mass ratio different from unity or a combination of both.

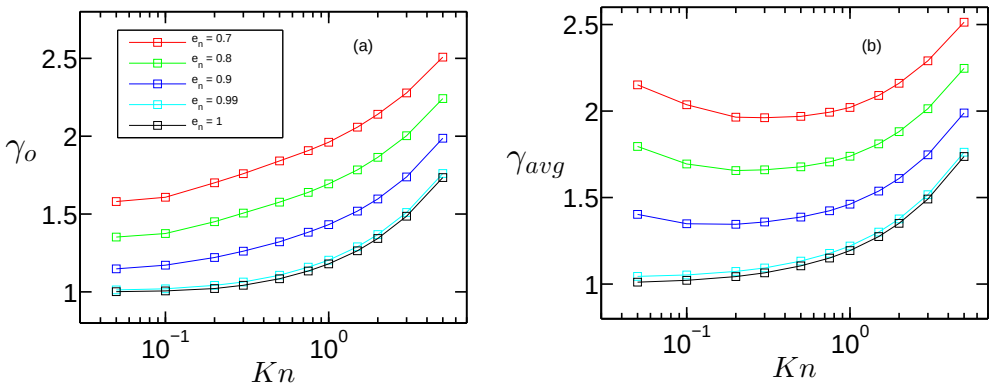

Figure 5.9: (a): γ_o vs Kn (b): γ_{avg} vs Kn, for different values of m_r and $e_n = 0.7$

5.6 Density and Segregation

In this section we focus on density profiles, in particular on segregation in a binary granular Poiseuille flow. Because the focal point of discussion is segregation, we only analyze data for the lowest value of Kn, i.e. 0.05, because as the average solid fraction in the system increases segregation is found to increase (Liu *et al.* 2007), and segregation will be minimal for rarefied flows. A typical mixture density profile is shown in Fig 5.10(a) and the individual densities are displayed in Fig 5.10(b), clearly showing segregation. As is noticed from both figures there is a heterogeneity in the total mixture density as well as in the species number density profiles. We

can quantify the heterogeneous behavior by specifying two parameters

$$I_{so} = \frac{\sum_{i=1}^{i=nb} (\frac{n^m(i)}{2n_{avg}} - 1)^2}{nb} \tag{5.15}$$

$$I_{sp} = \frac{\sum_{i=1}^{i=nb} (\frac{n^2}{n^1+n^2} - 0.5)^2}{nb} \tag{5.16}$$

In the equations above nb is the number of bins used for averaging. I_{so} defines the extent of heterogeneity in the total number density in the system, also the mixture's number density. This term, $'intensity'$ of total solids segregation (Liu *et al.* 2007), puts a single number for a number density profile, a higher magnitude signifying a greater extent of inhomogeneity in the mixture's number density. I_{sp} is the $'intensity'$ of species segregation (Windows-Yule *et al.* 2014, 2015) and assigns a number to the difference in individual species number density. Essentially it quantifies the deviation from a completely mixed scenario where the number density fraction for each species would be 0.5. Again, a higher value of I_{ss} denotes a greater extent of species segregation.

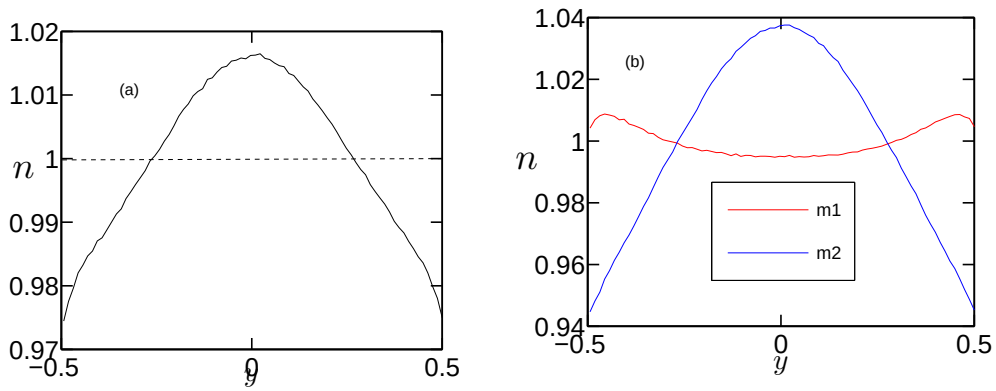

Figure 5.10: For $Kn, m_r, e_n = (0.05,50,0.99)$ (a): n^m vs y (b): n^1, n^2 vs y

The role of dissipation in inducing clustering and hence density inhomogeneity across the channel has been discussed in earlier chapters. In Fig 5.11 we see that m_r has a significant effect on the mixtures number density. From Fig 5.11(b,c) it is clear that the granular mixture becomes more uniform as we increase the mass ratio. While this effect is not clear in near inelastic particles, for the case of $e_n = 0.7,0.9$, there is a significant reduction in particle clustering, when compared to the case of $m_r = 1$, i.e. that of monodisperse flow. The above conclusion is supported by solids segregation plot shown in Fig 5.11(d), where for inelastic particles, I_{so} decreases with increasing m_r. This result is useful because it means that we can control the distribution of particles across the channel by tuning the amount of mass bidispersity.

Next we look at species segregation caused by mass bidispersity. In Fig 5.12 and Fig 5.13 we plot the individual number densities for a range of m_r for $e_n = 0.99$ and 0.9 respectively. Visually we can see that while for both e_n and all m_r, the heavier mass particle (species 2) has a higher tendency to cluster, the degree of segregation seems to differ for the two values of e_n shown. For $e_n = 0.99$, the segregation seems to increase with increasing m_r, whereas for

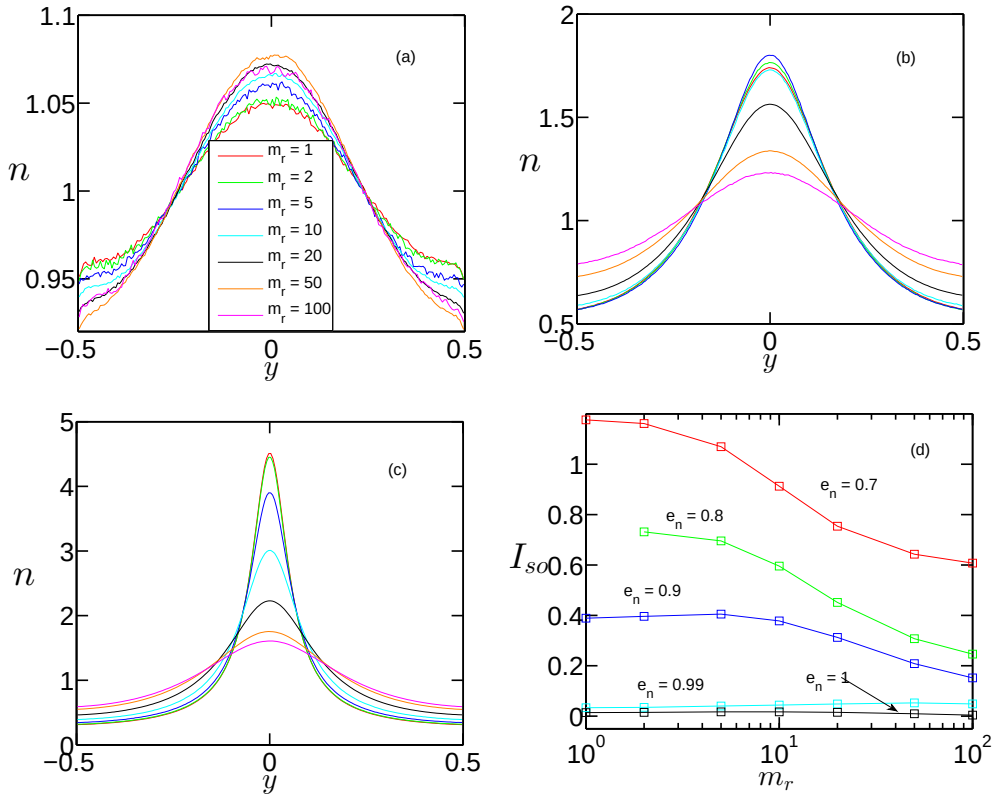

Figure 5.11: (a): n^m vs y for $e_n = 0.99$ (b): n^m vs y for $e_n = 0.9$, (c): n^m vs y for $e_n = 0.7$, (d): I_{so} vs m_r for different e_n

e_n=0.9, the segregation initially increases but then beyond a certain m_r, the segregation begins to decrease. Essentially our simulations reveal that for inelastic particles ($e_n \leq 0.9$), species segregation follows a nonmonotonic trend with m_r. This result is in agreement with kinetic theory calculations in (Liu *et al.* 2008) for channel flow. In Fig 5.14 the above discussed effect is summarized in a more quantitatively conclusive way and we see that for inelastic particles, I_{sp} varies in a nonmonotonic fashion with m_r with the transition point coming at lower m_r for lower value of e_n.

5.7 Conclusion

We have looked at a few features shown by a dilute binary granular Poiseuille flow. While, the results regarding energy nonequipartition are not surprising and in agreement with the results reported for other systems, the dependence of this nonequipartition on rarefaction has been shown. Rarefaction is also responsible for increasing the disparity between the individual mixture velocities, at least in the smooth wall limit as discussed here. Density profiles have been computed to qualitatively and quantitatively assess the amount of segregation in the system. To do the same we define two quantities and find that while the total mixture becomes more homogeneous as mass ratio increases, species segregation interestingly follows a non monotonic trend with mass ratio for inelastic particles. Centerline mixture velocity shows a similar trend, in contrast with previous work that suggests that mixture velocities are insensitive to mass

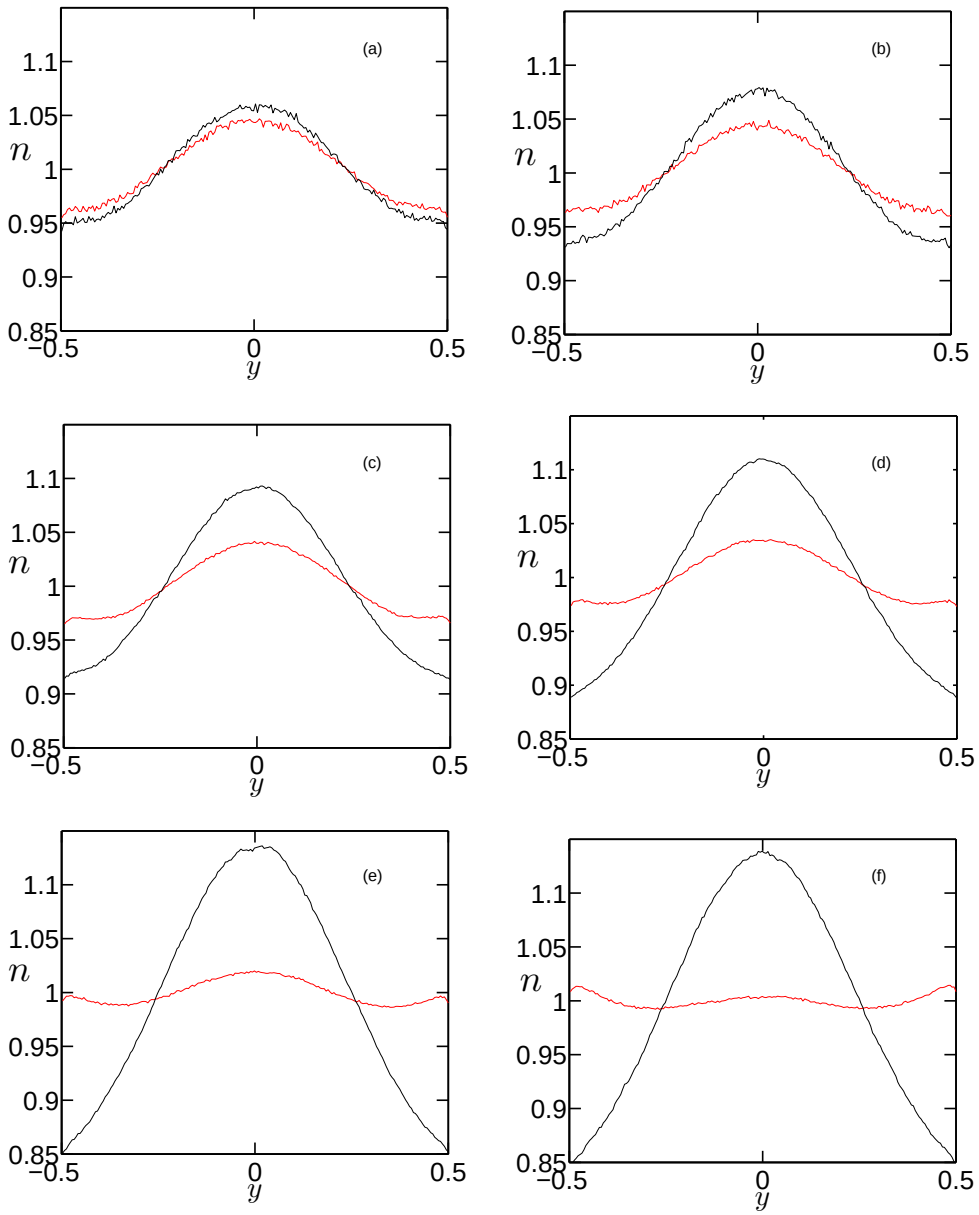

Figure 5.12: n^1, n^2 vs y for $e_n = 0.99$ and (a): $m_r = 2$, (b): $m_r = 5$, (c): $m_r = 10$, (d): $m_r = 20$, (e): $m_r = 50$, (f): $m_r = 100$

ratio. Work is in progress to present a physical explanation for the trend displayed by total and species segregation. While even the simpler case of only mass bidispersity ;ead to some interesting features it will be worthwile to carry out similar studies by varying diameter ratio as well as concentration ratio. Though the system will become tougher to analyze it is likely to yield some interesting physics much like the starting case of mass bidispersity pursued here.

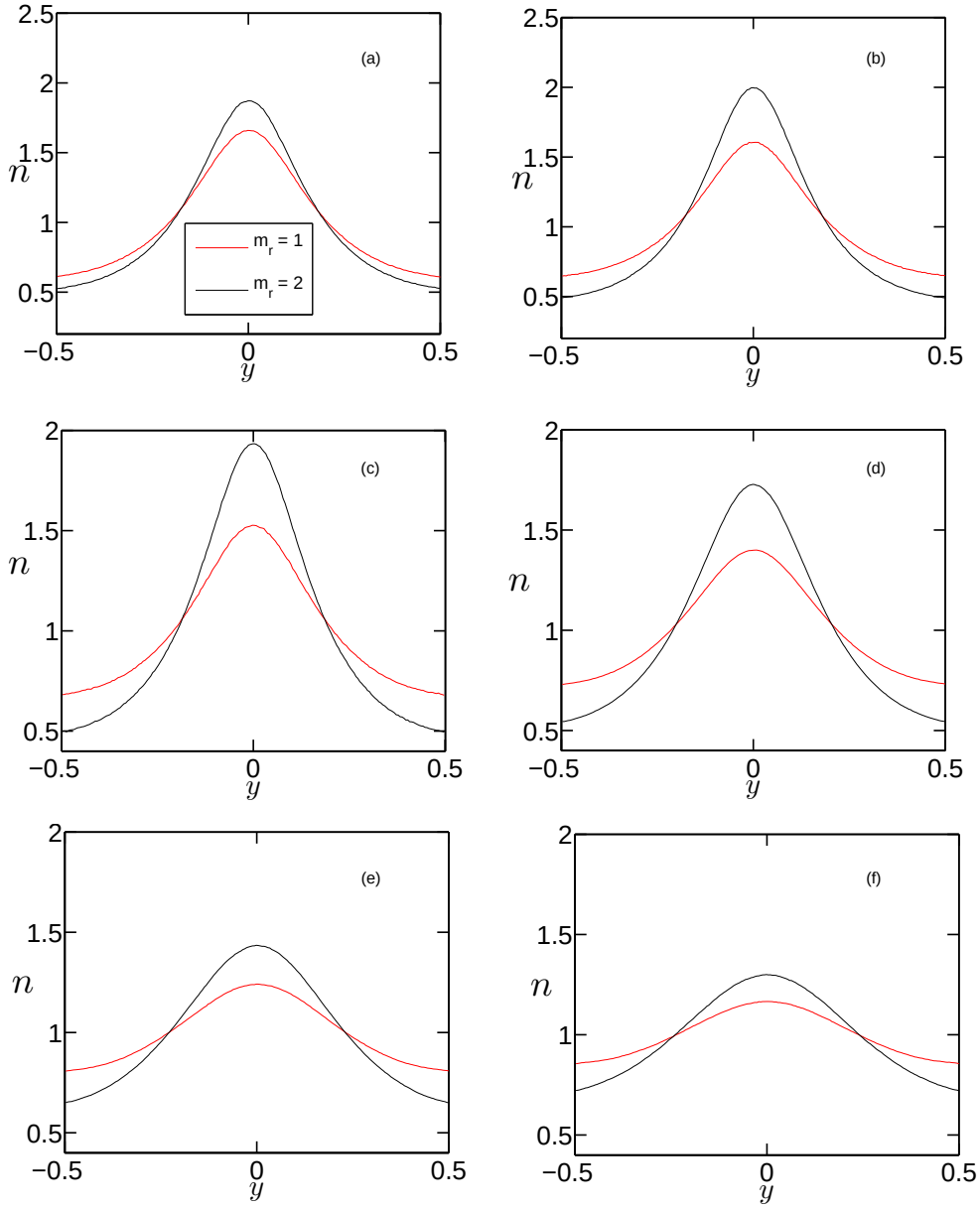

Figure 5.13: n^1, n^2 vs y for $e_n = 0.9$ and (a): $m_r = 2$, (b): $m_r = 5$, (c): $m_r = 10$, (d): $m_r = 20$, (e): $m_r = 50$, (f): $m_r = 100$

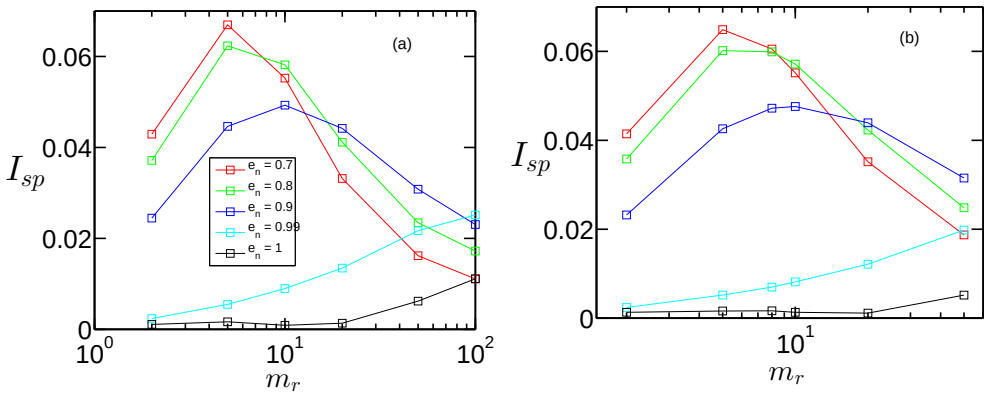

Figure 5.14: I_{sp} vs m_r for different e_n for (a): β_w = -0.9 (b): β_w = -0.9

Chapter 6

Summary and Conclusions

In this thesis we investigate the physics of the flow of a granular gas in a simple configuration, an acceleration driven Poiseuille flow. We employ the Direct Simulation Monte Carlo method to simulate a granular Poiseuille flow, a detailed description of which is presented in Chapter 2.

Starting with a monodisperse flow, we investigate the effects of rarefaction and dissipation on the hydrodynamics and rheology of a thermal wall driven granular Poiseuille flow in Chapter 3. For a fixed value of $\hat{a}$, we calculate the variation of hydrodynamic quantities across the width of the channel. Dissipation induces clustering near the channel center, due to cooling induced by inelastic collisions. This clustering leads to a density inhomogeneity that has important consequences on higher-order moments of the system. We invoke this clustering and subsequent rarefaction induced de-clustering to explain trends followed by slip and centerline velocity. A phenomenon that was found to be a result of rarefaction in a molecular gas flow, namely temperature bimodality was looked into and it was found that the bimodality in a granular gas is enhanced by inelasticity. There exist two distinct regimes within which dissipation and rarefaction are both independently responsible for the genesis of temperature bimodality. This result, while explored in (Alam *et al.* 2015), was independently obtained via the current DSMC simulations. Moving on from the system hydrodynamics, we look at rheological quantities. Shear stress shows a deviation from linearity for granular gases in the low Kn limit. While, rarefaction causes a nonuniform parabolic pressure profile in a molecular gas, inelasticity causes a deviation from a parabolic profile. Normal stress difference profiles show considerable variation across the channel and we quantify the effect of rarefaction and dissipation on centerline values of first and second normal stress differences. Our simulations reveal that for lower values of e_n, $\mathcal{N}_\infty(0)$ becomes negative in the low Kn limit. This finding must be explored further and it will be interesting to look if any theory for granular hydrodynamic predicts this non-trivial rheological feature. Dissipation is responsible for causing a bimodality in q_x as well as enhancing q_y in the bulk, and both effects are lost with increasing Kn. Work is in progress to investigate heat flux in a dilute GPF in detail, and in particular explain the double well shape of the q_x profile. Finally we study the effect of $\hat{a}$ on the system and we notice that there is a qualitative change in the behavior of centerline second normal stress difference and temperature bimodality. While, this effect could be a result of the system attaining a higher value of effective Kn at a higher $\hat{a}$, it could be a result of non linear effects as well.

An important result obtained in Chapter 3 was the observation of a Knudsen minimum for a granular gas. This finding was at odds with the conclusion drawn in Alam *et al.* (2015), where the authors found that except for nearly inelastic particles and almost smooth walls, a granular gas does not attain a Knudsen minimum. Our simulations indicate that the phenomena of a

Knudsen minimum is crucially dependent on wall boundary conditions, specifically the difference in boundaries for a molecular and granular gas. Bulk dissipation does not prevent the occurrence of a minimum in flowrate, as indicated by our thermal wall simulations. Hence, inelasticity was found to play a subdominant role in the presence or absence of a Knudsen minimum in a granular gas. We analyzed the problem of flowrate minimum in Chapter 4 using not only thermal walls, but two sets of athermal wall simulations - rough walls and adiabatic walls (Khain 2009) and tried to obtain a better understanding of the related velocity slip phenomena. In future work we will try to elucidate the mechanistic details of the boundary dependence of a Knudsen minimum in a GPF.

In Chapter 5 we add a degree of complexity to the system, by introducing a mass bidispersity in the system. Several interesting features of this dilute granular Poiseuille flow were uncovered. It was found that centerline velocities of the two species begin differing from each other and hence the mass averaged mixture velocity at higher values of Kn. This effect is sensitive to m_r, at lower values of m_r and shows a relatively weak dependence on e_n. Interestingly the centerline mixture velocity shows a non monotonic trend with m_r. The breakdown of energy equipartition manifests as a difference in species temperatures. As observed in a variety of systems, the nonequipartition is amplified by increasing inelasticity and m_r and is additionally found to be an increasing function of Kn. The mixture's total number density becomes more uniform with increasing m_r, whereas species segregation displays an interesting non monotonic variation with m_r.

In the thesis we have made an effort to study the individual and at times the competing effects of dissipation and rarefaction for the case of a dilute granular flow and have resolved the conundrum of Knudsen minima in a granular gas by highlighting the role of boundaries on the flow. A start is made to understand a dilute granular binary mixture in the Poiseuille flow configuration by limiting the amount of bidispersity to only a difference in masses. For conducting the above mentioned study we developed a 3D DSMC code which was rigorously tested and bench marked using various prototypical granular flows as test cases. For the monodisperse case, our DSMC code can be extended to simulate dense gases (Montanero & Santos 1996) and a systematic investigation of the rheology of a dense granular Poiseuille flow can be carried out. To the best of our knowledge, such a study is currently lacking. Moving from mass bidispersity, we can explore other regions of the phase space to study the hydrodynamics and segregation in the binary mixture system, a study similar to the one carried out in Chapter 5. Interesting results obtained in regard to heat flux and normal stress differences for a monodisperse case can be checked for parallels and possible deviation for a binary mixture. The rheological and hydrodynamic effects uncovered by DSMC simulations are likely to be useful in the development and testing of higher order hydrodynamic theories for rapid granular flows.

References

Alam, M. & Chikkadi, V. 2010 Velocity distribution function and correlations in a granular poiseuille flow. *Journal of Fluid Mechanics* **653**, 175.

Alam, M. & Luding, S. 2002 How good is the equipartition assumption for the transport properties of a granular mixture? *Granular Matter* **4** (3), 139–142.

Alam, M. & Luding, S. 2003*a* First normal stress difference and crystallization in a dense sheared granular fluid. *Physics of Fluids (1994-present)* **15** (8), 2298–2312.

Alam, M. & Luding, S. 2003*b* Rheology of bidisperse granular mixtures via event-driven simulations. *Journal of Fluid Mechanics* **476**, 69–103.

Alam, M. & Luding, S. 2005 Energy nonequipartition, rheology, and microstructure in sheared bidisperse granular mixtures. *Physics of Fluids (1994-present)* **17** (6), 063303.

Alam, M., Mahajan, A. & Shivanna, D. 2015 On knudsen-minimum effect and temperature bimodality in a dilute granular poiseuille flow. *Journal of Fluid Mechanics* **782**, 99–126.

Alam, M., Willits, J. T., Arnarson, B. Ö. & Luding, S. 2002 Kinetic theory of a binary mixture of nearly elastic disks with size and mass disparity. *Physics of Fluids (1994-present)* **14** (11), 4085–4087.

Alder, B. J. & Wainwright, T. E. 1959 Studies in molecular dynamics. i. general method. *The Journal of Chemical Physics* **31** (2), 459–466.

Aranson, I. S. & Tsimring, L. S. 2006 Patterns and collective behavior in granular media: Theoretical concepts. *Reviews of modern physics* **78** (2), 641.

Astillero, A. & Santos, A. 2005 Uniform shear flow in dissipative gases: Computer simulations of inelastic hard spheres and frictional elastic hard spheres. *Phys. Rev. E* **72**, 031309.

Bagnold, R. A. 1954 Experiments on a gravity-free dispersion of large solid spheres in a newtonian fluid under shear. In *Proceedings of the Royal Society of London A: Mathematical, Physical and Engineering Sciences*, , vol. 225, pp. 49–63. The Royal Society.

Barrat, A. & Trizac, E. 2002 Lack of energy equipartition in homogeneous heated binary granular mixtures. *Granular Matter* **4** (2), 57–63.

Bird, G. 1963 Approach to translational equilibrium in a rigid sphere gas. *Physics of Fluids (1958-1988)* **6** (10), 1518–1519.

Bird, G. 1994 Molecular gas dynamics and the direct simulation monte carlo of gas flows. *Clarendon, Oxford* **508**.

Brilliantov, N. & Pöschel, T. 2004 *Kinetic Theory of Granular Gases*. Oxford University Press.

Campbell, C. S. 1990 Rapid granular flows. *Annual Review of Fluid Mechanics* **22** (1), 57–90.

Cercignani, C. 2000*a* *Rarefied gas dynamics: from basic concepts to actual calculations*, , vol. 21. Cambridge University Press.

Cercignani, C. 2000*b* *Rarefied gas dynamics: from basic concepts to actual calculations*, , vol. 21. Cambridge University Press.

Cercignani, C. & Daneri, A. 1963 Flow of a rarefied gas between two parallel plates. *Journal of Applied Physics* **34** (12), 3509–3513.

Chapman, S. & Cowling, T. G. 1970 *The mathematical theory of non-uniform gases: an account of the kinetic theory of viscosity, thermal conduction and diffusion in gases*. Cambridge university press.

Chikkadi & Alam 2007 Velocity distribution and the effect of wall roughness in granular poiseuille flow. *Physical Review E* **75** (5), 051306.

Chikkadi, V. & Alam, M. 2009 Slip velocity and stresses in granular poiseuille flow via event-driven simulation. *Physical Review E* **80** (2), 021303.

Duran, J. 2012 *Sands, powders, and grains: an introduction to the physics of granular materials*. Springer Science & Business Media.

Eshuis, P., van der Meer, D., Alam, M., van Gerner, H. J., van der Weele, K. & Lohse, D. 2010 Onset of convection in strongly shaken granular matter. *Physical review letters* **104** (3), 038001.

Eshuis, P., van der Weele, K., van der Meer, D. & Lohse, D. 2005 Granular leidenfrost effect: Experiment and theory of floating particle clusters. *Physical review letters* **95** (25), 258001.

Faraday, M. 1831 On the forms and states assumed by fluids in contact with vibrating elastic surfaces. *Philos. Trans. R. Soc. London* **121** (319), 1831.

Farrell, M., Lun, C. & Savage, S. 1986 A simple kinetic theory for granular flow of binary mixtures of smooth, inelastic, spherical particles. *Acta Mechanica* **63** (1-4), 45–60.

Feitosa, K. & Menon, N. 2002 Breakdown of energy equipartition in a 2d binary vibrated granular gas. *Physical review letters* **88** (19), 198301.

Forterre, Y. & Pouliquen, O. 2008 Flows of dense granular media. *Annu. Rev. Fluid Mech.* **40**, 1–24.

Galvin, J., Dahl, S. & Hrenya, C. 2005 On the role of non-equipartition in the dynamics of rapidly flowing granular mixtures. *Journal of Fluid Mechanics* **528**, 207–232.

Garzó, V. 2004 On the einstein relation in a heated granular gas. *Physica A: Statistical Mechanics and its Applications* **343**, 105–126.

Goldhirsch, I. 1999 Scales and kinetics of granular flows. *Chaos: An Interdisciplinary Journal of Nonlinear Science* **9** (3), 659–672.

Goldhirsch, I. 2003 Rapid granular flows. *Annual review of fluid mechanics* **35**, 267–293.

Goldhirsch, I. & Zanetti, G. 1993 Clustering instability in dissipative gases. *Physical review letters* **70** (11), 1619.

Grad, H. 1949 On the kinetic theory of rarefied gases. *Communications on pure and applied mathematics* **2** (4), 331–407.

Graur, I., Perrier, P., Ghozlani, W. & Méolans, J. 2009 Measurements of tangential momentum accommodation coefficient for various gases in plane microchannel. *Physics of Fluids (1994-present)* **21** (10), 102004.

Hadjiconstantinou, N. G. 2003 Dissipation in small scale gaseous flows. *Journal of heat transfer* **125** (5), 944–947.

Haff, P. 1983 Grain flow as a fluid-mechanical phenomenon. *Journal of Fluid Mechanics* **134**, 401–430.

Hagan, G. 1839 Uber die bewegung des wassers in engen cylindrischen rohren. *Ann. Phys. Chem* **46**, 423–444.

Hrenya, C., Galvin, J. & Wildman, R. 2008 Evidence of higher-order effects in thermally driven rapid granular flows. *Journal of Fluid Mechanics* **598**, 429–450.

Hui, K., Haff, P., Ungar, J. & Jackson, R. 1984 Boundary conditions for high-shear grain flows. *Journal of Fluid Mechanics* **145**, 223–233.

Hünenberger, P. H. 2005 Thermostat algorithms for molecular dynamics simulations. *Advanced computer simulation* pp. 130–130.

Iddir, H. & Arastoopour, H. 2005 Modeling of multitype particle flow using the kinetic theory approach. *AIChE journal* **51** (6), 1620–1632.

Jaeger, H. M. & Nagel, S. R. 1992 Physics of the granular state. *Science* **255** (5051), 1523.

Jaeger, H. M., Nagel, S. R. & Behringer, R. P. 1996 Granular solids, liquids, and gases. *Rev. Mod. Phys.* **68**, 1259–1273.

Jenkins, J. & Mancini, F. 1989 Kinetic theory for binary mixtures of smooth, nearly elastic spheres. *Physics of Fluids A: Fluid Dynamics (1989-1993)* **1** (12), 2050–2057.

Jenkins, J. & Richman, M. 1985 Kinetic theory for plane flows of a dense gas of identical, rough, inelastic, circular disks. *Physics of Fluids (1958-1988)* **28** (12), 3485–3494.

Jenkins, J. & Savage, S. 1983 A theory for the rapid flow of identical, smooth, nearly elastic, spherical particles. *Journal of Fluid Mechanics* **130**, 187–202.

Kadanoff, L. P. 1999 Built upon sand: Theoretical ideas inspired by granular flows. *Reviews of Modern Physics* **71** (1), 435.

Karniadakis, G. & Beşkök, A. 2001 *Microflows: fundamentals and simulation*. Springer.

Khain, E. 2009 Bistability and hysteresis in dense shear granular flow. *EPL (Europhysics Letters)* **87** (1), 14001.

Knight, J. B., Jaeger, H. M. & Nagel, S. R. 1993 Vibration-induced size separation in granular media: the convection connection. *Physical review letters* **70** (24), 3728.

Knudsen, M. 1909 Die gesetze der molekularstromung und der inneren reibungsstromung der gase durch rohren. *Ann. Phys.* **333**, 75–130.

Kogan, M. 1969 Rarefied gas dynamics. *Plenum Press, New York* **2**, l.

Lees, A. & Edwards, S. 1972 The computer study of transport processes under extreme conditions. *Journal of Physics C: Solid State Physics* **5** (15), 1921.

Liu, X., Metzger, M. & Glasser, B. J. 2007 Couette flow with a bidisperse particle mixture. *Physics of Fluids (1994-present)* **19** (7), 073301.

Liu, X., Metzger, M. & Glasser, B. J. 2008 Granular and gas–particle flows in a channel with a bidisperse particle mixture. *Chemical Engineering Science* **63** (23), 5696–5713.

Majmudar, T., Sperl, M., Luding, S. & Behringer, R. P. 2007 Jamming transition in granular systems. *Physical review letters* **98** (5), 058001.

Mansour, M. M., Baras, F. & Garcia, A. L. 1997 On the validity of hydrodynamics in plane poiseuille flows. *Physica A: Statistical Mechanics and its Applications* **240** (1), 255–267.

Martin, P. A. & Piasecki, J. 1999 Thermalization of a particle by dissipative collisions. *EPL (Europhysics Letters)* **46** (5), 613.

Mathieu, E. 1863 Sur le mouvement des liquides dans les tubes de très petit diamètre. *CR* **57**, 320–324.

Mei, Y., Chen, Y. & Wang, W. 2015 Kinetic theory of binary particles with unequal mean velocities and non-equipartition energies. *arXiv preprint arXiv:1508.02871* .

Montanero, J. M. & Garzó, V. 2002 Monte carlo simulation of the homogeneous cooling state for a granular mixture. *Granular Matter* **4** (1), 17–24.

Montanero, J. M. & Santos, A. 1996 Monte carlo simulation method for the enskog equation. *Physical Review E* **54** (1), 438.

Montanero, J. M. & Santos, A. 1997 Simulation of the enskog equation a la bird. *Physics of Fluids* **9** (7), 2057–2060.

Ohwada, T., Sone, Y. & Aoki, K. 1989 Numerical analysis of the poiseuille and thermal transpiration flows between two parallel plates on the basis of the boltzmann equation for hard-sphere molecules. *Physics of Fluids A: Fluid Dynamics (1989-1993)* **1** (12), 2042–2049.

Ottino, J. & Khakhar, D. 2000 Mixing and segregation of granular materials. *Annual Review of Fluid Mechanics* **32** (1), 55–91.

Poiseuille, J. L. M. 1847 *Recherches expérimentales sur le mouvement des liquides de nature différente dans les tubes de très petits diamètres*. Bachelier.

Pöschel, T. & Schwager, T. 2005 *Computational granular dynamics: models and algorithms*. Springer Science & Business Media.

Puglisi, A. 2001 The homogeneous cooling state.

Rao, K. & Nott, P. 2008 *An Intriduction to Granular Flow*. Cambridge university press.

Rapaport, D. 1980 The event scheduling problem in molecular dynamic simulation. *Journal of Computational Physics* **34** (2), 184–201.

Reyes Vega Francisco, Santos, A. & Vincente, G. 2013 Steady base states for non-newtonian granular hydrodynamics. *Journal of Fluid Mechanics* **719**, 431–464.

Risso, D. & Cordero, P. 1998 Generalized hydrodynamics for a poiseuille flow: theory and simulations. *Physical Review E* **58** (1), 546.

Saha, S. & Alam, M. 2014 Non-newtonian stress, collisional dissipation and heat flux in the shear flow of inelastic disks: a reduction via gradâs moment method. *Journal of Fluid Mechanics* **757**, 251–296.

Savage, S. & Jeffrey, D. 1981 The stress tensor in a granular flow at high shear rates. *Journal of Fluid Mechanics* **110**, 255–272.

Savage, S. & Lun, C. 1988 Particle size segregation in inclined chute flow of dry cohesionless granular solids. *Journal of Fluid Mechanics* **189**, 311–335.

Serero, D., Goldhirsch, I., Noskowicz, S. & Tan, M.-L. 2006 Hydrodynamics of granular gases and granular gas mixtures. *Journal of Fluid Mechanics* **554**, 237–258.

Shinbrot, T. & Muzzio, F. J. 1998 Reverse buoyancy in shaken granular beds. *Physical Review Letters* **81** (20), 4365.

Stokes, G. 1845 On the theories of the internal friction of fluids in motion, and of the equilibrium and motion of elastic solids. *Trans. Camb. phil. Soc* **8**, 287–341.

Tehver, R., Toigo, F., Koplik, J. & Banavar, J. R. 1998 Thermal walls in computer simulations. *Physical Review E* **57** (1), R17.

Tij, M. & Santos, A. 1994 Perturbation analysis of a stationary nonequilibrium flow generated by an external force. *Journal of statistical physics* **76** (5), 1399–1414.

Umbanhowar, P. 2003 Granular materials: Shaken sandâa granular fluid? *Nature* **424** (6951), 886–887.

Uribe, F. & Garcia, A. L. 1999 Burnett description for plane poiseuille flow. *Physical Review E* **60** (4), 4063.

Wang, M. & Li, Z. 2004 Simulations for gas flows in microgeometries using the direct simulation monte carlo method. *International Journal of Heat and Fluid Flow* **25** (6), 975–985.

Wildman, R. & Parkar, D. 2002 Energy nonequipartition in a vibrated granular gas mixture. *Phys. Rev. Lett.* **88** (19).

Willits, J. & Arnarson, B. 1999 Kinetic theory of a binary mixture of nearly elastic disks. *Physics of Fluids (1994-present)* **11** (10), 3116–3122.

Windows-Yule, C., Douglas, G. & Parker, D. 2015 Competition between geometrically induced and density-driven segregation mechanisms in vibrofluidized granular systems. *Physical Review E* **91** (3), 032205.

Windows-Yule, C., Weinhart, T., Parker, D. & Thornton, A. 2014 Influence of thermal convection on density segregation in a vibrated binary granular system. *Physical Review E* **89** (2), 022202.

Wu, L., Liu, H., Reese, J. M. & Zhang, Y. 2016 Non-equilibrium dynamics of dense gas under tight confinement. *Journal of Fluid Mechanics* **794**, 252–266.

CALVIN: I think we've got enough information now, don't you?

HOBBES: All we have is one 'fact' you made up.

CALVIN: That's plenty. By the time we add an introduction, a few illustrations, and a conclusion, it will look like a graduate thesis.

Bill Watterson, Calvin and Hobbes

List of Corrections (Response to External Review)

- Correct spelling and typographical errors.

  An effort was made to rid the thesis of all spelling and typographical errors.

- The thesis should contain a page on Nomenclature and abbreviations used at the start, this would be placed after the abstract.

  A page on nomenclature was added after the abstract that includes a list of Roman Letters, Abbreviations, Greek letters and subscripts used.

- Compute and state average percentage error for Fig 2.5(a) and (b) to understand accuracy of prediction

  Computation of error for Fig 2.5 (a,b) is not possible because data points for time don't match for computed and extracted data. While there is some error in the steady state values, I found that slightly changing the imposed shear rate could lead to such errors in steady state temperatures. Such errors could creep in if there is a difference in the approximation for π in the original and current study as well. Considering that the data has been manually extracted from a log-log plot the match is reasonable.

- In Fig. 2.7 9a), state possible reason for why at low reduced shear rates, the results for reduced shear viscosity coefficient using DSMC methods does not follow Grad's method.

  The authors in the original study related the mismatch to the curvature of temperature profiles and the mismatch is more for more curvature and curvature is large for smaller shear rates. Our DSMC matches the DSMC results of the paper very well, though

- State what you understand by thermostat, and types of thermostat used in DSMC.

  Added information about thermostats used in DSMC and MD along with relevant references.

- Check valdiity of Eq. 3.13 and include references for Eq's 3.10-3.13.

  Equation 3.13 is simply Newton's law of motion for a particle undergoing uniform acceleration for pre and post collision cases. Even though it isn't necessary to update the x coordinate for the current system, we write down the equation for completeness and as such its validity is general. Added references for boundary conditions.

- Variation of Knudsen number along y is shown (Fig 3.7), how would Knudsen number vary for developing Poiseuille flow or with respect to x. when should one consider that the rarefaction effect has started.

For calculating the variation of Kn in X direction we will have to have something that breaks symmetry in X direction like end walls, X variation of wall temperature, roughness or a different acceleration field. That is a different problem and it is difficult to make predictions based on the current much more idealized problem. For discussing parallels for fully developed flow and entrance length in the context of rapid granular flows we might have to bring in concepts of boundary layer which are not very established in the kind of systems we are studying. Maybe we can discuss it by invoking the Knudsen layer, but I can't be sure. I must point out that the DSMC code developed can handle flows that depend on X and Y, but depending on the number of cells we might have to convert the serial code to a parallel version.

- for low Kn, Fig 3.9 shows drop in slip velocity for $e_n = 0.7$, state the reason for this to happen.

  The dip in slip velocity for low e_n and Kn is because the velocity profiles deviate from a parabolic shape and this leads to an imperfect fit. This could be a physical result or a consequence of not ideal fitting, but we can't say for sure. For such low e_n we don't simulate for $Kn \leq 0.05$ because Boltzmann equation loses validity and DSMC becomes costly for such cases.

- What is the authors viewpoint on the Knudsen minimum phenomena for rough wall with granular gas Poiseuille flow.

  For rough walls we don't see a Knudsen minima. While the exact mechanistic reason is unclear at the moment and we are investigating it, my viewpoint is that because the slip velocity keeps decreasing with Kn instead of increasing with Kn, it doesn't allow flowrate to increase after a minimum leading to a monotonic decrease in flowrate.

- Check validity of Eq. 5.11

  Eq. 5.11 has been corrected. Equation 5.11's validity is general because it's how mixture temperature is defined and doesn't result from ay physical law. This definition has been used in many studies for binary systems.